Investigation of Point Doppler Velocimetry (PDV) for Transition Detection in Boundary Layers

Final Report for Grant NAG-1-1892
Mr. James F. Meyers, Technical Monitor
NASA Langley Research Center

November, 1999

Dr. John M. Kuhlman, PI
West Virginia University
Morgantown, WV 26506-6106
(304)293-3111, x2328

(Note that this final report consists of the MS thesis prepared by graduate student David L. Webb, under the direction of the PI)

DEVELOPMENT OF AND MEASUREMENTS USING A POINT DOPPLER VELOCIMETRY (PDV) SYSTEM

By

David L. Webb

THESIS

Submitted to the College of Engineering and Mineral Resources
West Virginia University
Morgantown, WV

In partial fulfillment of the requirements
for the degree of

Master of Science
in
Aerospace Engineering

John M. Kuhlman, Ph.D., Chair
Mridul Gautam, Ph.D.
Charles F. Stanley, Ph.D.

Department of Mechanical and Aerospace Engineering
December 1999

Keywords: Velocity Instrumentation, Point Doppler Velocimetry, PDV, NACA 0012 Airfoil

Abstract

Development of and Measurements Using a Point Doppler Velocimetry (PDV) System

David L. Webb

A two component Point Doppler Velocimetry (PDV) system has been developed and tested. Improvements were made to an earlier PDV system, in terms of experimental techniques, as well as the data acquisition and reduction software.

Measurements of the streamwise and spanwise mean and fluctuating velocities for flows from a rectangular channel and over an NACA 0012 airfoil were made, and the data were compared against hot wire data. The closest to the airfoil surface that PDV measurements could be made was on the order of 0.005 m (0.2", z/c = 0.0169).

When the PDV and hot wire data were compared, the time traces for each appeared similar. The mean velocities agreed to within ±2 m/sec, while the RMS velocities agreed to ±0.4 m/sec. While the PDV time autocorrelations agreed with those of the hot wire data, the PDV power spectral densities were noisier above 750 Hz.

A major source of error in these experiments was determined to be the drifting of the iodine cell stem temperatures. While the stem temperatures were controlled to within ±0.1 °C, this could lead to a frequency shift of as much as 6 MHz, which translates into an error of 1.6 m/sec for the back scatter channel, and up to 6.9 m/sec for the forward scatter channel. These error estimates are consistent with the observed error magnitudes.

Acknowledgments

I would like to begin by thanking the NASA Langley Research Center for their support under grants NAG-1-1892 and NAG-1-2132. I would especially like to thank Jim Meyers for the knowledge and support he provided for this project.

I would also like to thank everyone who has assisted me on this project, including Jasmin Bauer, Tom Scarberry, Jonathan "Tex" Smith, and Valentino Williams. I would especially like to thank Kelly James and Steve Naylor for all their help, and the foundations for this project they laid for me to build on.

A special thanks goes to the faculty and staff of the Mechanical and Aerospace Engineering Department at West Virginia University, especially Dr. John Kuhlman. The knowledge and experience I have gained, especially over the course of this research, is a debt which can never be repaid.

My thanks goes out to all the friends I have made at WVU. A special thanks goes to Alex Alvarez, Boldy Khatter, and David Yeater for keeping me focused on completing my thesis.

Finally, my deepest thanks and gratitude go out to my brother, Mark, my parents Bruce and Antoinette, and my wonderful fiancé, Kristan Petroski. Without your love and support, I would not be here today. I dedicate this thesis to all of you.

Table Of Contents

Figure List

Chapter 1: Introduction

Since the beginnings of aeronautics, it has been necessary to measure the properties of a flowing fluid, such as air. Only by measuring these properties can calculations and models for the fluid flow be developed and improved. There are two main classifications for these measurements: intrusive and non-intrusive.

As the name implies, an intrusive measurement involves placing something in the flow, such as a pitot probe, a hot wire probe, or a pressure or temperature probe, to measure the flow. This of course disturbs the flow downstream of the intrusion, and can also produce disturbances upstream, such as a bow shock in front of a pitot probe in high-speed flows.

Perhaps the simplest way of measuring the velocity of a flow is with the use of a pitot or pitot-static tube. This probe can be connected to a manometer in order to measure the pressure difference between the stagnation and static pressure taps, although the response time for this method is very slow and typically only used in constant velocity flows. A pitot-static tube can also be connected to a pressure scanner, which can provide much higher scan rates of the pressure, which is useful in flows where the velocity changes.

Another intrusive method of measuring flow is with the use of a constant temperature hot-wire anemometer. In this method, a very thin wire of an electrically conductive metal is placed in the flow. An electrical current is then passed through this wire, which acts as a resistor in a Wheatstone bridge. A feedback amplifier is used to sense cooling of the wire by the flow, thus changing its resistance and causing an imbalance in the Wheatstone bridge. This imbalance is corrected by increasing the voltage applied to the bridge. The higher voltage reheats the wire so that its resistance and temperature remain a constant. Velocity calculations can then be made from the additional voltage applied to the wire. This method of measurement tends to be very responsive to changes in the flow, and can be used to measure turbulence levels in the flow. However, as stated earlier, this is an intrusive measurement, and care must be taken not to break the wire, as it is very fragile, and can be expensive to repair or replace. Additionally, a hot wire can not tell if the flow is moving in a positive or negative direction relative to itself.

An established non-intrusive measurement technique is laser Doppler anemometry, or LDA, or more properly, laser velocimetry (LV). In this measurement technique, two laser beams are focused to intersect at a point within the flow. A seeding material is also introduced into the flow upstream of the measurement area. The seed material has limitations of its own, as the particles must be small enough to accurately follow the flow. The light scattered from these seed particles is then measured. For conventional fringe LV systems, this scattered light displays a periodic variation of high to low intensity, which is due to the particles passing through the interference fringes in the probe volume. Velocity is obtained from the frequency of this oscillating light intensity. Unlike hot wire anemometry, LV can determine if the flow is positive or negative along an axis by means of a Bragg cell. A Bragg cell is an acousto-optical cell which is used to "add" a frequency shift as a known offset so that both positive and negative velocity directions are seen as positive shifts. Because of this, LV can be used in reversing flows.

The focus of this research was the refinement of a point Doppler velocimetry (PDV) system, which is also a non-intrusive, laser-based velocity measurement system. In a PDV system, a laser beam is passed through a seeded flow, which scatters the laser light. The scattered laser light is then collected from a point in the flow, and directed at a beam splitter. Part of the light is focused on a photodetector, while the rest is passed through a cell filled with iodine vapor, and then is collected by a different photodetector. The iodine vapor absorbs some of the scattered laser light, where the amount of light absorbed varies as the frequency of the scattered light varies (Figure 1.1). By comparing the light intensities of the two photodetectors, the Doppler shift, and thus flow velocity, can be determined. The basic Doppler velocity equation is

$$\Delta f = \frac{f_o}{c}(\hat{a} - \hat{l}) \cdot \vec{V} \qquad \text{Eq. 1.1}$$

where Δf is the Doppler frequency shift, f_o is the laser frequency, c is the speed of light, $\hat{a}$ is a unit vector between the flow and the receiving optics, $\hat{\mathrm{l}}$ is a unit vector along the laser propagation direction, and $\vec{\mathrm{V}}$ is the particle velocity vector. From this equation and Figure 1.1, it can be seen that Δf is proportional to the component of $\vec{\mathrm{V}}$ along the $\hat{a} - \hat{l}$ direction.

While LV and PDV may seem similar, there are many differences. For one, PDV is a simpler setup because only one laser beam is used, instead of two laser beams which much be aligned to intersect in the portion of the flow where the measurements are to be made. Also, LV requires low seeding levels, whereas PDV requires higher seeding levels, which reduces laser speckle, as well as producing a more continuous signal.

The goals of this project were to determine the accuracy of the PDV technique for turbulence measurements, and to determine how close to a “wall”, in this case an airfoil surface, measurements could be made.

Chapter 2: Previous Work in Absorption Cell Doppler Velocimetry

The summary below reviews both point Doppler velocimetry (PDV) and Doppler global velocimetry (DGV) papers. They are organized by institution when a significant number of papers have been published by researchers at that institution. Other papers are included at the end of this chapter.

2.1 Initial Work

Almost every PDV and DGV researcher uses iodine vapor confined in an optical cell as an absorption line filter to measure the Doppler shift of light scattered from a seeded flow. A study of the absorption spectrum of iodine was presented in Tellinghuisen (1982).

A patent on the basic PDV/DGV concept was obtained by Komine (1990). This patent covers a velocity measurement system using a laser light sheet to illuminate a flow seeded with small particles. An optical system and frequency-to-intensity converter are then used to measure the Doppler shift of the scattered laser light. The flow images can then be viewed directly, or processed with a computer.

2.2 NASA Langley and NASA Ames Research Centers

A large amount of work in DGV has been carried out at NASA Langley, most of it with the involvement of Mr. James F. Meyers. In Meyers and Komine (1991), a one-component DGV system is described. A description is also given of measurements on a rotating wheel and a small jet flow in a laboratory, as well as the vortical velocity field above a delta wing.

In Meyers, et al. (1991), two signal processing schemes for DGV are presented. One is a real-time analog method using a monochromatic frame grabber and producing a standard NTSC video signal. The other is a digital approach that uses the full resolution of the acquisition cameras, and allows for greater image correction options in post-processing. Results for each method over a delta wing in a wind tunnel are also presented. The greater capabilities of the digital processing scheme made it superior to the analog processing scheme. Meyers (1992) compares the results of the previous two papers with results obtained with a three component laser velocimeter.

This system was later expanded to three components and tested on the jet flow from a High Speed Civil Transport (HSCT) engine model (Meyers, 1995). At this stage in its development, the NASA Langley three component DGV system had a spatial resolution of 1.25 mm, and stated velocity uncertainties of approximately ±2 m/sec independent of mean velocity. Meyers (1996) described how to correct for errors due to optical distortions, electronic noise, and camera misalignment. Meyers, et al. (1991) and Meyers (1996) have made significant contributions to identifying error sources, as well as developing image processing techniques to reduce these errors.

A description of the problems encountered in hardening the NASA Langley three component DGV system for wind tunnel applications can be found in Meyers, et al. (1998). This hardening involved switching from an argon-ion laser to a pulsed Nd:YAG laser. One problem caused by this change in setup was that the software written to remove laser speckle could not adequately handle the speckle caused by the Nd:YAG laser. Other problems were also encountered in maintaining a stable, single frequency laser output due to the extreme temperature fluctuations within the wind tunnel.

Also at NASA Langley, Michael W. Smith has developed and tested a single channel DGV system utilizing a pulsed Nd:YAG laser. In Smith and Northam (1995), only a single camera and lens were used to make measurements due to the presence of an image splitter/recombiner system. Measurements were made on a pressure-matched sonic jet, as well as an overexpanded supersonic jet with a design Mach number of 1.9. These experiments were able to detect the average shock diamond structure and shear layer growth. Noise due to speckle was found to be the largest source of error in the experiments. These results are again presented, and compared against computational fluid dynamics (CFD) solutions in Smith, et al. (1996).

The above system was also utilized to study a high Reynolds number compressible jet in the Small Anechoic Jet Facility (SAJF) at NASA Langley (Smith, 1998). The conditions for these experiments were a Mach number of 0.85 at ambient pressure, which yielded a Reynolds number of approximately 650,000 based on diameter. Because laser speckle had been such an issue in the previous experiments, system components were selected in order to minimize speckle noise. Also, velocity errors due to laser drift were reduced by the use of a laser frequency monitoring leg. Mean and RMS velocity images were presented, as well as instantaneous velocity images for various flow seeding conditions.

Additional DGV research has been conducted at NASA Ames under R. McKenzie, mainly into low-speed flows. As with Smith, McKenzie utilizes a pulsed Nd:YAG laser, as well as a split image system. In McKenzie (1995), the limitations on the DGV system due to the CCD cameras were evaluated, and an analysis of the scattering properties of different aerosols was given. Measurements were made on a rotating wheel with a surface speed between 5 and 56 m/sec. For all speeds above 10 m/sec, an RMS error of ±2.5 m/sec was observed. The results also predict that errors as low as 2 m/sec should be obtainable in flows with velocities up to at least 20 m/sec.

In McKenzie (Jan. 1997), this research is continued by developing an uncertainty model based on laser light scattering, radiometric noise, and uncertainties introduced by the image processing. Additionally, measurements made in a low-speed, turbulent flow are compared against measurements made with an impact pressure probe, with good agreement. These methods can also be applied to large-scale wind tunnels, as described in McKenzie (Sep. 1997).

2.3 Ohio State University

Much DGV research has been carried out at Ohio State University. Investigation of compressible mixing layers has been carried out, as described in Elliot, et al. (1992). As with most other DGV researchers, a pulsed Nd:YAG laser was used. Two cases were studied, a lower compressibility case (Mach = 0.51), and a higher compressibility case, (Mach = 0.86). For the lower Mach number, roller-type spanwise structures were observed, as well as streamwise streaks. The structures observed at the higher Mach numbers were "more three dimensional and oblique" (Elliot, et al., 1992, pg. 2569). In later experiments (Elliot, et al., 1994), pressure broadening was used to optimize the absorption profile of a filter for the experimental flowfield and optical arrangement. This research also showed that when significant background light was present, a second filter could be added to the system in order to exclude this extraneous signal from reaching the signal camera. An error analysis was also performed on the results which showed that the error for the current measurements was approximately ±8% of full scale.

Improvements were later made to this DGV configuration (Clancy, et al, 1996). These improvements included using a split image system and laser frequency monitoring, with good results. Experiments were then made in an ideally expanded Mach 2 axisymmetric jet, and compared against Laser Doppler Velocimetry (LDV) measurements. The results agreed fairly well, but demonstrated that the DGV system required further refinements. Clancy and Samimy (1997) documented the procedures used to obtain quality data in the flow described above, as well as demonstrated the importance of the calibration of the splitter/recombiner system. This paper also presented RMS uncertainty results of approximately ±25 m/sec, and a mean velocity component that is within 6% of the velocity of the jet core.

This research was then expanded from two-dimensional to three-dimensional measurements in the same Mach 2 flow (Clancy, et al, 1998). Both the instantaneous and mean velocity measurements agreed well with LDV measurements made in the same flow. Improvements to the splitter/recombiner system and methods to remove laser speckle noise were also described. An overview of various DGV techniques, with an emphasis on high speed flows, were summarized in Samimy (1998). This paper included the results of the previous Ohio State experiments as well as results for a supersonic jet.

2.4 Princeton University

The focus of the research at Princeton University has been on Filtered Rayleigh Scattering (FRS). In Miles, et al. (1991), measurements were made on nitrogen molecules and other particles in a Mach 2.5 flow. The measured flow velocity was accurate to within ±20%. A theoretical analysis was also performed which indicated that measurements with an accuracy of better than 1% were possible. In Forkey, et al. (1995) and Forkey, et al. (1996), a theoretical FRS model including model parameters and uncertainties was described. Experimental velocity results for both ambient air and a Mach 2 free jet were presented, as well as preliminary results for temperature and pressure data. The errors in the experimental velocity results were greater than the ±4 m/sec and ±5 m/sec predicted in the theoretical model, at about 20 m/sec. This was blamed on a laser frequency "chirp" across the laser beam, which has not been observed by other researchers.

Lempert, et al. (1997) describes measurements made in the turbulent boundary layer over a zero pressure gradient flat plate in a Mach 8 flow. Additionally, a framing CCD camera was paired with a Titanium:Sapphire pulsed laser in order to capture "movies" of a turbulent Mach 2.5 flow over a 14° wedge. This system allowed the acquisition of FRS images at rates up to one MHz.

2.5 West Virginia University

At West Virginia University, Doppler Velocimetry work was begun with Ramanath, 1997. This research consisted mainly of the development of a three-dimensional linear positioning system for the flows to be measured. This was done because the complexity of this system was less than that of developing a system to move the measurement DGV or PDV optical systems. A continuous-wave (cw) argon-ion laser was used to illuminate the flow, and four photodetectors were used to measure the scattered light. Preliminary PDV data was also obtained, although these experiments produced inaccurate results, due to an inadequate method of calibration of the iodine cells.

This research was continued by James (1997). In this work, measurements were made both of a rotating wheel, and of a flow exiting from a 3.81 cm (1.5") diameter copper pipe. The calibration method was improved for these experiments by acquiring multiple calibration curves, and then "sliding" them along the frequency axis so that the curves overlaid one another. These curves were subsequently averaged, and then curve-fit, to obtain a more accurate calibration curve. For the rotating wheel, sensitivity errors of less than ±2% were obtained, and the linearity of the data was approximately ±0.6 m/sec, or about 1% of full scale. Data for the pipe was obtained at the pipe exit, as well as 7.62 cm (3") and 15.24 cm (6") downstream of the pipe exit. The mean velocity profiles observed showed good shape agreement with pitot static probe measurements. Additionally, turbulence quantities were calculated and compared against hot wire measurements, also with good agreement. The above two papers are also summarized in Kuhlman, et al. (1997).

A later effort was made at developing, and accuracy studies of, a two-component DGV system (Naylor and Kuhlman, 1998). This system used a cw argon-ion laser, iodine vapor cells acting as discriminating filters, and a frame grabber in conjunction with four 8-bit CCD cameras for image acquisition. Initial measurements were made on the surface of a rotating wheel. RMS noise levels on the order of ±1 m/sec were observed, as well as velocity range errors of ±1-2 m/sec. However, a zero velocity offset as large as -20 m/sec of unknown source was also seen. Similar zero velocity offset errors had been observed by James (1997).

Results obtained with the above DGV system for a rotating wheel, a fully-developed pipe flow, and a free jet were presented in Naylor (1998) and Naylor and Kuhlman (1999). A reference tab was placed in the field of view of the cameras for the pipe and jet measurements in order to provide a zero velocity signal in an attempt to eliminate the zero velocity offset. The results of the wheel measurements were the same as those given in the previous paper. For the pipe and jet flows, the DGV data agreed with pitot-static probe measurements to within about 2-4 m/sec.

PDV measurements over the surface of an NACA 0012 airfoil have also been made, as described in a preliminary version of this thesis (Kuhlman and Webb, 1999). These measurements were made both along the chord of the airfoil, as well as at a fixed chord position and varying distances from the airfoil surface. These measurements are also compared against single component hot wire data obtained at similar locations. The time series of the streamwise velocities for these two measurement techniques appeared similar. The mean and RMS velocities agreed to within approximately ±3 m/sec and ±0.5 m/sec, respectively.

2.6 Other Work

In Komine, et al. (1991), two different DGV methods are described. One uses a cw laser, and images of the flow are captured over an entire camera frame, typically 1/30th of a second. Because of this relatively long time frame, this method is only applicable to flows which have small variations over a given time frame. The second DGV method uses a pulsed laser with a pulse length of 1 μs to effectively take a "snapshot" of the flow. Thus, this method can be applied to rapidly changing flows. Results were also presented for measurements on a free-expansion jet at near sonic velocities for both DGV methods. For the cw laser, the results for the streamwise and spanwise velocities were consistent with expected velocities. However, instead of zero radial velocities, velocities of ±50 m/sec were also observed. It was speculated this was due to a rotary motion about the jet axis. The pulsed laser data did not display the relatively smooth velocity variations across the flow that was observed with the cw laser. It was theorized that the flow was somewhat irregular, as the pulsed laser data showed, while the cw laser presented time averaged data about the flow. This system was later expanded to three components, and used to demonstrate the ability of the system to make instantaneous velocity measurements in unsteady flows.

Elliot, et al. (1997) have made measurements on both circular and elliptical sonic jets injected transversely into a near Mach 2 flow. As with most other researchers, a pulsed Nd:YAG laser was used. Measurements were made of the streamwise velocities and turbulence intensities both upstream and downstream of the jet injections. The researchers were able to "see" the separation shock, bow shock, and the mixing layer of the jet. The shear layer of the elliptical jet displayed a faster spanwise spreading, while a greater turbulence intensity was also observed. The elliptical jet also did not penetrate the main flow as deeply as the circular jet.

Beutner, et al. (1998) describes measurements made on a flow typically produced by vortex-tail interactions, such as those observed on twin-tail fighter aircraft. These experiments were carried out using a pulsed Nd:YAG laser and two 16-bit CCD cameras with a resolution of 512 X 512 pixels and a shutter speed of 60 ms. Tests were conducted on a delta wing model with and without tails at 23° angle of attack in a Mach 0.2 flow, and many details of the flow were clearly visible. A discussion of the difficulties encountered in using DGV in large-scale wind tunnels is also presented. A later paper (Beutner, et al., 1999) presents results for a rotating wheel, an empty wind tunnel, and a wing model in this wind tunnel. Additionally, system accuracy and example DGV applications are discussed.

An early PDV system is described by Hoffenberg and Sullivan (1993). This experiment used a cw argon-ion laser, whose beam was focused down to a diameter of 0.25 mm by a lens of focal length 300 mm. An iodine cell was used as a filter to measure the Doppler shift of the experimental flow. The researchers found that velocity and turbulence measurements could be made at a point, and that the results showed good agreement with LDV data. Errors due to laser frequency drift, detector alignment, probe volume, and particle concentrations were also discussed.

A variation on the typical PDV setup was described by Crafton, et al., (1998). In this setup, a Distributed Brag Reflector (DBR) diode laser was paired with a Cesium vapor Faraday cell. This Cesium cell holds the promise of a finer resolution than that which is possible with Iodine cells, which in turn could make them more applicable to low-speed flows. Measurements were made on a disk spinning between 0 and 11 m/sec, with the results showing an RMS of less than 0.05 m/sec. Results were also presented for a 1.27 cm (1/2") jet with a velocity of 6.9 m/sec. The PDV system gave results of 7.4 m/sec, a difference of 0.5 m/sec, or about 8%.

Reeder (1996) describes DGV measurements of streamwise and lateral velocities in a supersonic jet. This system utilized a pulsed Nd:YAG laser and an image combiner system so that only one CCD camera was required. Measurements were made in a Mach 1.14 jet, and good agreement was shown when the DGV data was compared with particle imaging velocimetry (PIV) and pitot probe data.

Morrison, et al., (1994) describes the inaccuracies encountered when measurements were made using a one dimensional DGV system. These inaccuracies resulted from the performance of individual DGV components, including the video cameras, the transfer lens, the beam splitter, the iodine cell construction and charging, and the video capture boards. Individual descriptions of the problems, along with their corrections, were also discussed.

A DGV system has been developed by Chan, et al., (1995). This system used a cw argon-ion laser and a single CCD camera for both the signal and reference signals. Measurements were made on a spinning disk with a rim velocity of approximately 120 m/sec as measured by an optical tachometer. The techniques used in the image processing are also discussed.

Ford and Tatum (1995) developed a system which made use of a cw argon-ion laser which was frequency stabilized. The CCD cameras employed had a resolution of 560 X 450 and a frame rate of 25 Hz. Measurements were then made on a spinning disk with a diameter of 15 cm. The plane of the disk was offset from the illumination direction by 15°. The measurements of disk velocity were in good agreement with velocity measurements made by other techniques. It was also found that significant errors began to occur at points that were more than approximately 5° from the center of the field of view. Significant errors were also observed for divergence angles of the illumination beam that were greater than 10° at a distance of 5 cm from the beam axis.

DGV research has also been conducted at Oxford on transonic turbo-machinery flows (Ainsworth and Thorpe, 1994). As with several other researchers, Ainsworth and Thorpe utilized a single CCD camera to acquire both signal and reference images. A cw argon-ion laser was also used to image the flow. Measurements were made on a rotating disk with a tip speed of approximately 90 m/sec. The errors observed were much higher than would be acceptable in measuring a flow, mostly due to the use of a 6-bit frame grabber in these experiments. Error analyses for the frame grabber and Gaussian beam profile were also presented. This research was later continued on an axisymmetric free-jet air flow (Thorpe, et al., 1996). The DGV results showed excellent agreement with published results for the flow. An error analysis was also included, which showed errors to be on the order of ±4 m/sec. Ainsworth, et al. (1997) also presented an overview of different approaches to DGV research, as well as reiterated results from the papers listed above.

In Germany, Roehle and Schodl (1994) developed a one component PDV system and made measurements on a free jet in order to determine the accuracy of such a PDV system. A frequency stabilized argon-ion laser was used, as well as photodiodes to detect the light scattered from the flow. The speed of the flow was varied from 40 m/sec to

130 m/sec. The PDV data was compared against Laser-2-Focus data, with an uncertainty of less than ±3 m/sec.

Roehle later developed a three component DGV system, as described in Roehle (1996). This system utilized the frequency stabilized argon-ion laser, as well as two CCD cameras for image acquisition. Long-time records with low levels of seeding smoke were obtained for the flow field of a swirl spray nozzle in a cylindrical casing, and in the wake of a car model in a wind tunnel. The results of these experiments were in good agreement with laser velocimetry (LV) measurements. The DGV data acquisition was also faster than the LV data acquisition by several orders of magnitude.

2.7 Summary

Many researchers have contributed to the development of PDV/DGV. While there are similarities between most of the research, such as the use of pulsed Nd:YAG lasers by the majority of workers, there are also some original ideas being applied, such as using a Cesium vapor Faraday cells or Mercury vapor cells instead of iodine cells as frequency discriminators. Many advances and refinements have been made since Komine obtained his patent for the basic DGV concept in 1990. In that time, several of the researchers listed above have documented results with errors of about 4 to 5 % of full scale. Work is continuing to improve upon this level of accuracy.

Chapter 3: Apparatus And Configuration

3.1 Laboratory Configuration

A schematic of the laboratory setup as viewed from above can be found in Figure 3.1. Instead of attempting to develop a method of moving the laser and the sensing optics, and keeping them in the same plane, it was decided to keep the above components stationary, and instead develop a method of moving the flow facility. The result was a stepper-motor driven traverse which could be moved anywhere within a volume measuring 0.61 m by 0.46 m in the horizontal plane, by 0.305 m in the vertical plane (2' by 1.5' by 1'). For a typical move of a few inches, the accuracy of this system was found to be better than 25.4 μm (0.001"). A full description of this system has been given in Ramanath (1997).

A rectangular flow channel was then mounted on top of this traverse. This flow channel was constructed from Plexiglas, and measured 8.41 cm wide by 10.16 cm tall by 127 cm long (3 5/16" by 4" by 50"). Additionally, at the exit, two wooden pieces were attached to the roof and floor of the channel in order to form a two-dimensional nozzle with dimensions 8.255 cm (3 ¼") wide by 5.3975 cm (2 1/8") tall. The nozzle block contours were formed from two tangent, reverse curvature cubic curves to form S-shaped profiles. The flow for this channel was supplied by a Dayton model 4C108 blower. The blower was powered by a Dayton 5K901C motor. This was a one horsepower motor which turned at 3450 rpm. It was necessary to provide some flow resistance because the motor was not powerful enough for the blower without a load. Otherwise, the motor would overheat and shut down. This resistance was accomplished by placing grids of drinking straws both in the exit of the blower, as well as in the flow channel approximately 0.762 m (30") downstream of the blower exit. Additionally, whenever the blower was run, a control device was placed over the blower inlet to help limit the flowrate, and thus the velocity, of the flow, as well as to keep the motor from overheating.

3.2 Velocity Measurement Apparatus

3.2.1 Laser

The laser used in these experiments was a Coherent Innova Model 305. This was a 5 watt, continuous wave, argon-ion laser operating in single line mode at a wavelength of 514.5 nm, which corresponds to the color green in the visible spectrum. In order to achieve this single line mode, it was necessary to insert a heated, tilted etalon into the laser cavity. An etalon is a cylindrical piece of fused silica which, when inserted into the laser cavity, allows only a narrow wavelength range of light to be transmitted through itself. Typically, due to mode competition, the strongest mode of the laser cavity that lies within the frequency range where the laser gain exceeds the etalon loss will be the only mode permitted. This etalon also had the effect of lowering the power output of the laser, from the maximum of 5 watts, to approximately 1.5 watts.

3.2.2 Iodine Cells

The iodine cells used in these experiments were made by Opthos Instruments, Inc. They measured 6.35 cm (2.5") in length, 5.08 cm (2") in diameter, and had an internal optical path length of 5.08 m (2"). The ends of the cells were optically flat crown glass coated with an anti-reflective material. These ends were fused to the body of the cell by direct contact.

During construction, the cells were carefully evacuated, and a few iodine crystals were then placed inside. The glass stem by which both of these processes occur was then melted shut. Because of the low pressure, some of the iodine crystals undergo sublimation, which fills the cell with iodine vapor. When the temperature of the cell stem is varied while maintaining the body at a constant, but hotter, temperature, the amount of iodine vapor in the cell also varies. In order to maintain the cell bodies at a constant temperature, a copper sleeve was fitted around each cell. The copper sleeves were heated by band heaters, which were controlled by Omega model CN9000A temperature controllers. These temperature controllers were able to maintain a constant stem temperature to within an RMS fluctuation of ±0.1 °C.

3.2.3 Laser Frequency Monitoring System

When the laser beam exits the aperture of the laser, it is split into two beams by a piece of Pyrex glass. The main beam continues on to be passed through the flow, while the other beam is sent into the laser frequency monitoring system, which is used to monitor laser frequency drift (Figure 3.2).

The laser frequency monitoring system is totally enclosed within a wooden box in order to prevent stray light from interfering with the measurements. When the secondary laser beam enters the box through a hole drilled in the side, it is again split in two by Pyrex glass. One beam is then sent to a laser spectrum analyzer, while the other beam continues on to the signal and reference legs of the laser frequency monitoring system.

The spectrum analyzer is a Burleigh Instruments model number SA-200 Plus, which is connected to a Burleigh Instruments DA-100 detector amplifier. The second beam then passes through a neutral density filter, and then a pinhole. The pinhole is used to pick out only one beam, as some secondary beams are introduced as a result of passing through the Pyrex glass. A 5.08 cm (2") diameter dielectric beamsplitter is then used so that the beam can be sent down both legs of the laser frequency monitoring system.

The laser beam that passes straight through the beamsplitter is sent down the reference leg of the laser frequency monitoring system. It first hits a mirror, so that the beam can be deflected 90°. The beam then passes through a lens, which focuses the beam down to a point on the reference leg photodetector. The photodetectors used are described in a separate section below.

The laser beam that is deflected by the beamsplitter is sent down the signal leg of the laser frequency monitoring system. It first passes through a 10:1 beam expander in an effort to prevent local iodine vapor absorption saturation due to the laser light which is passing though the iodine cell. The beam expander is a CVI Instruments cw beam expander which has variable ratios from 4.5:1 up to 10:1. This beam expander is rated for wavelengths between 488 and 515 nm, and was factory-set to 515 nm. Once the beam exits the beam expander, it passes through the iodine cell for the laser frequency monitoring system. It then encounters a 5.08 m (2") diameter lens, which focuses it down to a point on the signal leg photodetector. The laser and the laser frequency monitoring system are mounted on a 0.5842 m by 1.1938 m (23" by 47") optical breadboard from Aerotech, model 91012. The entire optical breadboard has been mounted on a box filled with sand to dampen vibrations, and small inner tubes to allow for leveling of the breadboard.

In order to provide a safe working environment, a laser shutter was mounted in front of the emission aperture of the laser. This shutter was connected to an interlock, as well as a magnetic proximity switch mounted on the door to the lab.

3.2.4 PDV Velocity Measurement System

In order to measure flow velocity, two PDV components were used in order to ensure accurate measurements of the flow in two dimensions. These two components were functionally the same, although one component was the mirror image of the other when viewed from the front of the components. Because of this, only the geometry of one of the components will be described below. Additionally, a diagram of a component can be found as Figure 3.3.

To begin with, two Melles Griot rails were mounted on a Thor Labs optical breadboard measuring 0.46 m (18 1/8") by 0.765 m (30 1/8"). All of the components, with the exception of the heating controller for the iodine cells, were mounted on these rails. These rails were marked from 0 to 700 mm in 1 mm increments for precise placement of the optical components. The breadboard and all the mounted components were also enclosed in order to reduce the amount of stray light.

To enter the component, the scattered light first passes through a hole in the enclosure which is cut to be slightly larger than the first 5.08 cm (2") diameter lens that the light will pass through. This lens focuses the light down to a point, and a pinhole is placed at the focal point of the lens in order to only collect scattered light from a single point in the flow. Once the light passes through the pinhole, it expands until it reaches a diameter which is slightly less than 5.08 cm (2"). This is important because the diameter of both the next lens and the iodine cell is 5.08 cm (2"). At this point, the light passes through another lens which restores the beam to a constant diameter. The beam then strikes a beamsplitter in a gimbaled mount. The beamsplitter is a 10,16 cm (4") diameter dielectric model 68.0475 from Rolyn Optics, with a transmission/reflection ratio of 55/45. The mount is a Newport series 605-4. The light which passes through the beamsplitter is passed into the signal leg of the component, while the reflected light is passed to the reference leg. In order to ensure accuracy, both the signal and reference legs have been adjusted so that they have the same optical path length.

In the reference leg, once the light is reflected from the beamsplitter, it strikes a mirror in a gimbaled mount. The mirror is a Newport 10.16 cm (4") diameter mirror, part number 40D10BD.1. It is anti-reflective coated, and rated for 1 kW/cm^2. The mount is from Aerotech, Inc., and is model number A0M110-4. The light then passes through a lens, which focuses the beam down to a point on the reference leg photodetector.

In the signal leg, once the light is passed through the beamsplitter, it passes through the iodine cell. The light then passes through a lens, which focuses the beam down to a point on the signal leg photodetector.

The optic posts, rail mounts, and other positioning equipment were a mix from Thor Labs, Melles Griot, and Creative Star.

3.2.5 Photodetectors

The photodetectors used in the laser frequency monitoring system were model number PDA150 fixed gain amplified silicon detectors from Thor Labs. These photodetectors have a spectral response from 320 to 1100 nm, and a rise time of 7 ns. They operate from a 12 V DC power supply. Their voltage output is between 0 and 1.5 V, and they have a BNC connector for signal output. The active area of the detector is 1.5 mm^2. The spectral sensitivity in amps per watt (A/W) reaches a maximum of 0.6 between wavelengths of approximately 900 and 925 nm. At the wavelength used in this experiment (514.5 nm), the sensitivity was approximately 0.3 A/W. These photodetectors have lower noise levels than the PDA50's in the two sensing components, as well as a lower gain. This lower gain did not present a problem due to the stronger light signal in the laser frequency monitoring system. Because there was a need for variable gains in the two sensing components, these PDA150's could not be used, despite their advantages over the PDA50's.

The photodetectors used in the two sensing components were model number PDA50 variable gain amplified silicon detectors from Thor Labs, and have a spectral response from 320 to 1100 nm. They have a rise time of $\leq$ 35 ns, and operate from a 12 V DC power supply. Their voltage output is between 0 and 3.5 V, and they have a BNC connector for signal output. The active area of the detector is 13.7 mm^2. The spectral sensitivity in amps per watt (A/W) reaches a maximum of 0.6 at a wavelength of approximately 850 nm. At the wavelength used in this experiment (514.5 nm), the sensitivity was approximately 0.32 A/W. These photodetectors were chosen for use partly because they had a variable gain which was higher than that of the PDA150. The gain can be adjusted by a 12-turn potentiometer.

During the course of experimentation, it was suspected that one of the photodetectors in component 2 (streamwise direction) was no longer functioning properly. Because of this, the two PDA50's were replaced with Thor Labs PDA55s, which have 5 discrete gain settings. They have a spectral response from 320 to 1100 nm, and operate from a 120 V AC power supply. They have a DC bandwidth to 10 MHz for the detector, but for the amplifier setting at which data was acquired, the DC bandwidth was limited to 60 kHz. Their voltage output is between 0 and 5 V, and they have a BNC connector for signal output. The active area of the detector is 12.96 mm^2. The spectral sensitivity in amps per watt (A/W) reaches a maximum of 0.625 at a wavelength of approximately 900 nm. At the wavelength used in this experiment (514.5nm), the sensitivity was approximately 0.3 A/W.

3.2.6 Smoke Injection

In order to make measurements of the flow, it was seeded with theatrical fog. A Rosco 1500 fog machine was used, along with Rosco fog fluid. After the fluid was vaporized to fog in the fog machine, it was pumped into a plenum. This was done in order to maintain a more constant smoke flow to the flow facility. From the plenum, the fog was drawn into the intake of the Dayton blower described above, which then propelled it through the flow facility. After passing through the PDV measurement area, the flow entered an exhaust cone (Figure 3.1). This cone could only exhaust a limited amount of smoke, which limited the range of velocity measurements which could be made.

An attempt was also made to improve the quality of the data by introducing a coflow into the shear layers of the flow. The smoke for this coflow was produced by a Ness ULF-700 theatrical fog machine. The fog from this machine was injected directly into a plenum. The fog from the plenum was then drawn into a box designed to only release smoke into the upper and lower shear layers of the flow.

3.2.7 Hot Wire and Pitot Probe

In order to determine the flow velocity from the rectangular channel using an established velocity measurement technique, a 0.3175 cm (1/8") diameter pitot static probe from United Sensor was used. This probe was connected to an ESP32 pressure transducer via a Star 2000 interface. Both the transducer and interface were manufactured by Pressure Systems, Inc. The pressure transducer had a range of ±18.68 mm Hg (±10" water gage).

Various other measurements were made using a hot wire. This hot wire was a 1-axis probe, type 55P04 manufactured by Dantec. This probe was connected to an IFA 300 constant temperature anemometer from TSI Incorporated.

3.3 Computer Related Equipment

3.3.1 Computers

The main data acquisition computer was an IBM compatible PC running Microsoft Windows 95 OSR2. This computer used an Intel Pentium® microprocessor running at 200 MHz, and contained 64 megabytes of RAM. It also had three hard drives, with a total capacity of 13 gigabytes. This space was needed because once some of the datasets were reduced, the total hard drive space required was over 600 megabytes. This computer was the one connected to the IOtech A/D board described below. During the course of the research, this computer was upgraded to an Intel Pentium® microprocessor running at 400 MHz. The main effect of this upgrade was that the time required for data reduction was reduced from approximately two hours to one hour.

The other computer, which was used to run the traverse, was an IBM compatible PC running Microsoft Windows 95. This computer used an Intel-compatible microprocessor running at 80 MHz, and contained 8 megabytes of RAM.

3.3.2 A/D Boards

The main A/D board was an external IOtech model ADC488/8SA. This board used the IEEE 488 interface to communicate with the PC, as well as to send digitized voltage values to the data acquisition PC at rates up to 100 kHz. It was a 16-bit, variable gain board, and had 8 differential input channels with simultaneous sample-and-hold capabilities. These input voltages were converted in sequential order at intervals of 10 μs, and were then either stored in the memory buffer, or transmitted via the IEEE bus to PC memory. Six input channels were used in these experiments, one for each photodetector in each component. In this configuration, the maximum sampling rate for data acquisition was 10 kHz.

The other A/D board was a National Instruments AT-GPIB/TNT that was located inside the data acquisition PC. This board was also 16-bit and variable gain, but the maximum sampling rate over the 8 channels was 20 kHz. It was not a simultaneous sampling board. This board was used to collect temperature data from thermocouples mounted on the bodies and stems of the iodine cells. These temperature signals varied slowly, so high-speed data acquisition and precise matching of the sampling times were not necessary.

3.4 NACA 0012 Airfoil Model

The NACA 0012 airfoil model was designed to have a chord length of 0.3048 m (12") (a diagram of this geometry and commonly used airfoil definitions can be found as Figure 3.4.). The model design was begun by using Microsoft Excel to calculate discrete points using the following equation for NACA 4-digit series airfoils:

$$y = \frac{t}{0.2}\left(0.2969x^{0.5} - 0.126x - 0.3516x^2 + 0.2843x^3 - 0.1015x^4\right) \qquad \text{Eq. 3.1}$$

where y is the vertical distance from the airfoil chord, t is the maximum thickness of the airfoil, and x is the distance along the chord, all in fractions of chord length. These points were then imported into AutoCAD 14, and exported to an Initial Graphic Exchange Specification (IGES) file. This file was then taken to DeVall Brothers, Inc., a local machine shop. Once there, the file was used to program an N/C controlled milling machine to make a female airfoil template from 0.635 cm (¼") thick aluminum. This template was beveled in order to facilitate its use in the making of the actual model.

The airfoil template was then taken to General Woodworking Co., the company which actually made the wooden airfoil. A 0.9144 m (3') length of poplar was hand worked to a shape close to that of a NACA 0012 airfoil. The aluminum template was then drawn down over the length of poplar, producing a wing section. This section was then hand-sanded to remove any rough spots. Naturally, there were some imperfections in the wing section, so measurements were made to find a section that was closest to the desired shape. A 0.3048 m (12") span was then cut out to become the model. The actual chord length was measured to be 0.3 m (11.8125"). The contour of the airfoil was measured by mounting it in a milling machine which allowed for precise movements of the airfoil. A dial caliper was then used to measure coordinates on both surfaces of the airfoil. A comparison of the theoretical and actual airfoil profiles can be found in Figure 3.5.

In order to mount this airfoil in the flow, an aluminum frame was constructed which would attach to the traverse and position the airfoil at the exit of the flow channel. A picture of this frame with the airfoil mounted in it can be found as Figure 3.6. During the course of this research, it became apparent that the upper part of this frame was interfering with measurements over a streamwise distance of about 2.54 cm (1"). To solve this problem, the upper half of the frame was cut off. After this modification was made, the measurements of this frame were 0.2953 m by 0.3222 m by 0.1556 m (11 5/8" by 12 11/16" by 6 1/8"). It was designed with a pivot point 1.27 cm (0.5") from the leading edge. At the trailing edge, grooves were cut from the support frame, and the airfoil was mounted such that it could be moved through angles of attack of 0 to +10°. When attached to the traverse, the leading edge was 0.635 cm (¼") from the exit of the flow channel, and the shoulder was 9.684 cm (3 13/16") from the exit. Also, during the course of experimentation, the airfoil and frame were painted flat black in an effort to reduce the amount of light scattered from the airfoil surface.

Chapter 4: Data Acquisition and Post-Processing

In order to acquire and reduce the data for this research, custom software was developed using Microsoft Visual Basic 4.0 (32-bit) (Loew 1997). The initial version of this software has been described in James (1997). Since the time that thesis was written, numerous improvements have been incorporated into the software. These include:

- An error that reversed the X and Y component calibration curves in the data reduction software has been fixed.
- The sensitivities of each component originally had been calculated by taking the angles of each component, drawing a graph of the lab configuration, including the sensitivity angles, and then calculating the sensitivities from the graph. The sensitivities are now directly calculated from the angles, without the small errors that were induced by the conversions to and from the graph.
- The orthogonal velocities are now also calculated by dot product calculations. The equations for these calculations are:

$$U = \lambda_o \frac{\Delta f_1 S_2 - \Delta f_2 S_1}{C_1 S_2 - C_2 S_1} \qquad \text{Eq. 4.1}$$

$$V = \lambda_o \frac{\Delta f_1 C_2 - \Delta f_2 C_1}{C_2 S_1 - C_1 S_2} \qquad \text{Eq. 4.2}$$

where U is the spanwise velocity, and V is the streamwise velocity. λ_o is the laser wavelength used in this experiment, equal to 514.5 nm. Also, Δf_1 and Δf_2 are the frequency shift measured by components 1 and 2, respectively. The "constants", C_1, C_2, S_1, and S_2, are given by the equations

$C_1 = \cos\theta_1 + \cos\gamma_L \qquad S_1 = \sin\theta_1 + \sin\gamma_L$ Eq. 4.3

$C_2 = \cos\theta_2 + \cos\gamma_L \qquad S_2 = \sin\theta_2 + \sin\gamma_L$ Eq. 4.4

In the above equations, γ_L is the angle that the laser makes with the x-axis, θ_1 is the angle between the x-axis and the viewing direction of the first component, and θ_2 is the angle between the x-axis and the viewing direction of the second component. These equations were described in Naylor, 1998.

- Thresholding of the voltage levels was added to the Data Reduction program to eliminate data due to the extremes in the ratio normally caused by low smoke levels on the edges of the flow. These threshold values are user selectable, and can be changed for each data file. Normally, one set of values is used for all files from a given data run (data taken in one day.)
- All of the above programs have been through some minor cosmetic changes. In order to speed the data reduction progress, the ability to select multiple files and run them sequentially was added to each of the data reduction programs.
- Some of the data reduction process that was performed within Microsoft Excel was tedious, repetitive, and prone to user error. To reduce the errors, Excel macros were written wherever possible to automate the data reduction process. As with the data reduction programs, these macros give the user the ability to select multiple files, and run them sequentially. It is estimated that these Excel macros have reduced the time needed for data reduction by over 80%.

4.1 Overview

The laser, IOTech A/D board, and all other components were turned on at least 1 hour, and typically over 2 hours, before aligning the components. This time was required because some drift has been observed in both the laser and the IOTech board. This drift was significantly reduced in both after 2 hours. When the experiment was ready to begin, the fog machine(s) were turned on, and the overhead lights in the laboratory were turned off.

The next step was to align the two components so that they were both viewing the same location in the flow. In order to accomplish this, a triangle of velum attached to the traverse was placed in the horizontal center of the flow channel, nominally 10.16 cm (4") from the exit of the channel. Or, for the airfoil measurements, the velum triangle was placed at the shoulder of the airfoil, and in the horizontal center of the flow channel. The location of the traverse was then adjusted so that the tip of the velum triangle was placed approximately in the diametric center of the laser beam. The two PDV components were then adjusted so that they were both viewing the laser light scattered from the tip of the velum triangle. For each component, the adjustable pinholes were closed down to their smallest size, and then adjusted so that the light scattered from the velum triangle and focused by the initial lens was centered on the pinhole (Figure 3.3). This adjustment typically consisted of left/right and up/down movements, but occasionally the pinhole would also be moved along the optical path. The pinhole was then opened to a diameter of 1-3 mm. The iodine cells were then checked to make sure all of the light was still passing through them, and not striking the edges. Finally, the two photodetectors in each component were adjusted so that the light focused by the lenses directly in front of them fell only on the sensing area.

The velum triangle was then removed from the flow channel exit or airfoil shoulder. The blower was started, and the intake partially blocked so that the desired flow rate was achieved. Smoke injection was begun, and three to five minutes were allowed to pass so that the smoke level could reach steady state, as determined by relatively constant photodetector voltages. The computer monitors were then blocked from the view of the components. A dark voltage (the voltage output of the photodetectors when the laser beam is not allowed out into the laboratory) was then recorded. This dark voltage is then subtracted from each subsequent voltage measurement by the data acquisition software to compensate for photodetector noise and light not originating from the laser beam. The voltage levels from the photodetectors were then checked, and, if necessary, the smoke level, laser power, or photodetector gains were adjusted.

The laser wavelength was such that the ratio of the signal to the reference channels in the laser frequency monitoring system was typically between 0.4 and 0.6. Data was then taken under the conditions to be described in Chapter 5. The ratio had to periodically be reset since it would change as the laser drifted. This laser drift was caused by changes in the room temperature and/or changes in the temperature of the laser cooling water. A calibration run was then performed as described in Chapter 4.2 below. Data acquisition and calibration runs were then repeated as desired. The angles of the two components with respect to the laser propagation direction were then measured, and the data was reduced according to the procedure explained in the Data Processing section below.

4.2 Iodine Cell Calibration

For a calibration run, the laser beam was positioned in the vertical center of the flow channel, and the blower intake was blocked so that the flow rate through the channel was minimal. This was done so that the PDV component iodine cells could be calibrated *in situ* using scattered light from the same smoke particles used for velocity measurements. The calibrations were taken using the continuous mode hop technique developed in James (1997), and also described in Naylor (1998). Typically 6-10 different calibrations were obtained during a calibration run. Each calibration run was then reduced according to the calibration curve shifting procedure detailed below to produce a calibration curve for each iodine cell.

4.3 Data Reduction Procedure

The data reduction procedure can be broken up into two main procedures: obtaining the calibration curve, and data processing. Flowcharts to outline each of these procedures can be found as Figures 4.1 and 4.2, while the procedures will be described in detail below.

4.3.1 Obtaining the Calibration Curve

To begin the data reduction process, the program New Calibration was run. The purpose of this program was to find the mode hops for each component in the calibration files. When run, the first calibration file is read by the program. It then marks the lines where the mode hops occur. To do this, the voltage of the signal photodetector on the laser frequency monitoring system is used. The voltage at each time step is compared against the voltage at the previous time step. When the laser mode hops, this voltage increases. If the current voltage multiplied by a user-selectable value (typically 0.9 to 0.95) is greater than the previous voltage, that line is marked as a mode hop. Generally, an average calibration was used, which means that the program takes all the ratio values between any two mode hops, and averages them to provide a ratio at that mode hop. The ability to do left-edge and right-edge calibrations is also included in these programs. For these two types of calibrations, the first 5 points after a mode hop, or the last 5 points before a mode hop, respectively, are averaged. These two calibration methods did not work as well as the average calibration method (James, 1997), and have not been used in this research. The mode hop values are then written to an output file. If there are calibration files remaining, the above steps are repeated for each file.

Next, the Excel macro Trim Cal Files was run to eliminate extra points from the beginning and end of the calibration files. To do this, the calibration file is read into an array, and processing is begun from the end of the array. When the i-1 voltage is greater than the i voltage, the bottom of the absorption well has been found, and all points i and greater are deleted. The truncated calibration file is again read into an array, and the macro again begins processing at the end of the array. This time, if the i-1 voltage is less than the i voltage, the top of the well has been reached, and anything else is actually starting into another absorption well. All points before, and including, i-1 in the array are then deleted. The trimmed data for all three components are then plotted on a graph, and the shortened calibration file is saved. The above steps are then repeated for each calibration curve in the calibration run. Once all the curves have been processed, a new Excel workbook is created to hold all the reduced calibration files. These files are then copied into a single worksheet, and three graphs are plotted from it. Each graph shows all of the calibration curves for one of the components. This graph is then manually checked to make sure each of the calibration curves is acceptable, i.e. no double mode hops. This graph is also used to decide which curve to shift to, and which curves, if any, to exclude from the next data processing step.

The program Calibration Curve Combination was then run in order to “slide” the calibration curves on top of one another. To do this, the user first inputs the “fixed” calibration curve (the curve to shift to) as chosen above. This curve is used for the laser frequency monitoring system as well as the two sensing components. Each of the calibration curves to be shifted to this curve are then chosen. The user also selects the maximum and minimum voltage ratios to be used in the shifting, typically 0.8 and 0.2 for these experiments. The program then takes each calibration curve and “slides” it along the frequency axis in order to minimize the sum of the squares of deviations from the fixed calibration curve. The sum of the squares of deviations are calculated by linear interpolation. A new calibration file is then generated containing every point from the fixed calibration curve, as well as each of the other calibration curves. This file has three sets of data, one for each iodine cell.

Next, the Excel macro Plot Cal Curves is run to check that the calibration curves for each component are acceptable (sufficiently “smooth”). This macro simply takes the combined calibration curve and plots each component on a separate graph. If the curves are not acceptable, Calibration Curve Combination and Plot Cal Curves are run iteratively, varying the curve shifted to, and which curves are excluded, until the calibration curves are acceptable.

4.3.2 Data Processing

The work described above was performed simply to produce a calibration curve for each of the iodine cells. The main data reduction is done within the program Data Reduction. To begin, the viewing angles of the two viewing components are input so that the sensitivities of each component can be calculated. Next, the combined calibration file is read in. A Boltzmann fitting function is then used to fit a curve to the data. The equation for this function is

$$y = \frac{A_1 - A_2}{1 + e^{\left(\frac{x - x_0}{D_x} + A_2\right)}} \qquad \text{Eq. 4.5}$$

where A_1 and A_2 are the upper ratio bound and lower ratio bound, respectively, of the curve, x_0 is the frequency shifting factor, and D_x is the scaling factor. This fitting function was used because it closely approximates the shape of one side of an iodine absorption line. A more complete description of this function can be found in Naylor (1998). After the curve fitting is completed, the first of the data files is then read in. High and low threshold values for the voltages from each photodetector are then set by the user. These values can be changed for each data file, but generally the same values are used for every data file from a given day. Each voltage in the data file is checked against its respective threshold value. If it is within the acceptable voltage range, it is input into a new array to continue being processed. If it is outside of the acceptable range, it is skipped. A point that is skipped for any one of the components is also skipped for the other two components. The program then calculates a frequency for each data point using the Boltzmann curve fit described above, as well as a frequency shift between each point. This frequency shift is calculated by subtracting the frequency of the laser frequency monitoring system iodine cell, as computed from its curve fit, from the frequency of the individual component. From this, the velocities along each viewing direction are computed, as well as the orthogonal velocities. The mean and standard deviations are also calculated. Finally, the mean velocities and standard deviations are written to a velocity output file. The above steps are then repeated for each subsequent file.

In order to facilitate an easy understanding of the data, the Import Vel Data macro is run. This macro imports a velocity file, and plots the time traces of the velocities. Also 10-point running averages of the mean velocity and standard deviations are computed and plotted. These files are manually inspected to gauge the accuracy of the data.

In the last few months of experimentation, the quantity of data acquired on any given day made the manual inspection of each velocity data file all but impossible. To rectify this situation, the macro Summarize Stats was written. This macro took all the data files from a given data run, and created a spreadsheet with graphs of the streamwise and spanwise mean and RMS velocities. In this way, the statistics for each data file could be viewed easily, and if a more thorough analysis was required, the individual velocity data file could be inspected.

Chapter 5: Velocity Measurement Experiments

5.1 Rectangular Channel

Initial velocity measurement experiments were conducted on the rectangular channel described in Chapter 3.1. These traverses were performed without the NACA 0012 airfoil positioned in the flow. For these traverses, PDV data was recorded while moving continuously at a speed of 2.54 cm/sec (0.1"/sec). The sampling rate was 100 Hz, and the exit velocity was typically about 20 m/sec. This velocity was observed using the pitot-static probe described in Chapter 3.2.7. While the blower could maintain a higher maximum velocity, 20 m/sec was the maximum speed where the seeding smoke could still be exhausted from the laboratory.

To begin, several initial attempts were made at collecting data from traverses over varying distances at varying axial distances downstream of the exit of the rectangular channel. The sampling rate for all of these data runs was 100 Hz. Data was taken at increments downstream of the channel exit, ranging from 2.54 cm to 15.24 cm (1" to 6") in 2.54 cm (1") increments. The lateral distances of these traverses ranged from 6.604 cm to 10.67 cm (2.6" to 4.2"), with the traverse distances increasing with increasing distance from the channel exit. The typical number of data points can be calculated by taking the traverse distance, subtracting 0.1, and then multiplying by 1000.

In attempts to improve the quality of the data, many aspects of the data taking process were varied. These included:

- The A/D voltage range was either ±1 or ±2 V.
- The coflow smoke was on or off.

- The computer monitors were or were not blocked from the view of the component pointing in their direction.
- The smoke level was varied between 1.5 and 2.5, as measured on the control of the fog machine.
- The size of pinholes were varied between nominally 1 mm and 3 mm.
- The components were positioned so that either both channels were in forward scatter, or there was one component each in forward and back scatter.
- The calibrations were varied in that between 7 and 10 calibrations were averaged, they were taken either between data runs or after all the data was taken, and were done with the flow moving either at slow speed or at the same speed data was taken.

After many data-taking attempts, it was determined that the optimal conditions were a voltage range of ±2 V, no coflow, with the view of the monitors blocked, the smoke level about 2.25, the components one each in forward and back scatter, the pinhole size about 3 mm for backscatter, and 1-2 mm for forward scatter, the calibrations done between data runs and at slow speed. No clear evidence was found that averaging a larger number of calibrations improved the quality of the data.

The PDV data to be presented in Figures 6.1 through 6.4 were taken at 2.54 cm (1”) downstream of the exit of the flow channel. Traverses of 7.112 cm (2.8”) were performed, and 2700 data points were taken at a sampling rate of 100 Hz. Additionally, the PDV data to be presented in Figures 6.5 through 6.8 were taken at 7.62 cm (3”) downstream of the exit of the flow channel. Traverses over a distance of 8.382 cm (3.3”) were performed, and 3200 data points were taken at a sampling rate of 100 Hz. This data was also taken at the optimal conditions described above.

5.2 NACA 0012 Airfoil Model

The setup for these experiments were similar to those described in Chapter 5.1, except that an NACA 0012 airfoil was mounted at the exit of the rectangular flow channel described in Chapter 3.1. The Reynolds number for this flow was approximately 394,000, based on airfoil chord. For the NACA 0012 airfoil, data was typically taken at discrete stations along the chord of the airfoil separated by 2.54 cm (1"). These were taken from 5.08 cm (2") upstream of the airfoil shoulder (x/c = 0.130) to 20.32 cm (8") downstream of the airfoil shoulder (x/c = 0.977) (Figure 3.4). Also, data was taken at a constant vertical distance relative to either the airfoil surface, or the laboratory floor. Typically, either 1000 or 4096 data points were taken at each station at a sampling rate of 10 kHz.

Traverses were also made at the shoulder of the airfoil, starting at 1.27 cm (0.5", z/c = 0.0423) above the airfoil surface and descending to 0.127 cm (0.05", z/c = 0.00423) above the airfoil surface in 0.127 cm (0.05") increments. Typically 4096 data points were taken at each station at a sampling rate of 10 kHz.

Additionally, some continuous traverses were taken from 5.08 (2") upstream of the shoulder (x/c = 0.130) to 17.78 cm (7") downstream of the shoulder (x/c = 0.892). Typically, 3000 data points were taken at a sampling rate of 100 Hz. This method of data taking was not used very much because data could not be gathered over the entire airfoil, and also because correlation coefficients and spectra could not be calculated.

5.3 Unsuccessful Experimental Methods

Several methods were used in attempts to improve the quality of the data. Some of these techniques have been mentioned above, and both those techniques and other methods not mentioned are discussed below.

When the experiments were begun, both PDV channels were in a forward scatter configuration. This configuration provided a better signal to noise ratio, as well as requiring less smoke to get a strong signal from the flow. However, this configuration had little sensitivity to the spanwise velocity, leading to large errors in both the mean and RMS spanwise velocities.

In order to obtain better zero velocity data in the upper and lower shear layers of the flow, a secondary fog machine was used in order to seed these shear layers, while the primary fog machine was used to seed the main part of the flow. This method was unsuccessful because it was not possible to control the smoke level of the secondary fog machine, even with the use of the plenum to help regulate the smoke flow.

Decreasing the probe volume was also attempted in order to produce better results. To this end, a beam expander fitted with a lens of focal length equal to 310 mm was placed in the flow so that the focal point of lens was approximately in the transverse center of the flow. This model 0055 X0121 beam expander was manufactured by DISA. The diameter of the probe volume generated by this lens was on the order of 0.3 mm, as opposed to 2-3 mm for the unfocused laser beam. On one data taking attempt, the mean streamwise and spanwise velocities were approximately correct, but the RMS velocities were too large (up to 15 m/sec). Two possible explanations for this problem are noise due to laser speckle, or perhaps non-uniform seeding levels.

Other attempts to improve the data included varying the pinhole size and the amount of smoke injected into the flow. These variations did not appear to have a large effect on the quality of the data, except that if the pinhole size were made too small, then the data did not appear to be correct. This could perhaps be explained if the two components were not focused on the same point in the flow. Additionally, if the pinhole on the spanwise sensitive channel was too small, the signal to noise ration was too small to generate reliable data. In contrast, the larger pinholes would allow a greater chance of the two sensing areas to overlap, thus improving the data. The larger sensing areas would also tend to average out the effects of uneven seeding in the flow.

An attempt was also made to improve the data by placing polarizing film at the optical entrance of each component. The polarizing film should help eliminate the sensitivity to polarization of the beam splitter by only passing the original, in this case vertical, polarization. This method was not rigorously tested, but it appears to hold promise. Results for one run using this experimental method will be presented in Chapter 6.3.

Chapter 6: Results

6.1 Rectangular Channel

The first results presented are for the rectangular channel without the NACA 0012 airfoil installed. This data was taken in order to help track down programming errors in the data acquisition and data reduction software. These errors were first suspected to exist because a velocity of close to zero could not be measured at the edges of the jet, and the streamwise velocity was always incorrect. The data presented was acquired and reduced after these programs were corrected.

For PDV measurements at the exit of the rectangular flow channel, vertical traverses over a distance of 7.112 cm (2.8") were made at 2.54 cm (1") from the exit. A total of 2700 data points were taken at a sampling rate of 100 Hz, while continually traversing the flow channel at a rate of 0.254 cm/sec (0.1 "/sec). Time histories of the average streamwise and spanwise velocities of these measurements can be found in Figures 6.1 and 6.2, respectively. These time histories are the average of five different data runs. In these figures, the x-axis is in meters because the constant traverse speed allows the recorded time to be converted into distance. The measured average streamwise velocity in the core of the flow is approximately 22 m/sec. This agrees well with the pitot-static probe measurements on the jet centerline. Also, the measured mean velocity in the spanwise direction is approximately 3 m/sec, instead of the actual 0 m/sec. RMS velocity data for these traverses are also presented in Figures 6.3 and 6.4. These figures are also the average of five different data runs. In the streamwise direction, the average RMS is about 2 m/sec, while the spanwise RMS is slightly higher, about 2.5 m/sec. At this distance from the channel exit, the core flow appears to be approximately 0.045 m thick.

Additionally, vertical traverses over a distance of 8.382 cm (3.3") were made at an axial distance of 7.62 cm (3") from the channel exit. For these traverses, 3200 data points were taken at a sampling rate of 100 Hz. Profiles of the streamwise and spanwise velocities of these measurements can be found in Figures 6.5 and 6.6, respectively. These figures are the average of six different data runs. The measured average streamwise velocity in the core of the flow is approximately 25 m/sec, while in the spanwise direction it is approximately 9 m/sec. Again, the true spanwise velocity is 0 m/sec. Also, RMS velocity data for these traverses are presented in Figures 6.7 and 6.8. These figures are also the average of six different data runs. In the streamwise direction, the average RMS is again about 2 m/sec, while the spanwise RMS is again higher than the streamwise RMS, approximately 2.8 m/sec. At this distance from the channel exit, the core flow has shrunk to 0.04 m thick.

6.2 NACA 0012 Airfoil Measurements

The NACA 0012 airfoil measurements were taken in order to assess the accuracy of the PDV system for turbulence measurements in a flow with varying RMS levels. This assessment was carried out using conventional statistics such as mean and RMS velocity values, as well as time auto-correlations and power spectra, both calculated using MATLAB. Another part of this assessment was accomplished by comparing the PDV statistics with similar measurements made using a hot wire anemometer.

6.2.1 Chordwise Velocity Profiles

Figures 6.9 and 6.10 show the measured PDV streamwise and spanwise mean velocity at 11 stations along the airfoil chord, each spaced 2.54 cm (1") apart. These stations cover the distance between x/c of 0.130 and 0.977. The traverse was positioned so that the measurement volume of the PDV system was 1.27 cm (0.5") above the shoulder of the airfoil, which was set at an angle of attack of 0°. The traverse was then moved purely in the positive or negative direction of the airfoil chord, so that the distance of the measurement volume from the surface of the airfoil increased as the traverse was moved away from the airfoil shoulder (Figure 3.4). Additionally, Figure 6.9 compares the streamwise PDV velocity with hot wire data taken at the same stations, but at different times. For the PDV data, 1000 points were taken at each station at a sampling rate of 10 kHz. For the hot wire data, 1024 points were taken at 10 kHz. The number of points taken for the hot wire data differs from that of the PDV data due to the requirement in the hot wire data acquisition software that the number of points must equal 2^n, where n is an integer > 0.

In Figure 6.9, the hot wire data starts at 21 m/sec near the leading edge of the airfoil, increases to 22 m/sec at station 2, and decreases to approximately 13 m/sec at the last station on the airfoil. In comparison, the PDV data is about 23 m/sec for the first two stations, and drops to an average of about 11 m/sec at the last airfoil station. The total variation in range of velocity at any x/c location is about 2 m/sec for the hot wire data, and 7 m/sec for the PDV data. Figure 6.10 shows the corresponding spanwise PDV velocity data. The average spanwise velocity for each station is approximately 0 m/sec, as expected, while the largest velocity range between the data runs at a station is about

4.5 m/sec. No spanwise hot wire data is presented because the hot wire probe was only sensitive to one direction, and was aligned to the streamwise direction of the flow.

Figures 6.11 and 6.12 are the same as 6.9 and 6.10, except that these display the corresponding RMS velocities. The streamwise hot wire RMS data ranges from 3 m/sec to 4 m/sec, while the PDV data ranges from 2.5 m/sec to 3.75 m/sec. The largest variation in RMS range is about 1.2 m/sec for the hot wire data, and only 0.7 m/sec for the PDV data. Figure 6.12 shows the corresponding spanwise PDV RMS velocity. This RMS velocity ranges from 2.3 m/sec to 4 m/sec, while the largest RMS velocity range between the data runs at a station is about 0.6 m/sec. The PDV RMS is almost the same for both the streamwise and spanwise data, which one would expect to observe if the flow were isotropic.

Figures 6.13 through 6.16 present a second set of PDV data which corresponds to the data in Figures 6.9 through 6.12. The differences for this second data run were that the voltage range for the A/D board was ± 1 V instead of ± 2 V, and the number of data points in each run was 4096 instead of 1000. The streamwise PDV data in Figure 6.13 is compared against the same hot wire data as in the previous set of graphs. The PDV velocity ranges from 19 m/sec to 11 m/sec, with a maximum range of variation of 4 m/sec at any station. For the spanwise mean velocity in Figure 6.14, the average velocity is about -1 m/sec, but increases to 3 m/sec at the last station on the airfoil. In Figure 6.15, the streamwise PDV RMS velocity varies from 2.3 m/sec to 3.3 m/sec, and the largest range of variation is 0.4 m/sec. The largest variation in mean streamwise velocity is 7 m/sec at any given point. The PDV data is consistently lower than the hot wire data. In Figure 6.16, the spanwise RMS velocity varies from 3.5 m/sec to 5.1 m/sec, with a maximum range of variation of 0.3 m/sec. It can also be observed that the measured spanwise PDV RMS is significantly larger than the measured streamwise PDV RMS (1.2 to 1.6 m/sec), but only slightly higher than the measured streamwise hot wire RMS results (0.2 to 1.0 m/sec).

When the first and second data sets are compared, it can be seen that the streamwise and spanwise mean velocity profiles show less variation at each data point in the second data set than in the first, although the average velocity for the first data set is more comparable to that of the hot wire data. Very little difference can be seen between the two sets of streamwise RMS profiles, but the spanwise RMS profile of the first data set is lower than that of the second data set by about 1 m/sec.

Figures 6.17 and 6.18 present examples of streamwise hot wire time histories at 1.27 cm (0.5") from the surface of the airfoil. Figure 6.17 was taken at the shoulder of the airfoil (x/c = 0.3), while Figure 6.18 was taken at the next to last station on the airfoil (x/c = 0.89). The data was taken in blocks of 1024 points at 10 kHz. The measured average streamwise velocity at the shoulder was about 20 m/sec, while near the trailing edge it was 13 m/sec. The data at the shoulder also has higher frequency fluctuations than near the trailing edge.

Figures 6.19 and 6.20 are the corresponding PDV data to figures 6.17 and 6.18. This data was taken in blocks of 4096 points at a sampling rate of 10 kHz. Only the first tenth of a second of data is displayed so that these graphs can be better compared against the hot wire data. The average velocities for the PDV graphs are 17 m/sec and 10 m/sec, respectively. These velocities are offset from the hot wire data by -3 m/sec. The time traces of the hot wire and PDV data at the shoulder appear comparable. However, at x/c = 0.89, the PDV data shows activity at higher frequencies. It is believed that this may indicate that the PDV data is noisier than the hot wire data.

The streamwise hot wire correlation coefficients are shown in Figures 6.21 and 6.22. These coefficients were calculated from the time histories shown in Figures 6.17 and 6.18 using MATLAB. The x/c locations of these two figures are 0.3 and 0.89, respectively. The signal dies out at about 0.1 sec for both graphs, but higher frequencies can be seen at the shoulder. Additionally, the first zero crossing occurs at $t \cong 0.005$ sec for both of these figures. This may be indicative of the integral time scale of the flow. Figures 6.23 and 6.24 are the corresponding PDV correlation coefficient graphs. The correlation for these two graphs does not appear to die out in 0.1 sec as does the hot wire data, but higher frequencies can still be seen at the shoulder. Also, while the hot wire and PDV graphs at x/c = 0.89 appear comparable, the hot wire data shows higher frequencies than appear in the PDV data. Additionally, the first zero crossings for the hot wire and PDV correlation coefficients at x/c = 0.89 appear similar. These would be determined by the lower frequency large eddies.

The streamwise hot wire power spectral densities computed from the data in Figures 6.17 and 6.18 are shown in Figures 6.25 and 6.26. At the shoulder, the lowest frequencies have a power density of about 25 dB, but this decays to about -5 dB at 5000 Hz, for a dynamic range of about 30 dB. At x/c = 0.89, the power density again starts out at about 25 dB, but this time decays to -13 dB at 5000 dB, for a total dynamic range of about 38 dB. These ranges are larger than those observed in the corresponding PDV spectra which follow.

Figures 6.27 and 6.28 show the corresponding PDV power spectral densities. For the PDV measurements at x/c = 0.3, the power density starts out at about 17 dB, and decays to -3 dB around 1500 Hz, where it remains up through 5000 Hz. The total dynamic range is about 20 dB. Near the trailing edge, the power density starts at 23 dB, and again decays to about -3 dB between 1500 Hz and 5000 Hz, for a dynamic range of about 26 dB. It is important to note that the PDV dynamic range is approximately 10 dB less than the hot wire dynamic range.

6.2.2 Vertical Velocity Profiles

Starting with Figure 6.29, data is presented for locations at varying distances from the surface of the airfoil instead of varying locations along the chord of the airfoil. Generally, the locations which will be analyzed in detail are 1.27 cm (0.5") and 0.508 cm (0.2") above the shoulder of the airfoil, which correspond to z/c values of 0.0423 and 0.0169, respectively. These data were taken in order to assess PDV accuracy, but also to determine how close to a "wall" measurements could be made.

Figures 6.29 and 6.30 show PDV streamwise and spanwise velocity at 8 stations of varying heights above the shoulder of the airfoil, each spaced 0.127 cm (0.05") apart. The vertical location of these points range from 0.381 cm (0.15") to 1.27 cm (0.5") from the surface of the airfoil. Also, Figure 6.29 compares the streamwise PDV velocity with hot wire data taken at the same stations, but at different times. For the PDV data, 8192 points were taken at each station at a sampling rate of 10 kHz. For the hot wire data, 4096 points were taken at 10 kHz.

In Figure 6.29, the hot wire streamwise mean velocity data starts at 25 m/sec at 0.127 cm (0.05", z/c = 0.00423) from the airfoil surface, increases to 26 m/sec at 0.381 cm (0.15", z/c = 0.0127), and decreases to about 21 m/sec at 1.27 cm (0.5", z/c = 0.0423). The PDV data for 0.127 cm (0.05") and 0.254 cm (0.1") were inaccurate due to laser light scattered off the surface of the airfoil interfering with the data, and have been deleted from the graph. For the remaining PDV data, the measured velocity starts at 26 m/sec at 0.381 cm (0.15", z/c = 0.0127), and decreases to 18 m/sec at 1.27 cm (0.5", z/c = 0.0423). There does not appear to be a strong correlation between the hot wire and PDV data. This could perhaps be partially explained by not being set up at the exact same distance from the airfoil for both the hot wire and PDV data acquisition. It is also possible that the flow is not very repeatable, or the measurements could have inadvertently been made too close to the airfoil. The largest ranges of velocity variations appear to be 1 m/sec for the hot wire data, and 5 m/sec for the PDV data. Figure 6.30 shows the spanwise PDV velocity. The average velocity for each station is about -3 m/sec, instead of the true value of 0 m/sec, while the largest velocity range between the data runs at a station is about 5 m/sec.

Figures 6.31 and 6.32 display the measured PDV RMS velocities which correspond to the PDV mean velocities in Figures 6.29 and 6.30. Again, the PDV data at 0.127cm (0.05") and 0.254 cm (0.1") from the airfoil surface have been deleted due to inaccuracies caused by reflections off of the airfoil surface. The streamwise hot wire RMS data ranges from 2 m/sec to 3.7 m/sec, while the PDV RMS data ranges from 2.3 m/sec to 2.9 m/sec. The largest RMS range of variation is about 0.4 m/sec for the hot wire data, and 0.6 m/sec for the PDV data. Figure 6.32 shows the corresponding spanwise

PDV RMS velocity results. These RMS velocities range from 1.7 m/sec to 2.7 m/sec, while the largest RMS velocity range between the data runs at a station is about 1.1 m/sec. The spanwise PDV RMS data are reasonably close to the corresponding streamwise PDV RMS results.

Figures 6.33 through 6.36 present another PDV data set which corresponds to Figures 6.29 through 6.32, except that the number of data points for each time trace was 4096 instead of 8192. The streamwise PDV data in Figure 6.33 is compared against the same hot wire data as in the previous graphs. The PDV velocity goes from 26 m/sec at $z/c = 0.0127$ to 17 m/sec at $z/c = 0.423$, with a maximum range of variation of 6 m/sec at a fixed location. For the PDV mean spanwise velocity in Figure 6.34, the average velocity is about -4 m/sec. Also, one of the data runs gave an average mean spanwise velocity of approximately -10 m/sec. This could indicate a reflection off of the airfoil surface at this station. In Figure 6.35, the streamwise PDV RMS data varies from 2.1 m/sec to 2.7 m/sec, and the largest range of variation is 0.4 m/sec. The PDV data is consistent with the hot wire data up to 0.635 cm (0.25", $z/c = 0.0212$) from the surface of the airfoil, but then the PDV RMS velocity increases more slowly than the hot wire data. At 1.27 cm (0.5", $z/c = 0.0423$), the hot wire RMS velocity is approximately 1.1 m/sec greater than the PDV RMS velocity. In Figure 6.36, the spanwise RMS velocity varies from 2.3 m/sec to 3.6 m/sec. These RMS values are larger than the corresponding streamwise PDV RMS values, and more nearly match the hot wire RMS data in Figure 6.35.

When the first and second data sets are compared, it can be seen that there is little difference between the mean streamwise velocities for the two data runs. Likewise, the mean spanwise velocities are also very similar, with the exception of a single data run in the second data set. There appears to be less streamwise and spanwise RMS velocity variation at each data point in the second data set, and the first set of spanwise RMS velocities are also lower than the second set by about 0.75 m/sec.

Figures 6.37 and 6.38 present examples of hot wire time histories at the shoulder of the airfoil. Figure 6.37 was taken at 1.27 cm (0.5") from the surface of the airfoil (z/c = 0.0423), while Figure 6.38 was taken at 0.508 cm (0.2") from the surface of the airfoil (z/c = 0.0169). The data was taken in blocks of 1024 points at a sampling rate of 10 kHz. The measured average streamwise velocity at 1.27 cm (0.5") was approximately 18 m/sec, while at 0.508 cm (0.2") it was approximately 22 m/sec.

Figures 6.39 and 6.40 are the corresponding PDV data to Figures 6.37 and 6.38. This data was taken in blocks of 4096 points at a sampling rate of 10 kHz. Only the first tenth of a second of data is displayed so that these graphs can be better compared against the hot wire data. The average streamwise velocity at 1.27 cm (0.5") was approximately 18 m/sec, while at 0.508 cm (0.2") it was approximately 23 m/sec. The PDV and hot wire velocities at each location appear almost the same. Additionally, near the airfoil surface, the fluctuation levels are reduced. However, the PDV time histories again appear to have more high frequency fluctuations than the corresponding hot wire time histories.

The streamwise hot wire correlation coefficients are shown in Figures 6.41 and 6.42. These coefficients were calculated from the time histories shown in Figures 6.37 and 6.38 using MATLAB. Again, the data was taken at 1.27 cm (0.5", z/c = 0.0423) and 0.508 cm (0.2", z/c = 0.0169) from the shoulder of the airfoil. The correlation dies out at about 0.1 sec for both graphs, and higher frequencies (shorter times) can be seen at

1.27 cm (0.5"). Additionally, the first zero crossing occurs at t ≅ 0.004 sec for Figure 6.41, and t ≅ 0.001 for Figure 6.42, again indicating higher frequency fluctuations at z = 1.27 cm (0.5"). Figures 6.43 and 6.44 are the corresponding PDV correlation coefficient graphs. The correlation for these two graphs does not appear to die down like the hot wire data within 0.1 sec. The first zero crossing occurs at t ≅ 0.001 sec for both graphs, again indicating that the low frequency response of the PDV system is similar to that of the hot wire system. Also, the hot wire graphs show higher frequencies in the data than appear in the PDV data.

The streamwise hot wire power spectral densities are shown in Figures 6.45 and 6.46. At z = 1.27 cm (0.5", z/c = 0.0423), the lowest frequencies have a power spectral density of about 20 dB, and this decays to about -5 dB by 5000 Hz, for a dynamic range of 25 dB. At z = 0.508 cm (0.2", z/c = 0.0169), the power spectral density starts out around 10 dB, and decays to -15 dB at 5000 Hz, for a dynamic range of 25 dB. By moving 0.762 cm (0.3") closer to the airfoil, a decrease of 10 dB appears in the power spectra. In figure 6.46, a spike in the power spectrum can be seen at about 300 Hz. This is believed to be a manifestation of nearly periodic disturbances in the boundary layer of the airfoil.

Figures 6.47 and 6.48 show the corresponding PDV power spectral densities. For the measurements at z = 1.27 cm (0.5", z/c = 0.0423), the power spectral density starts out at approximately 14 dB, and decays to -2 dB by 5000 Hz, for a dynamic range of 16 dB. At z = 0.508 cm (0.2", z/c = 0.0169), the power spectral density starts at 15 dB, and decays to -3 dB between 1500 Hz and 5000 Hz, for a dynamic range of 18 dB. As with the hot wire data, a spike appears around 300 Hz in figure 6.48. which corresponds to the dip in the PDV correlation coefficient in Figure 6.42 at approximately 0.003 sec. Again, this is believed to be a manifestation of periodic flow phenomena in the boundary layer of the airfoil.

6.3 Error Analysis for Cell Stem Temperature Drift

The main source of error in the current experiments has recently been found to be due to the temperature drift of the iodine cells. This temperature drift changes the amount of iodine vapor in the cell, which in turn changes the cell calibrations. This was determined by running the theoretical iodine absorption code by Forkey (Forkey, 1995.) Because the stem temperature of the iodine cells was controlled to within ±0.1 °C (one standard deviation), the theory code was run twice, only varying the stem temperature by 0.1 °C. The frequency for each of the resulting curves was then recorded at an absorption ratio of 0.5, and a frequency offset of approximately 1.52 MHz was found. There are two iodine cells involved in any velocity measurement, the one in the sensing component and the one in the laser frequency monitoring system. If one would increase by 0.1 °C, while the other decreased by 0.1 °C, this would cause a difference of 0.2 °C, or two standard deviations. Also, in order to cover 95% of the possibilities, two standard deviations should be used. In all, calculations should be done assuming four standard deviations. With this in mind, the frequency offset increases to 6.08 MHz. When this number is divided by the sensitivities of the two sensing components for the current work, velocity offsets of 1.60 m/sec for forward scatter and 6.94 m/sec for back scatter are calculated. These velocity offset estimates are the same order of magnitude as the observed mean velocity errors in the current work.

6.4 Polarizing Film Results

In an attempt to improve the results obtained from the PDV system, polarizing film was placed where the scattered light enters the enclosure for each channel. The purpose of the polarizing film was to filter out the depolarized scattered light, and only pass scattered light which was still in the original vertically polarized orientation. This was done because the beam splitters were somewhat sensitive to polarization, and also because the intensity of the scattered light was sensitive to particle size and polarization (Meyers, PC 1998). If all the light striking the beam splitter has only one polarization, than the percent reflected and percent transmitted would always be a constant.

Figures 6.49 and 6.50 are the measured PDV mean streamwise and spanwise velocities with polarizing film in place for both channels. For this data, 4096 points were taken at each location at a sampling rate of 10 kHz. Each location was spaced 2.54 cm (1") apart from the next, and covered a distance between x/c of 0.130 and 0.977. The PDV measurement volume was again positioned 1.27 cm (0.5") above the surface of the airfoil shoulder. The streamwise mean velocity in Figure 6.49 starts at approximately 15 m/sec near the leading edge of the airfoil, increases to 17 m/sec at the shoulder, and decreases to approximately 9 m/sec near the trailing edge. Figure 6.50 shows the measured PDV spanwise mean velocity, which appears to average 0 m/sec over the length of the airfoil, with a total range of variation of 4 to 8 m/sec at a given streamwise location. When Figure 6.49 is compared with the PDV mean streamwise velocity data in Figures 6.9 and 6.13, it can be seen that the data has similar profile shapes, as well as similar variability at a given x/c. The same conclusions can be drawn when Figure 6.50 is compared to Figures 6.10 and 6.14. However, in Figure 6.49, the streamwise velocity data is decreased by 2-3 m/sec from Figure 6.9, and increased by 1 m/sec from Figure 6.13. The spanwise velocity is approximately the same for Figures 6.10, 6.14, and 6.50, at 0 or 1 m/sec. In contrast, the largest velocity variation range for Figure 6.50 is about 8 m/sec, larger than the 4.5 m/sec in Figure 6.10, or the 7 m/sec in Figure 6.14.

Figures 6.51 and 6.52 are the corresponding PDV RMS velocities for the data presented in Figures 6.49 and 6.50. The streamwise RMS in Figure 6.51 starts at 2.1 m/sec near the leading edge, and increases to 3.3 m/sec near the trailing edge. The spanwise RMS in Figure 6.52 begins at 2.7 m/sec near the leading edge, and increases to 4.4 m/sec near the trailing edge. The maximum range of variation is 1.2 m/sec at a given streamwise location. When Figure 6.51 is compared with the PDV RMS streamwise velocity data in Figures 6.11 and 6.15, or Figure 6.52 is compared with the PDV RMS spanwise velocity data in Figures 6.12 and 6.16, it can be seen that the data has similar profile shapes. Figures 6.11 and 6.51 have similar variability (1 m/sec) at a given x/c, but Figure 6.15 has a much smaller variability (0.3 m/sec). Also, the RMS variability for the polarizing film (Figure 6.52) is approximately 1.6 m/sec, which is larger than Figures 6.12 and 6.16, whose variability is approximately 0.5 m/sec.

Based on these initial results, it is not clear that the polarizing film improved the accuracy of the data. This may be because the polarizing film attenuates the scattered light by approximately 50%, which reduces the signal to noise ratio of the data.

Chapter 7: Conclusions and Recommendations

A two component Point Doppler Velocimetry (PDV) system has been developed and tested. Techniques for aligning the optical components and acquiring data were developed and refined. This work built on previous work and experience with an earlier PDV system, as well as a Doppler Global Velocimetry (DGV) system. The greatest increases in knowledge came in the areas of experimental techniques, types of measurements that can be made over an airfoil, and how closely to the airfoil surface these measurements can be made with the present configuration.

To begin, the software that was developed for the previous PDV system was modified to correct errors in the previous version, as well as improve usability. Specialized Excel macros were also written to reduce or eliminate user error in the data reduction process, as well as increase the speed of data reduction approximately five-fold.

Many variables in the setup of the PDV system, as well as data acquisition techniques, were investigated in an attempt to improve the quality of the data. Focusing the laser beam down to a smaller diameter introduced many difficulties into the data measurements, either due to laser speckle or nonuniform seeding of the flow, and did not appear to solve any major accuracy issues.

The size of the pinholes in the sensing components had a major effect on the quality of the PDV data. If the pinholes were too small, the signal to noise ratio was small, and it was difficult to focus both components on the same point in the flow. In contrast, if the pinholes were too large, any details of the flow were averaged out because of the larger sensing area. A moderately sized pinhole on the order of 1 to 2 mm provided the best data.

Smoke coflow was also used at the exit of the rectangular channel in order to seed the upper and lower shear layers of the flow and improve the accuracy of the PDV measurements at the edges of the flow. The seeding of this coflow could not be controlled to a sufficient degree of accuracy, and was thus discontinued in the current research.

A major source of error in early measurement with the NACA 0012 airfoil was laser light reflections from the airfoil support frame, as well as the airfoil surface itself. Both the airfoil and the frame were painted flat black, which greatly improved the quality of the data. However, reflections from the airfoil were still the major limiting factor in determining how close to the surface of the airfoil surface measurements could be made. The closest measurements that could be made were at a distance on the order of 0.508 cm (0.2", $z/c = 0.0169$) from the airfoil.

When the PDV and hot wire data were compared, the time traces for each appeared similar. The mean velocities agreed to about ±2 m/sec, while the RMS velocities agreed to ±0.4 m/sec. While the PDV time autocorrelations agreed with those of the hot wire, the PDV power spectral densities were noisier above approximately 750 Hz.

The major source of error in these experiments was the random drifting of the iodine cell stem temperatures. While the stem temperature was controlled to an RMS of ±0.1 °C, this could lead to a frequency shift of as much as 6 MHz, which translates into an error of 1.6 m/sec for the back scatter channel, and up to 6.9 m/sec for the forward scatter channel. These velocity error estimates are the same order of magnitude as the observed mean velocity errors in the current work.

There are still many modifications that could be made to the current setup in order to improve the data. One of these would be the use of vapor-limited iodine cells. Since the amount of iodine vapor in the cell would be a constant, more consistent calibration curves could be produced, and these calibrations should not vary versus time. It is expected that this should largely eliminate the mean velocity errors. Another modification would be to use a non-polarizing beam splitter and polarizing film. While initial experiments were conducted using polarizing film with somewhat promising results, a more thorough analysis still needs to be performed. Also, if testing were performed in a flow with a greater mean velocity, it could confirm that the zero and sensitivity errors are not dependent on the mean velocity range.

Another improvement would be to purchase new photodetectors that, when compared to the current photodetectors, would be less noisy, more stable, and more sensitive. Also, more efforts could be made to reduce the probe volume size while still being able to acquire accurate data. This approach might require a more powerful laser.

It would also be worthwhile to acquire hot wire and PDV data simultaneously. While both types of data acquisition could not occur at the same point in the flow, they could be made close enough to each other to allow a comparison of mean velocities, as well as turbulence and eddy characteristics. However, the smoke levels in the flow would have to be reduced from their current levels in order to prevent damage to the hot wire probe. Since reducing the smoke level would also reduce the signal strength, more sensitive photodetectors would be required, as mentioned above.

Longer data records could also be used to improve the accuracy of the measurements by averaging out any fluctuations, such as those due to the smoke level.

This would also have the effect of producing smoother power spectral densities and time auto correlations. This could not be performed with the current experimental configuration for various reasons, the main one being the temperature drift of the iodine cells.

Another intriguing possibility would be to develop a multi-point Doppler velocimeter. This would enable the calculation of both time and spatial correlations, since several simultaneous time records of velocity could be made.

References

Ainsworth, R.W., and Thorpe, S.J., "The Development of a Doppler Global Velocimeter for Transonic Turbine Applications," International Gas Turbine and Aeroengine Congress and Exposition, The Hague, Netherlands, June 13-16, 1994.

Ainsworth, R.W., Thorpe, S.J., and Manners, R.J., "A New Approach to Flow-Field Measurement - A View of Doppler Global Velocimetry Techniques," International Journal of Heat and Fluid Flow, Vol. 18, No. 1, pp. 116-30, Feb. 1997.

Beutner, T.J., Elliot, G., Mosedale, A., and Carter, C., "Doppler Global Velocimetry Applications in Large Scale Facilities," AIAA Paper 98-2608, 20th Advanced Measurement and Ground Testing Technology Conference, Albuquerque, NM, June 15-18, 1998.

Beutner, T.J., Williams, G.W., Baust, H.D., Elliot, G.S., Crafton, J., and Carter, C., "Characterization and Applications of Doppler Global Velocimetry," AIAA Paper 99-0266, 37th AIAA Aerospace Sciences Meeting and Exhibit, Reno, NV, Jan. 11-14, 1999.

Chan, V.S.S., Robinson, D.I., Turner, J.T., and Heyes, A.L., "A Simplified Doppler Global Velocimeter," Vol. 229, pp. 9-14, ASME FED Laser Anemometry Proceedings of the 1995 ASME/JSME Fluids Engineering and Laser Anemometry Conference and Exhibition, Hilton Head, SC, Aug. 13-18, 1995.

Clancy, P., Kim, J.-H., and Samimy, M., "Planar Doppler Velocimetry in High Speed Flows," AIAA Paper 96-1990, 27th Fluid Dynamics Conference, New Orleans, LA, June 17-20, 1996.

Clancy, P.S., and Samimy, M., "Multiple-Component Velocimetry in High Speed Flows Using Planar Doppler Velocimetry," AIAA Paper 97-0497, 35th Aerospace Sciences Meeting, Reno, NV, Jan. 6-9, 1997.

Clancy, P.S., Samimy, M., and Erskine, W.R., "Planar Doppler Velocimetry: Three-Component Velocimetry in Supersonic Jets," AIAA Paper 98-0506, 36th Aerospace Sciences Meeting, Reno, NV, Jan. 12-15, 1998.

Crafton, J., Messersmith, N.M., and Sullivan, J.P., "Filtered Doppler Velocimetry: Development of a Point System," AIAA Paper 98-0509, 36th Aerospace Sciences Meeting & Exhibit, Reno, NV, Jan. 12-15, 1998.

Elliot, G.S., Samimy, M., and Arnette, S.A., "Study of Compressible Mixing Layers Using Filtered Rayleigh Scattering Based Visualizations," AIAA Journal, Vol. 30. No. 10, pp. 2567-9, 1992.

Elliot, G.S., Samimy, M., and Arnette, S.A., "Details of a Molecular Filter-Based Velocimetry Technique," AIAA Paper 94-0490, 32nd Aerospace Sciences Meeting, Reno, NV, Jan. 10-13, 1994.

Elliot, G.S., Mosedale, A., Gruber, M.R., Nejad, A.S., and Carter, C.D., "The Study of a Transverse Jet in a Supersonic Cross-Flow Using Molecular Filtered Based Diagnostics," AIAA Paper 97-2999, 33rd AIAA/ASME/SAE/ASEE, Joint Propulsion Conference, Seattle, WA, July 6-9, 1997.

Ford, H.D., and Tatam, R.P., "Imaging System Considerations in Doppler Global Velocimetry," Vol. 2546, Proceedings of SPIE - The International Society for Optical Engineering, Optical Techniques in Fluid, Thermal, and Combustion Flow, San Diego, CA, July 10-13, 1995.

Forkey, J.N., Finkelstein, N.D., Lempert, W.R., and Miles, R.B., "Control of Experimental Uncertainties in Filtered Rayleigh Scattering Measurements," AIAA Paper 95-0298, 33rd Aerospace Sciences Meeting, Reno, NV, Jan. 9-12, 1995.

Forkey, J.N., Finkelstein, N.D., Lempert, W.R., and Miles, R.B., "Demonstration and Characterization of Filtered Rayleigh Scattering for Planar Velocity Measurements," AIAA Journal, Vol. 34, No. 3, March 1996.

Hoffenberg, R., and Sullivan, J.P., "Filtered Particle Scattering: Laser Velocimetry Using an Iodine Filter," ASME-FED, Vol. 161, pp. 135-8, June 20-24, 1993.

James, K.M., "Determination of the Accuracy of a Two-Component Point Doppler Velocimetry System," MS Thesis, Department of Mechanical and Aerospace Engineering, College of Engineering, West Virginia University, June 1997.

Komine, H., United States Patent, Patent No. 4,919,536, pp. 1-16, April 24, 1990.

Komine, H., Brosnan, S.J., Litton, A.B., and Stappaerts, E.A., "Real-Time, Doppler Global Velocimetry," AIAA Paper 91-0337, 29th Aerospace Sciences Meeting, Reno, NV, Jan. 7-10, 1991.

Komine, H., and Brosnan, J., "Instantaneous, Three-Component, Doppler Global Velocimetry," Laser Anemometry - Vol. 1, pp. 273-7, ASME 1991.

Kuhlman, J., Naylor, S., James, K, and Ramanath, S., "Accuracy Study of a 2-Component Point Doppler Velocimeter (PDV)," AIAA Paper 97-1916, 28th AIAA Fluid Dynamics Conference, Snowmass Village, CO, June 29-July 2, 1997.

Kuhlman, J., and Webb, D.L., "2-Component Point Doppler Velocimetry (PDV) Measurements of Turbulent Flow Over an Airfoil," AIAA Paper 99-3517, 30th AIAA Fluid Dynamics Conference, Norfolk, VA, June 28-July 1, 1999.

Lempert, W.R., Wu, P., Finkelstein, N., Erbland, P., and Miles, R.B., "Imaging Fluid Phenomena with Atomic and Molecular Vapor Filters," AIAA Paper 97-2520, 32nd Thermophysics Conference, Atlanta, GA, June 23-25, 1997.

Loew, C., "Visual Basic Programming for Data Acquisition," Desktop Engineering Vol. 1. No. 1, pp. 12, 14-6, Helmers Publishing, Inc., Apr. 1997.

McKenzie, R.L., "Measurement Capabilities of Planar Doppler Velocimetry Using Pulsed Lasers," AIAA Paper 95-0297, 33rd Aerospace Sciences Meeting, Reno, NV, Jan. 9-12, 1995.

McKenzie, R.L., "Planar Doppler Velocimetry Performance in Low-Speed Flows," AIAA Paper 97-0498, Aerospace Sciences Meeting, 35th, Reno, NV, Jan. 6-9, 1997.

McKenzie, R.L., "Planar Doppler Velocimetry for Large-Scale Wind Tunnel Applications," Paper No. 9, AGARD Fluid Dynamics Panel 81st Meeting and Symposium on Advanced Aerodynamic Measurement Technology, Seattle, WA, Sep. 22-25, 1997.

Meyers, J.F., and Komine, H., "Doppler Global Velocimetry A New Way to Look at Velocity," ASME Fourth International Conference on Laser Anemometry, Cleveland, OH, Aug. 3-9, 1991.

Meyers, J.F., Lee, J.W., and Cavone, A.A., "Signal Processing Schemes for Doppler Global Velocimetry," IEEE 14th International Congress on Instrumentation in Aero Simulation Facilities (ICIASF), Rockville, MD, Oct. 27-31, 1991.

Meyers, J.F., "Doppler Global Velocimetry *The Next Generation?*," AIAA Paper 92-3897, 17th Aerospace Ground Testing Conference, Nashville, TN, July 6-8, 1992.

Meyers, J.F., "Development of Doppler Global Velocimetry as a Flow Diagnostics Tool," Measurement Science and Technology, Vol. 6, No. 6, pp. 769-83, June 1995.

Meyers, J.F., "Evolution of Doppler Global Velocimetry Data Processing," Eighth International Symposium on Applications of Laser Techniques to Fluid Mechanics, Lisbon, Portugal, pp. 1-22, July 8-11, 1996.

Meyers, J.F., Lee, J.W., Fletcher, M.T., and South, B.W., "Hardening Doppler Global Velocimetry Systems for Large Scale Wind Tunnel Applications," AIAA Paper 98-2606, 20th AIAA Advanced Measurement and Ground Testing Technology Conference, Albuquerque, NM, June 15-18, 1998.

Meyers, J.F., Personal Communication, 1998.

Miles, R.B., Lempert, W.R., and Forkey, J., "Instantaneous Velocity Fields and Background Suppression by Filtered Rayleigh Scattering," AIAA Paper 91-0357, 29th Aerospace Sciences Meeting, Reno, NV, Jan. 7-10, 1991.

Morrison, G.L., Gaharan, C.A., and DeOtte, R.E., Jr., "Doppler Global Velocimetry: Problems and Pitfalls," Laser Anemometry 1994 Advances and Applications, ASME Publication FED-Vol. 191, June 1994.

Naylor, S., and Kuhlman, J., "Accuracy Studies of a Two-Component Doppler Global Velocimeter (DGV)," AIAA Paper 98-0508, 36th Aerospace Sciences Meeting & Exhibit, Reno, NV, Jan. 12-15, 1998.

Naylor, S.M., "Development and Accuracy Determination of a Two-Component Doppler Global Velocimeter (DGV)", PhD Dissertation, Department of Mechanical and Aerospace Engineering, College of Engineering and Mineral Resources, West Virginia University, July 1998.

Naylor, S., and Kuhlman, J., "Results for a Two-Component Doppler Global Velocimeter (DGV)," AIAA Paper 99-0268, 37th Aerospace Sciences Meeting & Exhibit, Reno, NV, Jan. 11-14, 1999.

Ramanath, S., "Development of a Point Doppler Global Velocimeter (DGV)," MS Thesis, Department of Mechanical and Aerospace Engineering, College of Engineering, West Virginia University, 1997.

Reeder, M.F., "Jet Entrainment Measurements Via Doppler Global Velocimetry," Proceedings of the ASME Fluids Engineering Division Summer Meeting, Vol. 239, No. 4, pp. 129-34, San Diego, CA, Jul 7-11, 1996.

Roehle, I., and Schodl, R., "Evaluation of the Accuracy of the Doppler Global Technique," Optical Methods and Data Processing in Heat and Fluid Flow, London, UK, pp. 155-61, Apr. 14-15, 1994.

Roehle, I., "Three-Dimensional Doppler Global Velocimetry in the Flow of a Fuel Spray Nozzle and in the Wake Region of a Car," Flow Measurement and Instrumentation, Vol. 7, No. 3/4, pp. 287-94, 1996.

Samimy, M., "A Review of Planar Multiple-Component Velocimetry in High Speed Flows," AIAA Paper 98-2509, 20th Advanced Measurement and Ground Testing Technology Conference, Albuquerque, NM, June 15-18, 1998.

Smith, M.W., and Northam, G.B., "Application of Absorption Filter-Planar Doppler Velocimetry to Sonic and Supersonic Jets," AIAA Paper 95-0299, 33rd Aerospace Sciences Meeting, Reno, NV, Jan. 9-12, 1995.

Smith, M.W., Northam, G.B., and Drummond, J.P., "Application of Absorption Filter Planar Doppler Velocimetry to Sonic and Supersonic Jets," AIAA Journal, Vol. 34, No. 3, pp. 434-41, March 1996.

Smith, M.W., "Application of a Planar Doppler Velocimetry System to a High Reynolds Number Compressible Jet," AIAA Paper 98-0428, 36th Aerospace Sciences Meeting & Exhibit, Reno, NV, Jan. 12-15, 1998.

Tellinghuissen, J., "Transition Strengths in the Visible-Infrared Absorption Spectrum of I_2," Journal of Chemical Physics, Vol. 76, No. 10, pp. 4736-44, May 15, 1982.

Thorpe, S.J., Ainsworth, R.W., and Manners, R.J., "Time-Averaged Free-Jet Measurements Using Doppler Global Velocimetry," FED-Vol. 239, Fluids Engineering Division Conference, Vol. 4, ASME 1996.

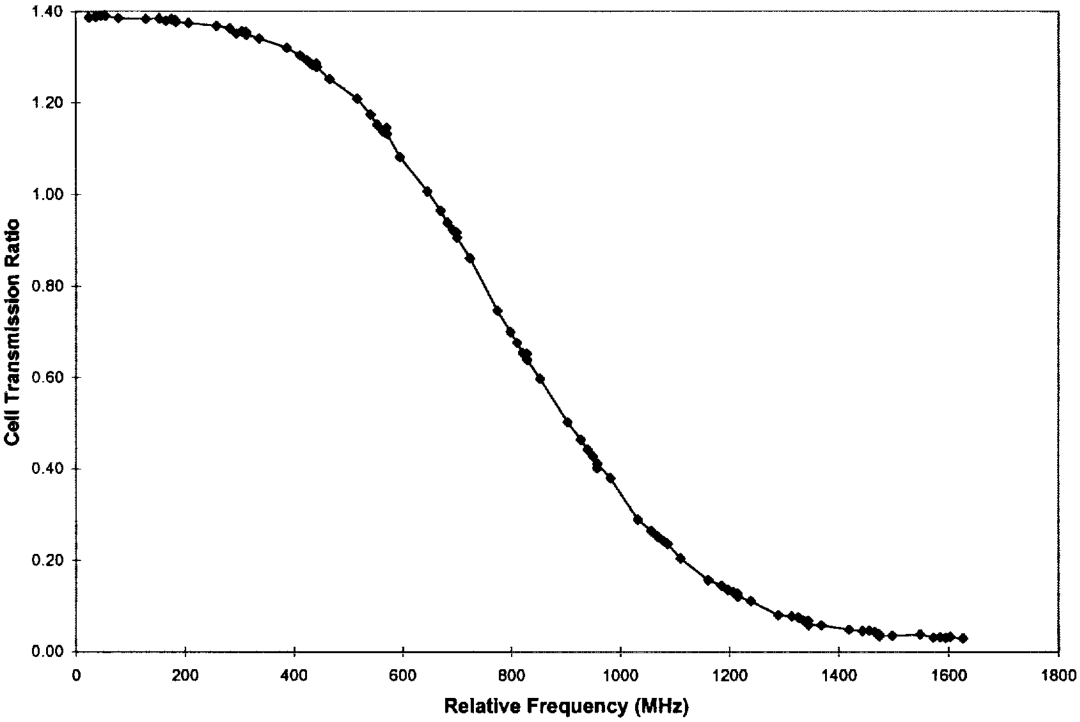

Figure 1.1. Iodine cell transmission ratio as a function of laser frequency.

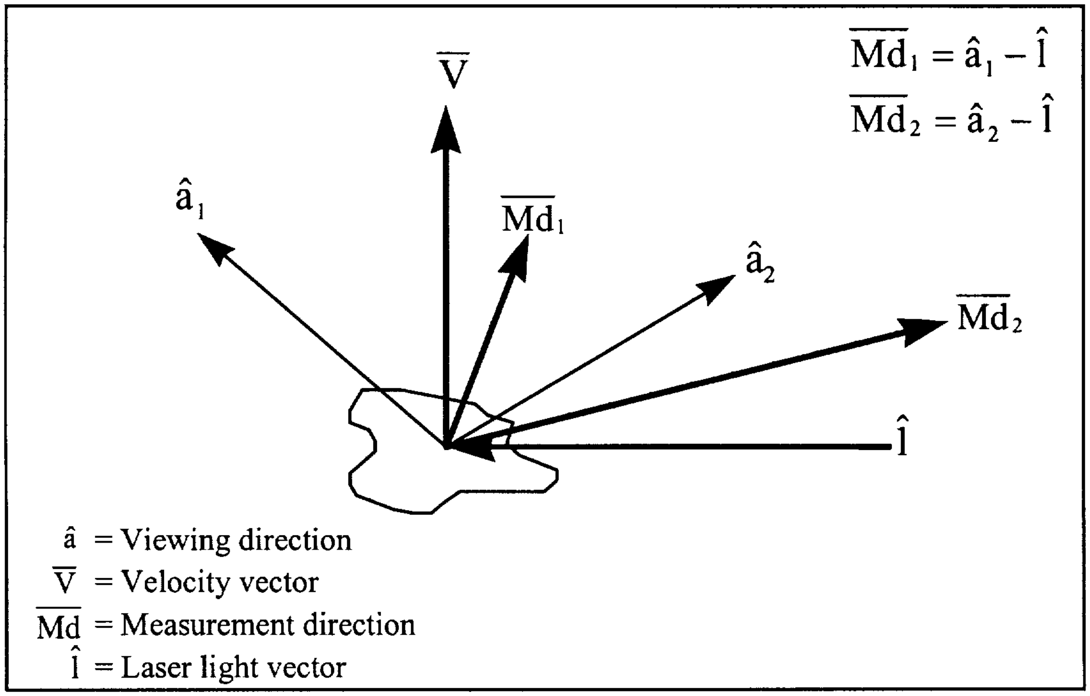

Figure 1.2. Vector geometry for a 2 component PDV system.

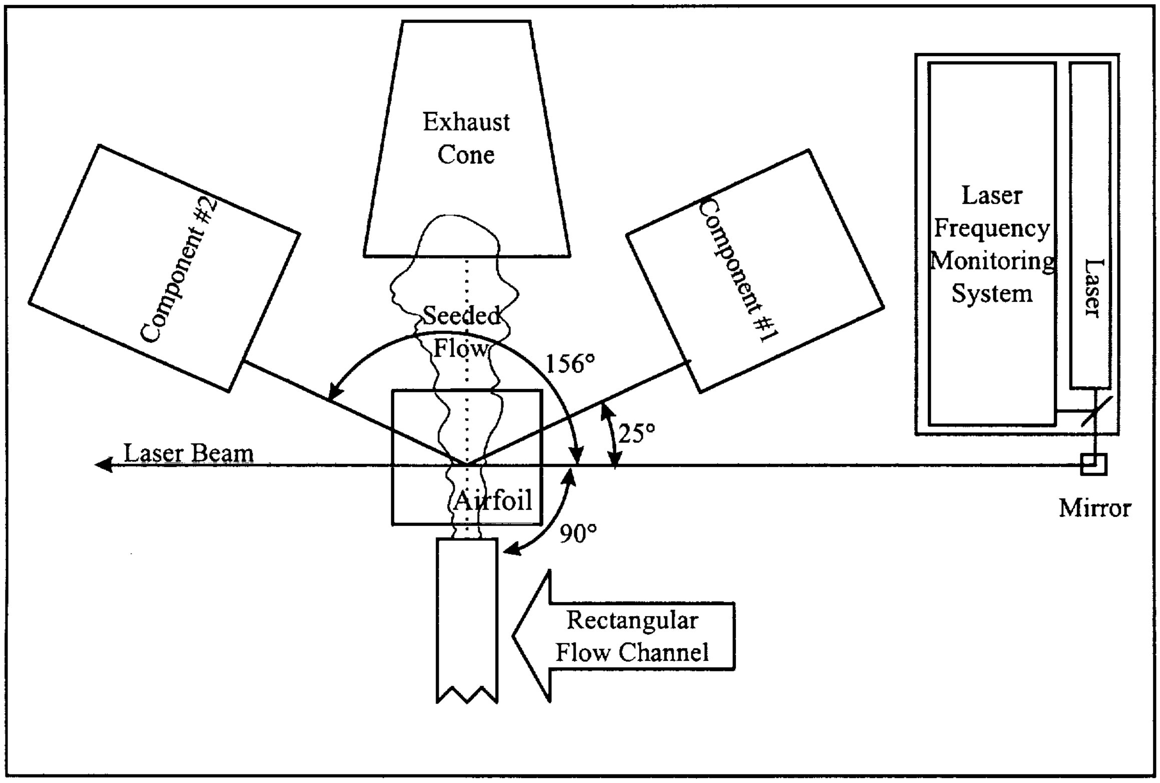

Figure 3.1. Overhead schematic of the laboratory setup, with typical component angles.

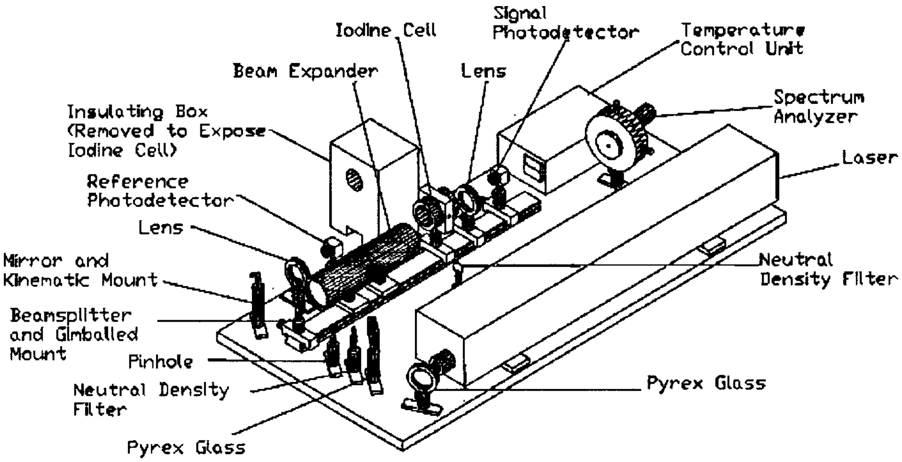

Figure 3.2. Schematic of the laser frequency monitoring system.

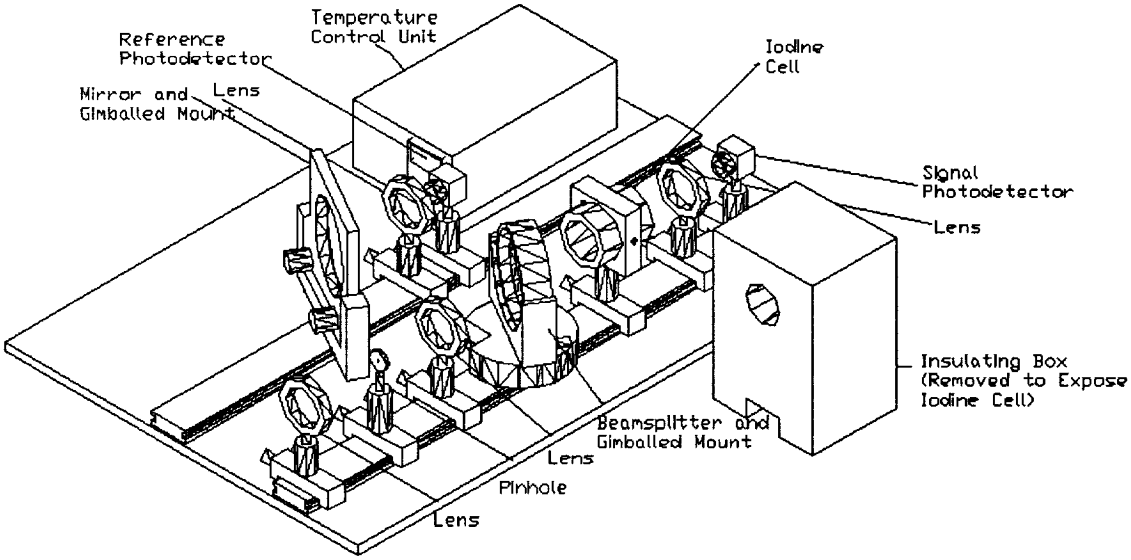

Figure 3.3. Schematic of a PDV sensing component.

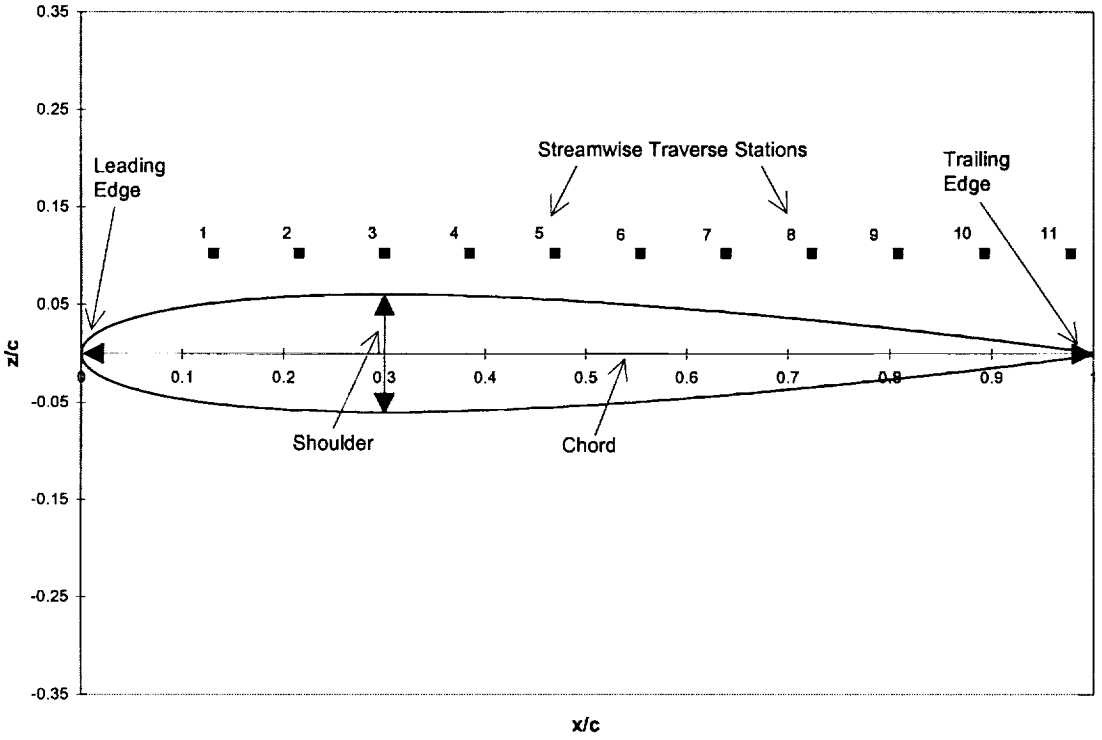

Figure 3.4. Diagram of current airfoil geometry, showing commonly used airfoil definitions.

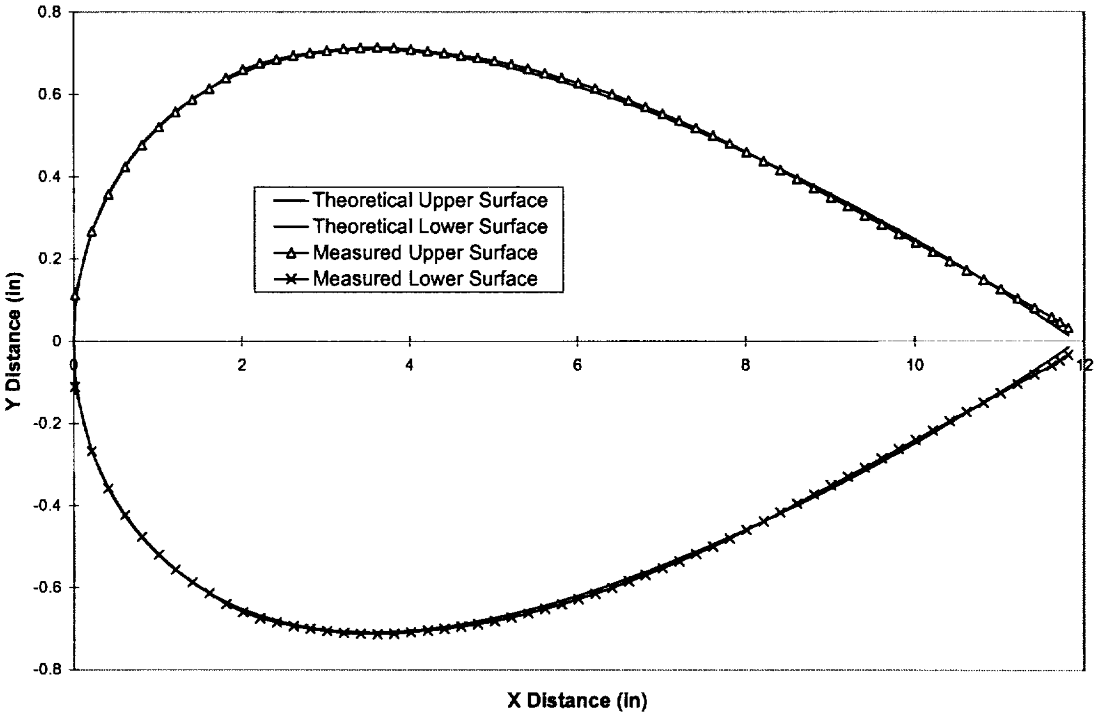

Figure 3.5. Comparison of theoretical and measured NACA 0012 airfoil coordinates.

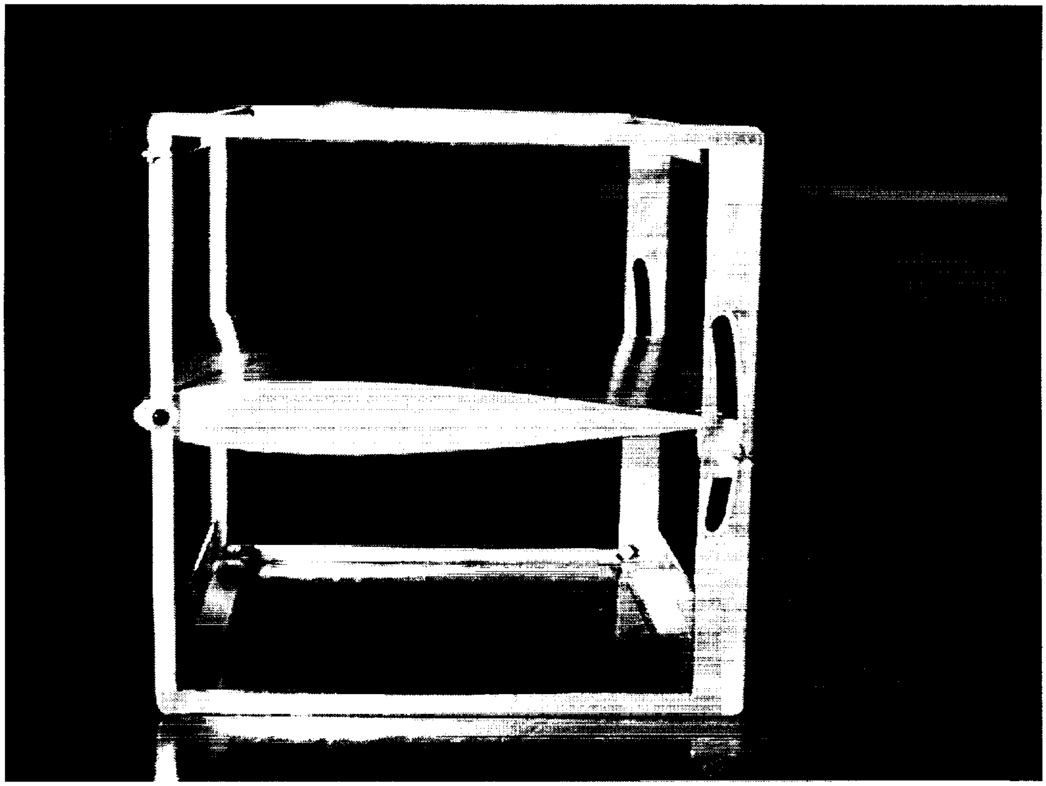

Figure 3.6. Airfoil frame with airfoil mounted in it.

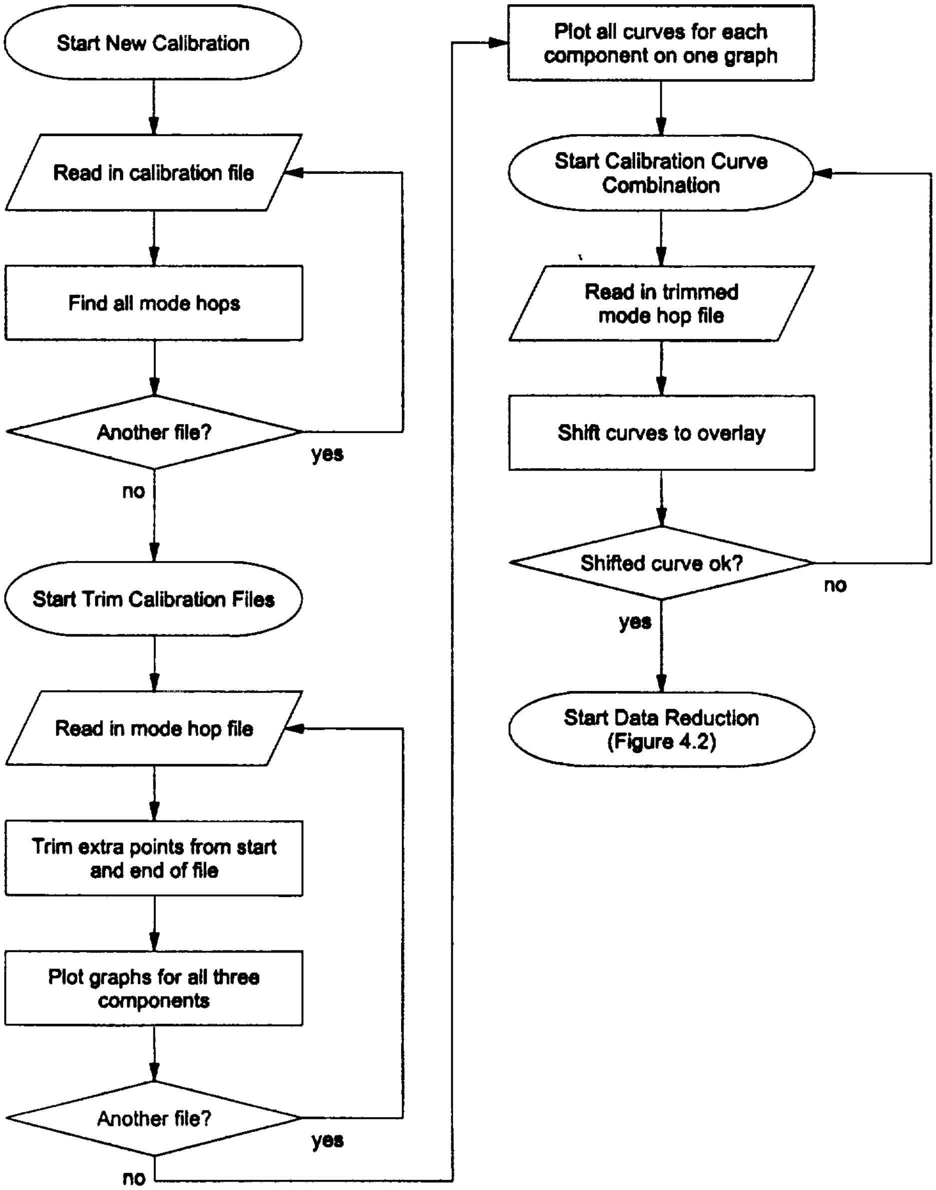

Figure 4.1. Flowchart of obtaining the calibration curve.

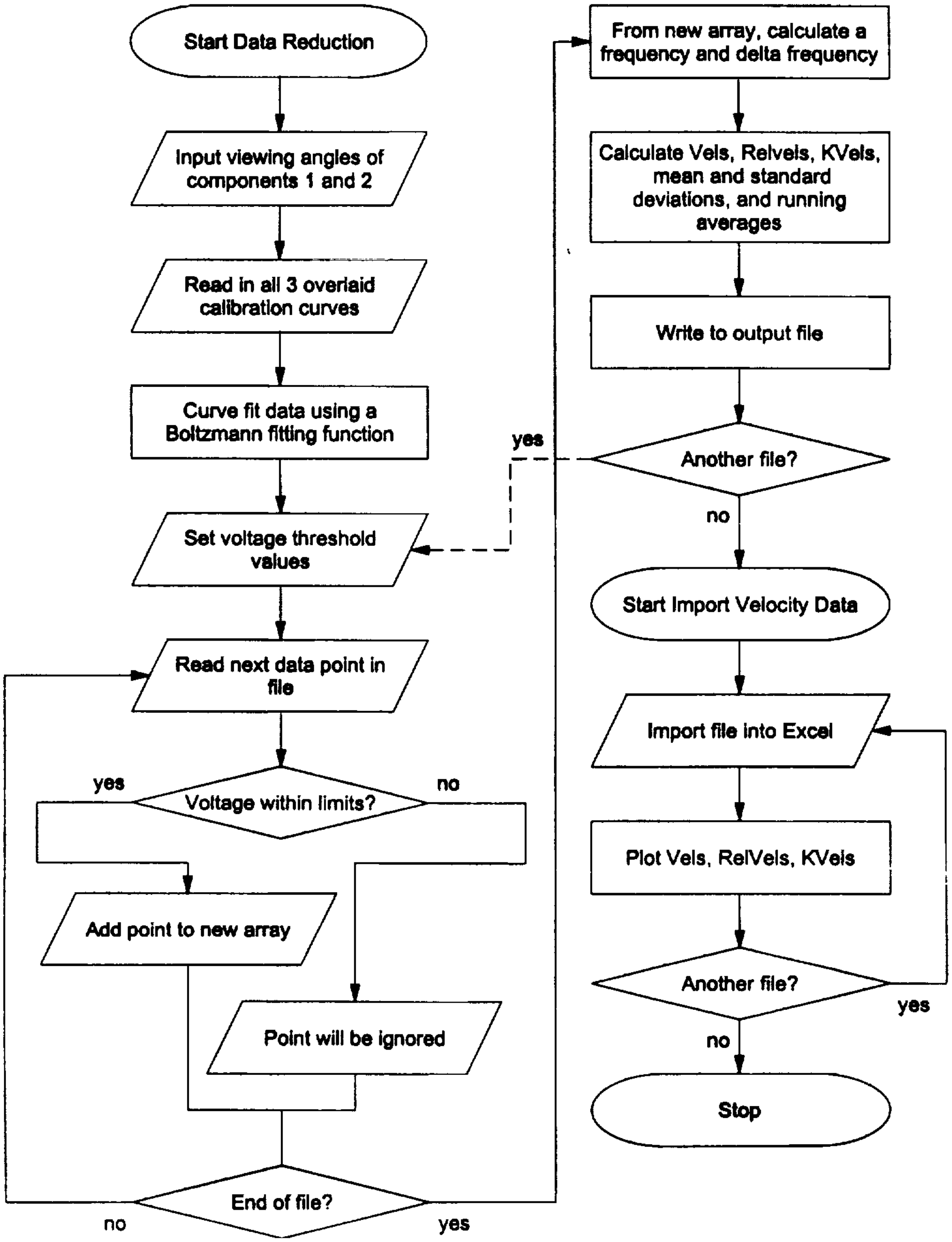

Figure 4.2. Flowchart of the data processing procedure.

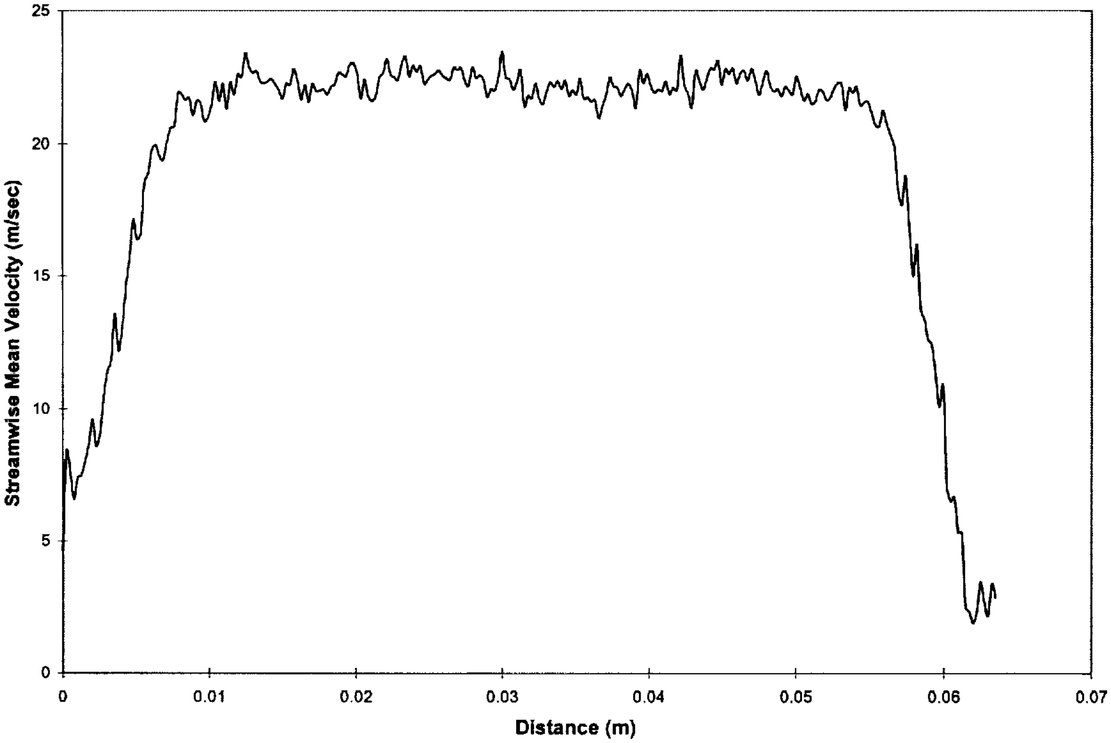

Figure 6.1. Streamwise PDV traverse mean velocity at 0.0254 m (1", 0.25D) from exit of the rectangular channel.

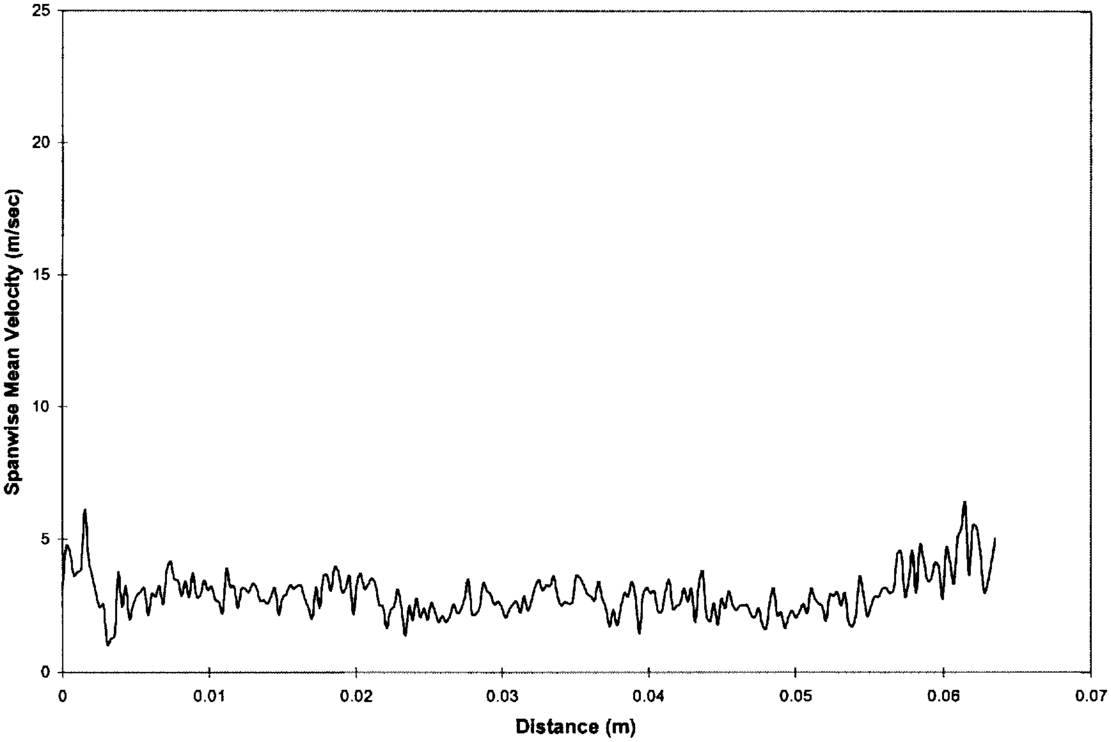

Figure 6.2. Spanwise PDV traverse mean velocity at 0.0254 m (1", 0.25D) from exit of the rectangular channel.

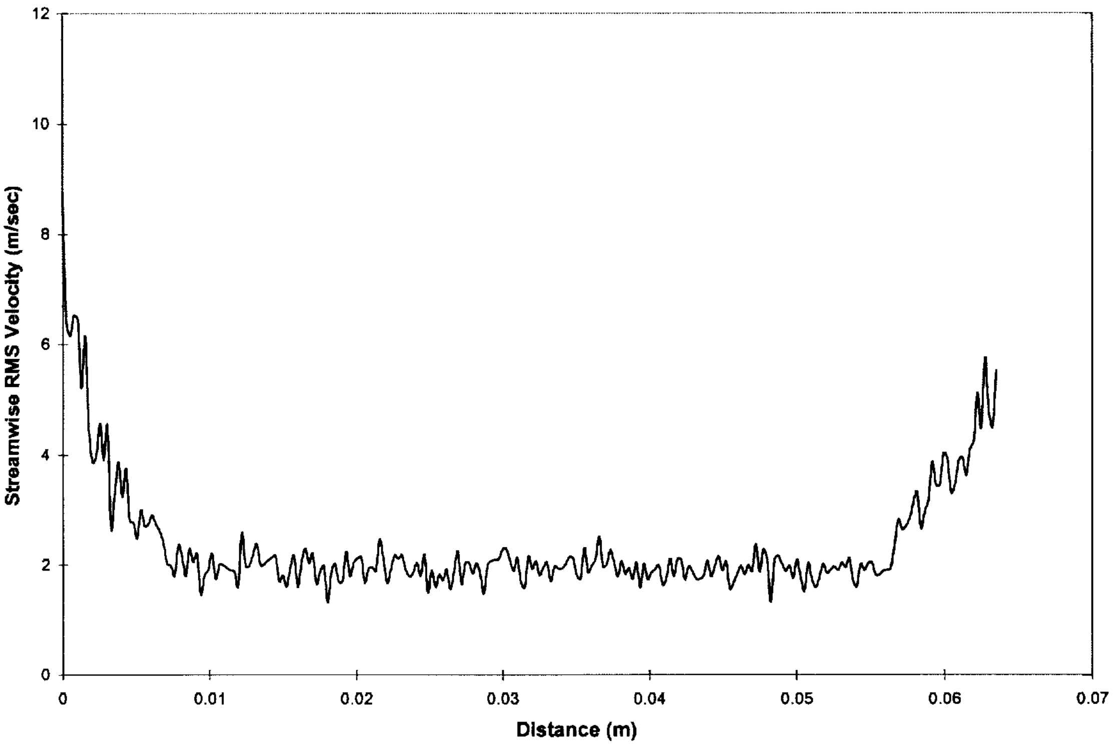

Figure 6.3. Streamwise PDV traverse RMS velocity at 0.0254 m (1", 0.25D) from exit of the rectangular channel.

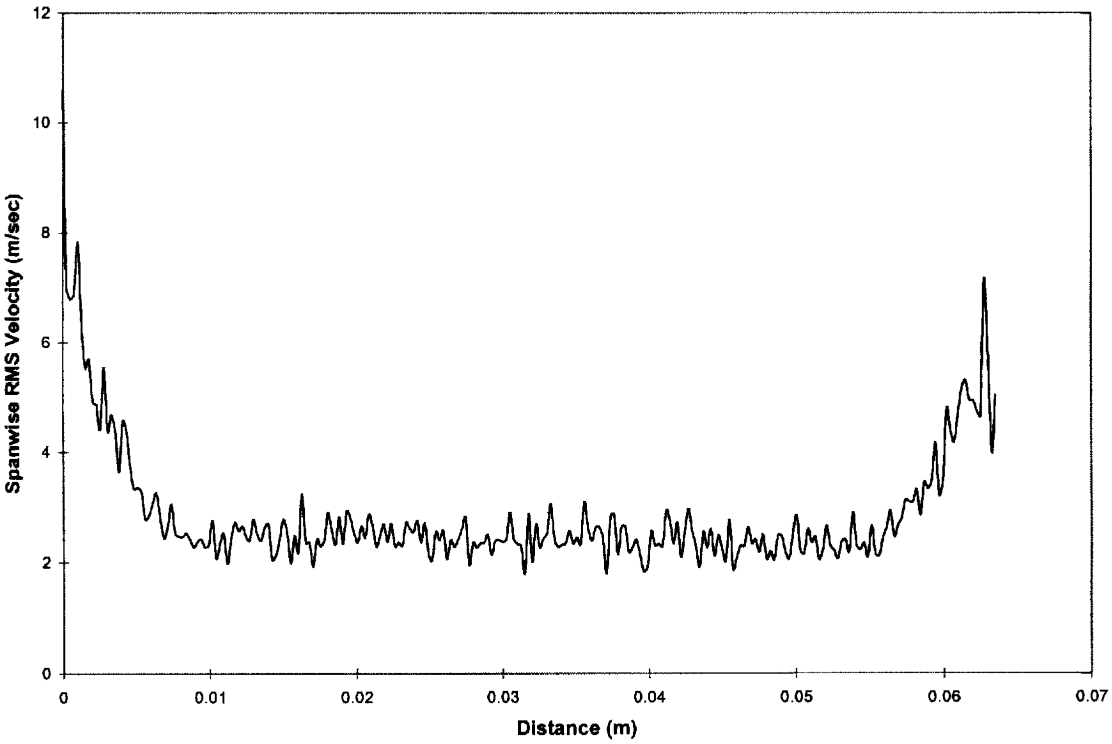

Figure 6.4. Spanwise PDV traverse RMS velocity at 0.0254 m (1", 0.25D) from exit of the rectangular channel.

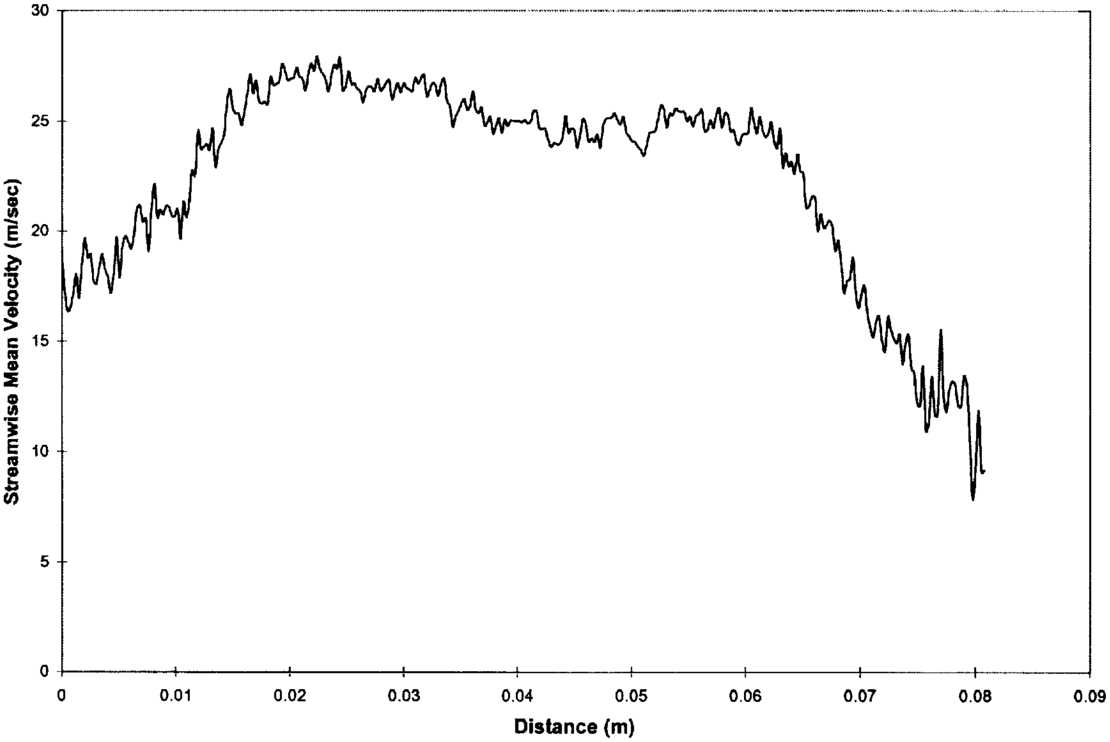

Figure 6.5. Streamwise PDV traverse mean velocity at 0.0762 m (3", 0.75D) from exit of the rectangular channel.

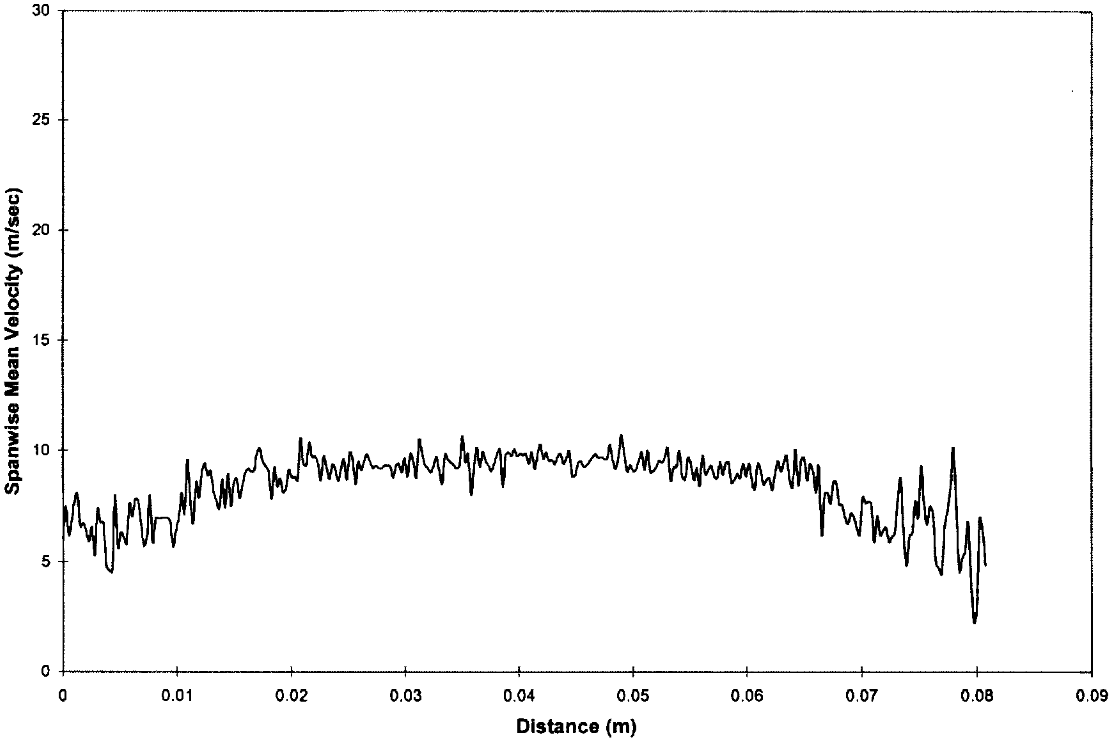

Figure 6.6. Spanwise PDV traverse mean velocity at 0.0762 m (3", 0.75D) from exit of the rectangular channel.

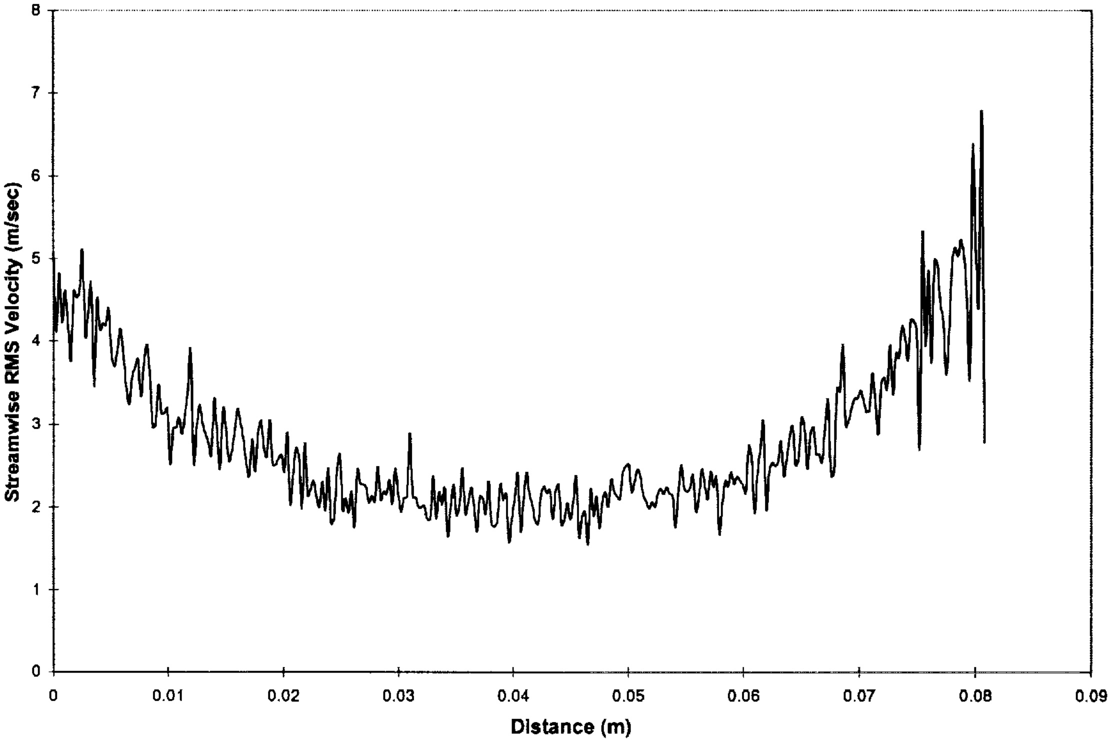

Figure 6.7. Streamwise PDV traverse RMS velocity at 0.0762 m (3", 0.75D) from exit of the rectangular channel.

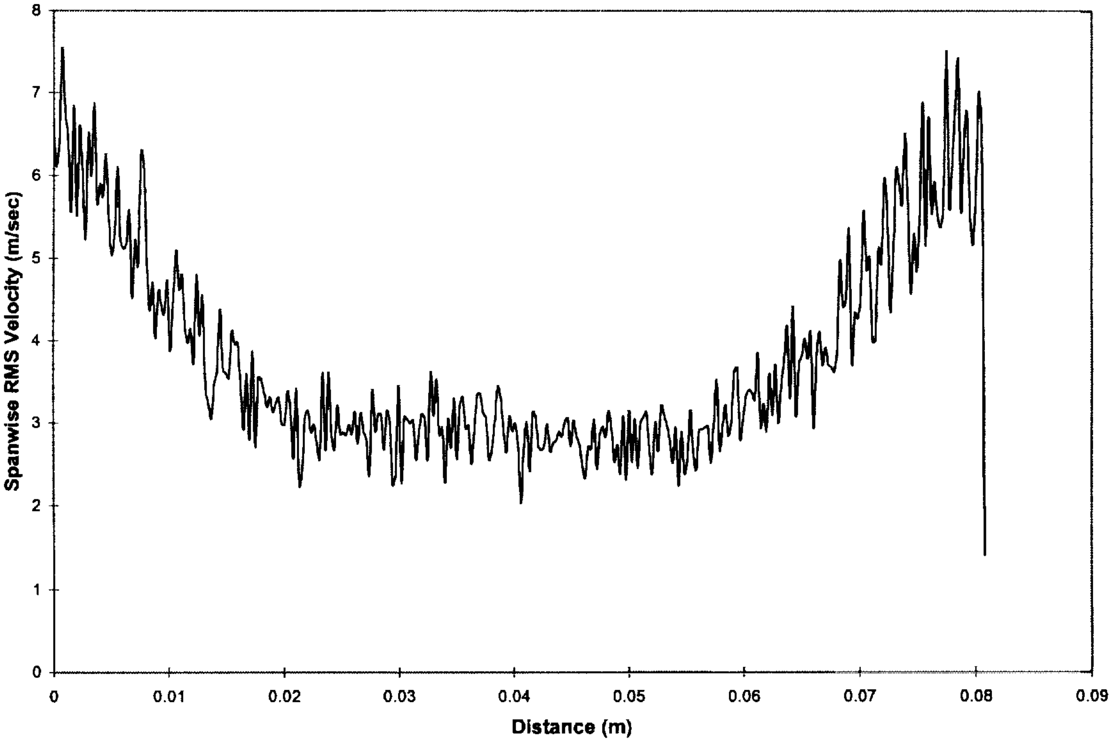

Figure 6.8. Spanwise PDV traverse RMS velocity at 0.0762 m (3", 0.75D) from exit of the rectangular channel.

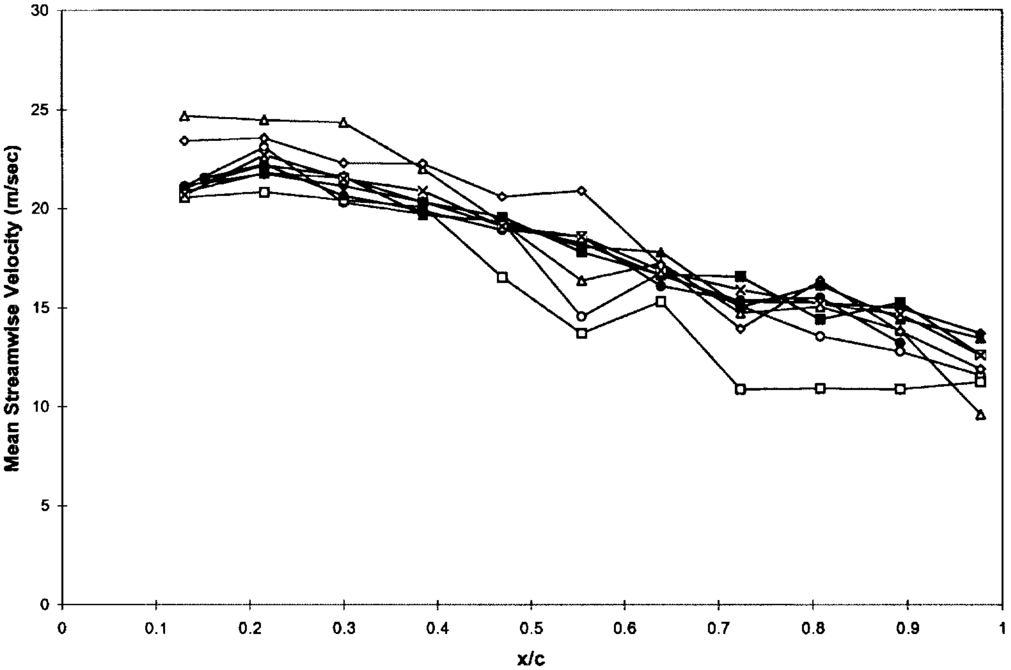

Figure 6.9. Comparison of hot wire and PDV mean streamwise velocity (open symbols - 4 repeat PDV runs, closed symbols - 5 repeat hot wire runs).

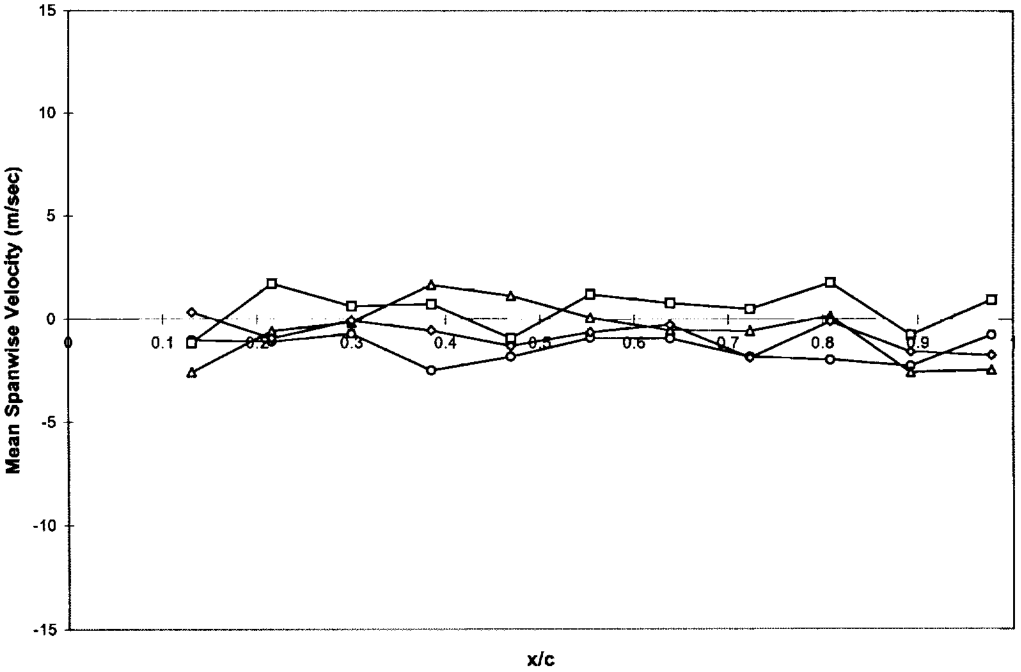

Figure 6.10. PDV mean spanwise velocity (4 repeat PDV runs).

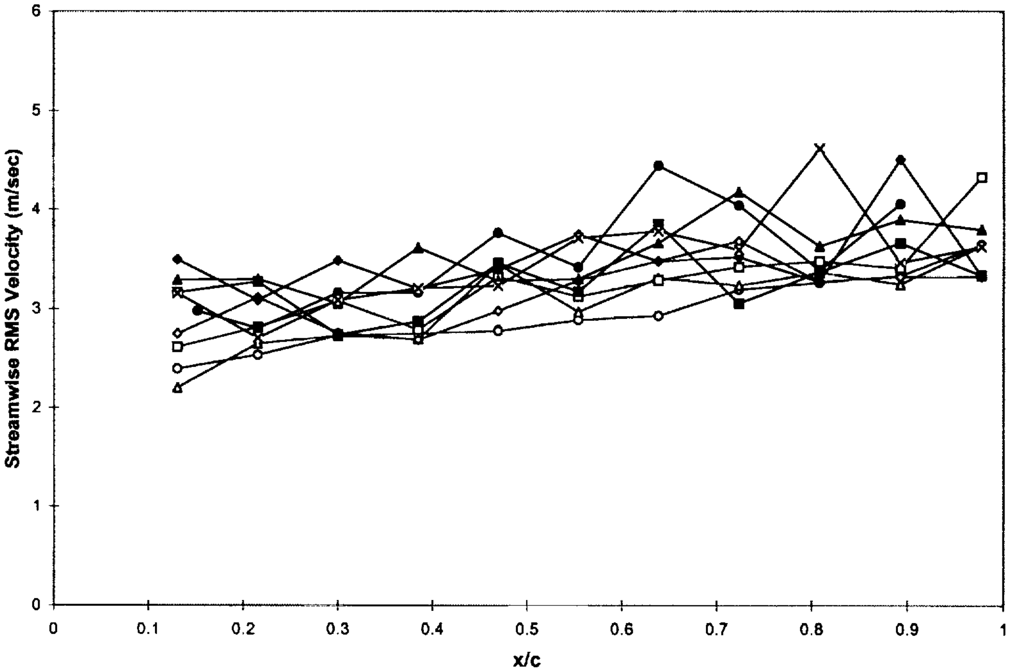

Figure 6.11. Comparison of hot wire and PDV streamwise RMS velocity (open symbols - 4 repeat PDV runs, closed symbols - 5 repeat hot wire runs).

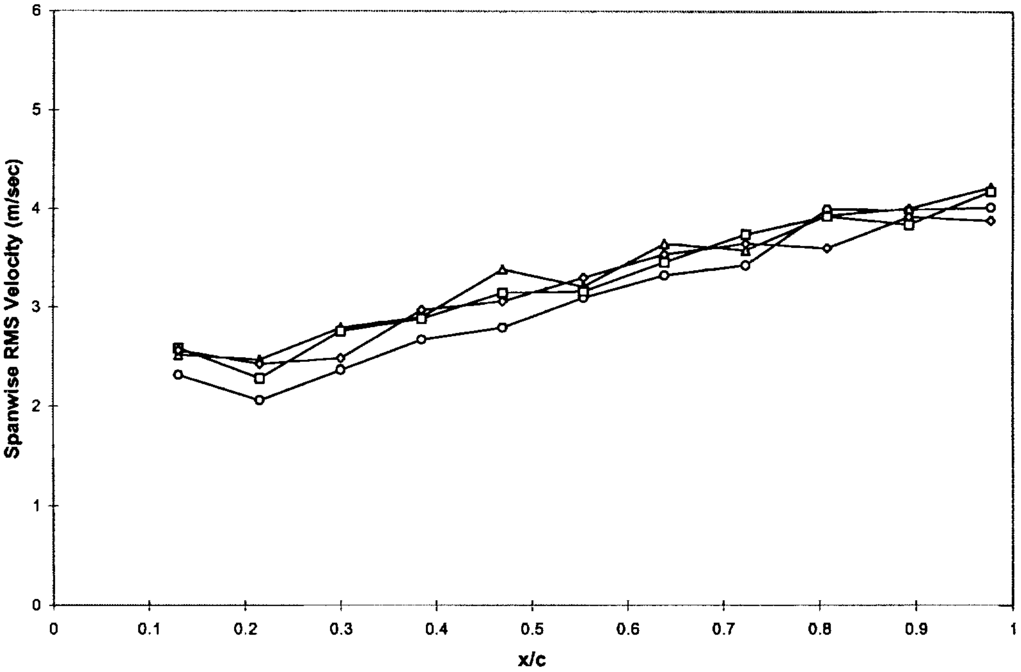

Figure 6.12. PDV spanwise RMS velocity (4 repeat PDV runs).

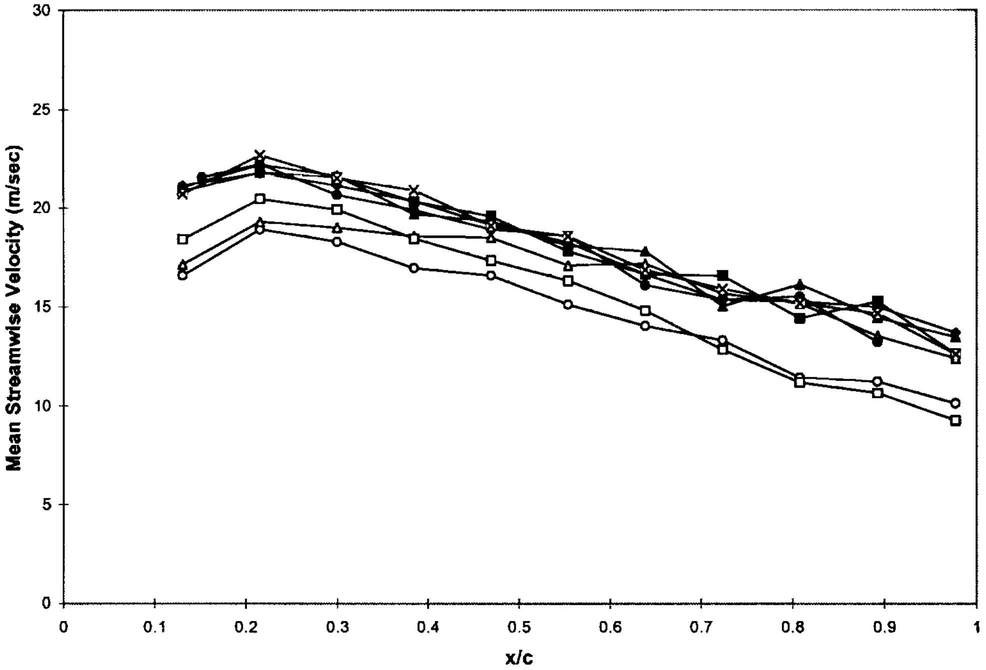

Figure 6.13. Comparison of hot wire and PDV mean streamwise velocity (open symbols - 3 repeat PDV runs, closed symbols - 5 repeat hot wire runs).

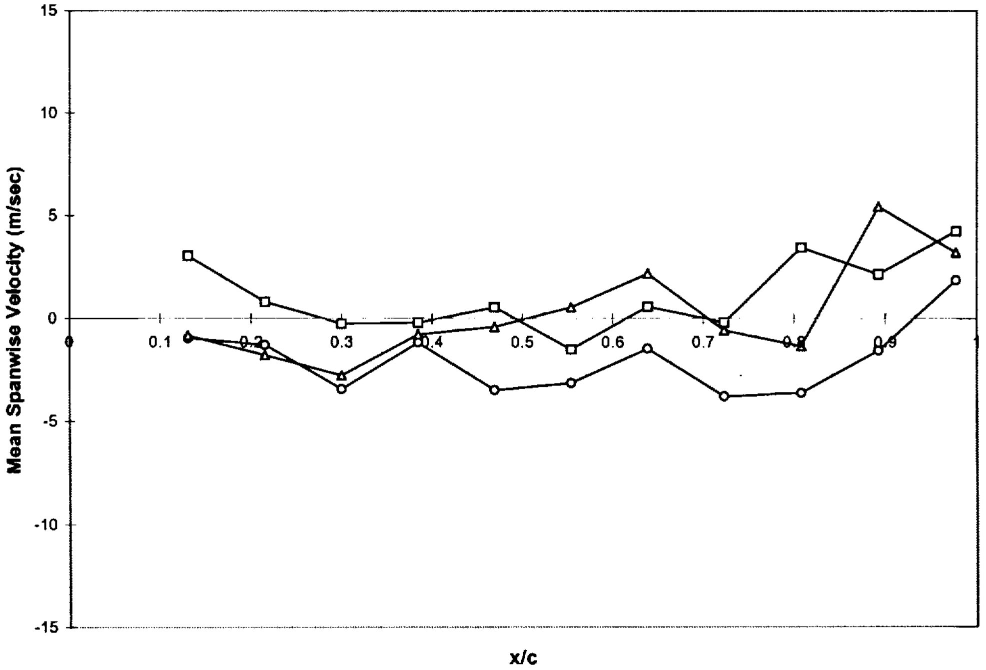

Figure 6.14. PDV mean spanwise velocity (3 repeat PDV runs).

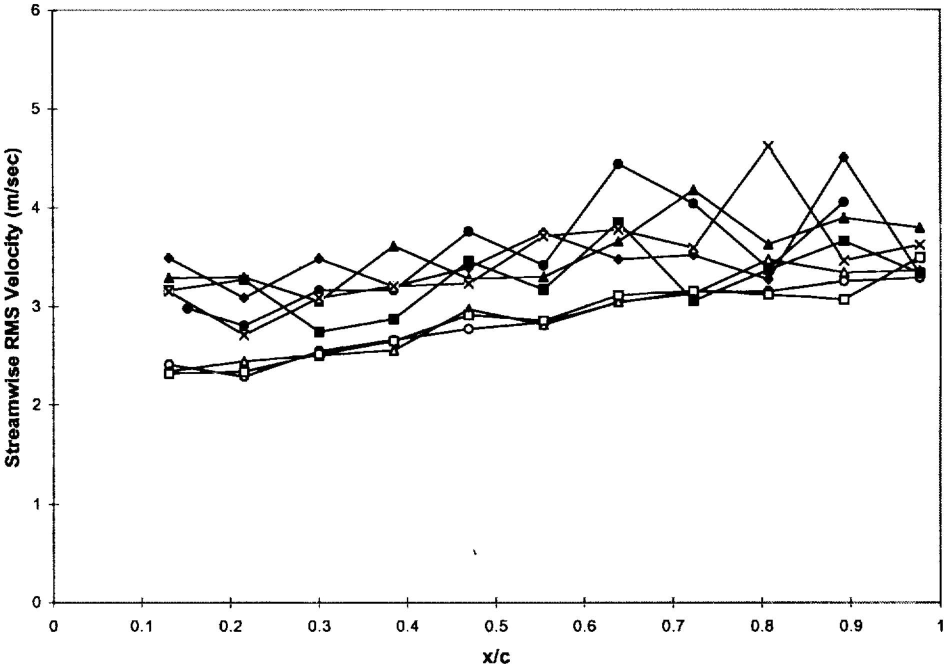

Figure 6.15. Comparison of hot wire and PDV streamwise RMS velocity (open symbols - 3 repeat PDV runs, closed symbols - 5 repeat hot wire runs).

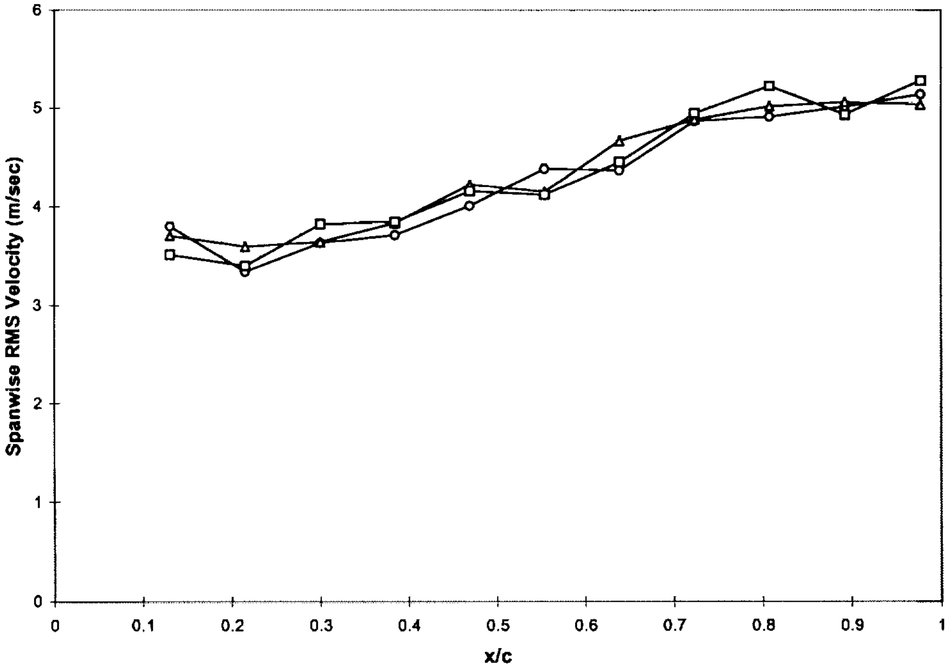

Figure 6.16. PDV spanwise RMS velocity (3 repeat PDV runs).

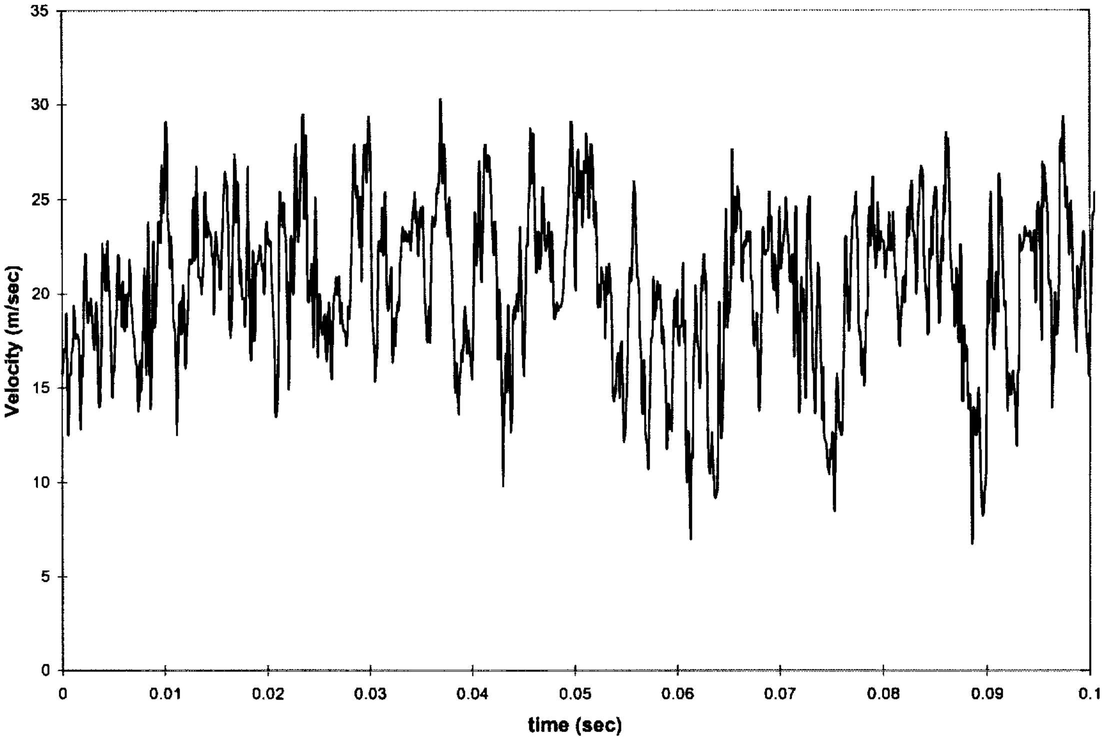

Figure 6.17. Streamwise hot wire time history, x/c = 0.30, z = 1.27 cm (0.5").

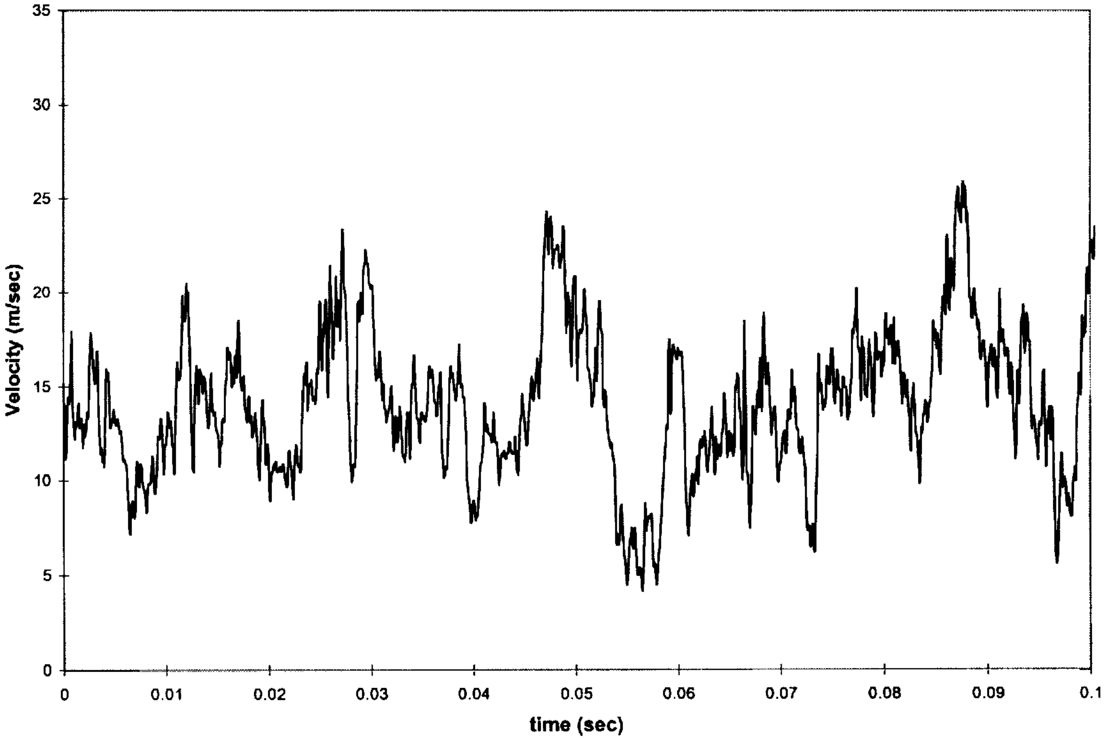

Figure 6.18. Streamwise hot wire time history, x/c = 0.89, z = 1.27 cm (0.5").

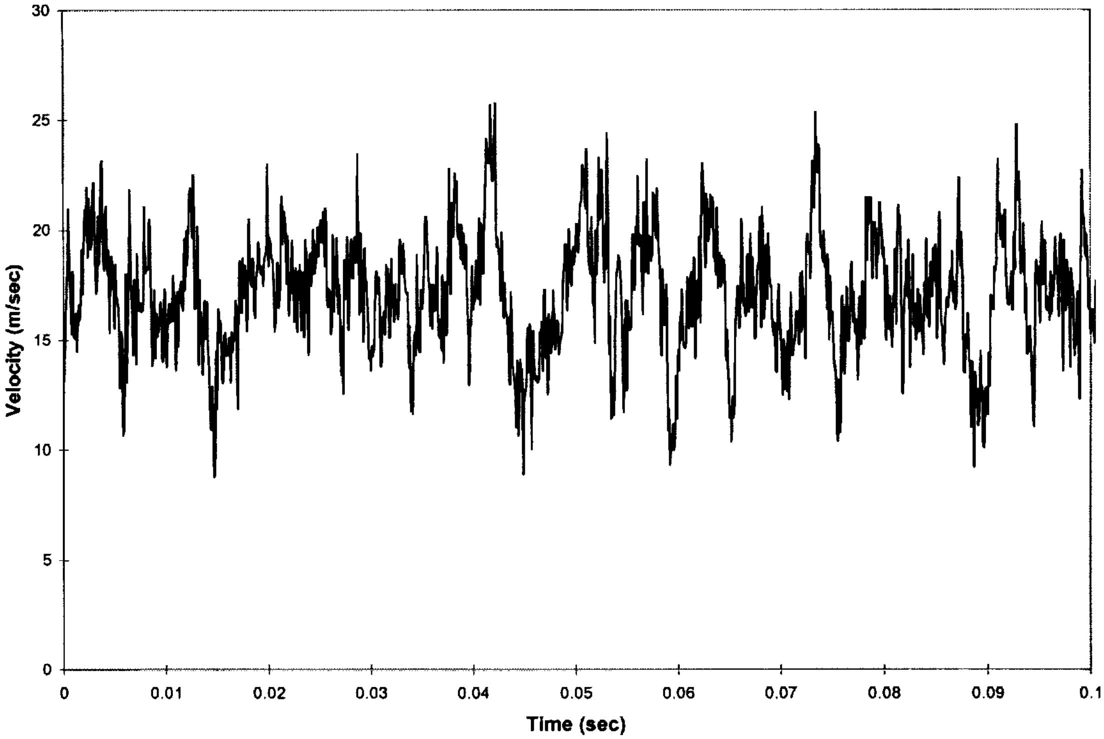

Figure 6.19. Streamwise PDV time history, x/c = 0.30, z = 1.27 cm (0.5").

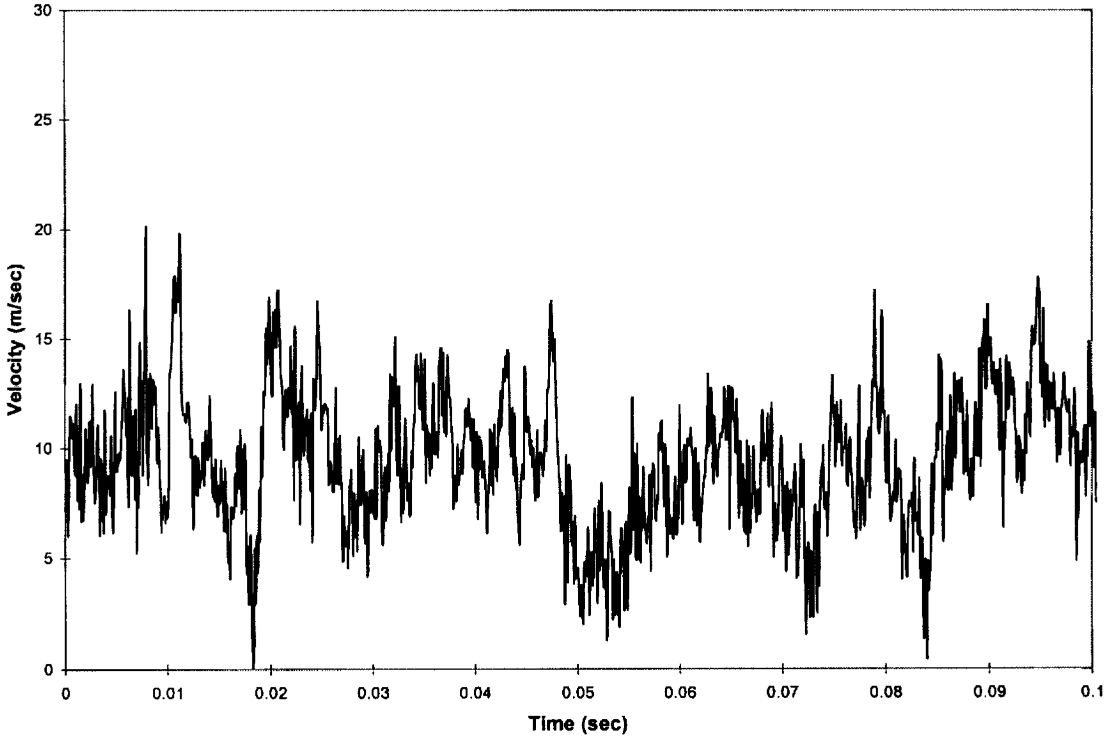

Figure 6.20. Streamwise PDV time history, x/c = 0.89, z = 1.27 cm (0.5").

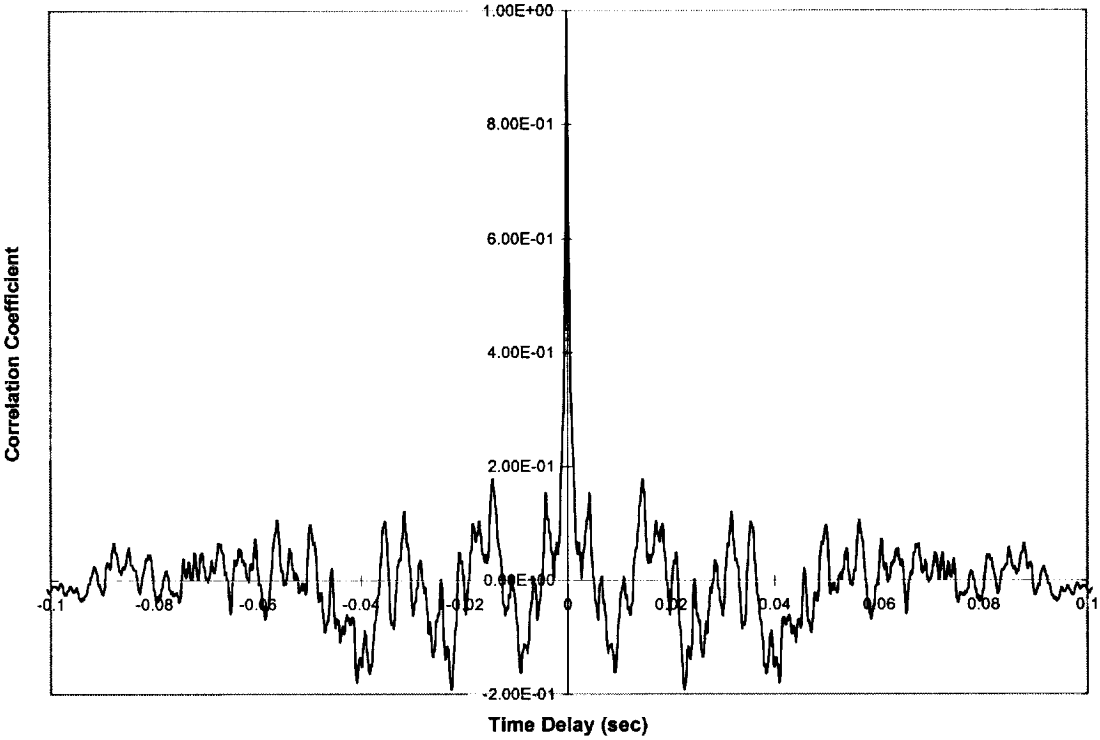

Figure 6.21. Streamwise hot wire correlation coefficient, x/c = 0.30, z = 1.27 cm (0.5").

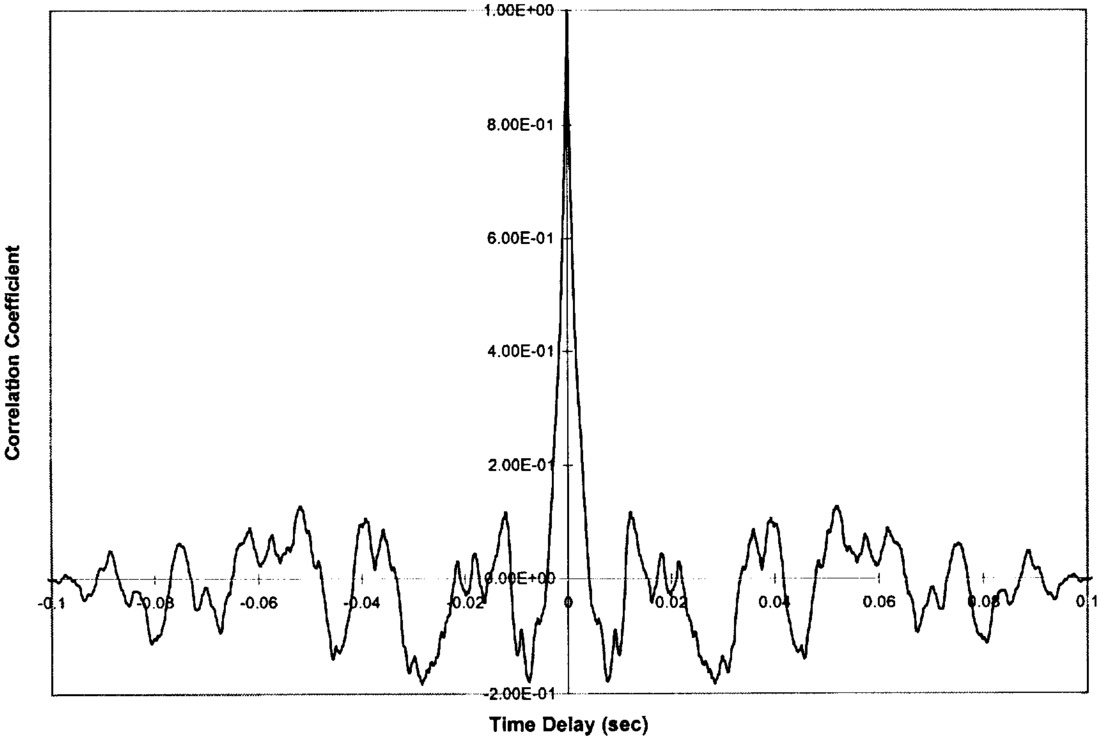

Figure 6.22. Streamwise hot wire correlation coefficient, x/c = 0.89, z = 1.27 cm (0.5").

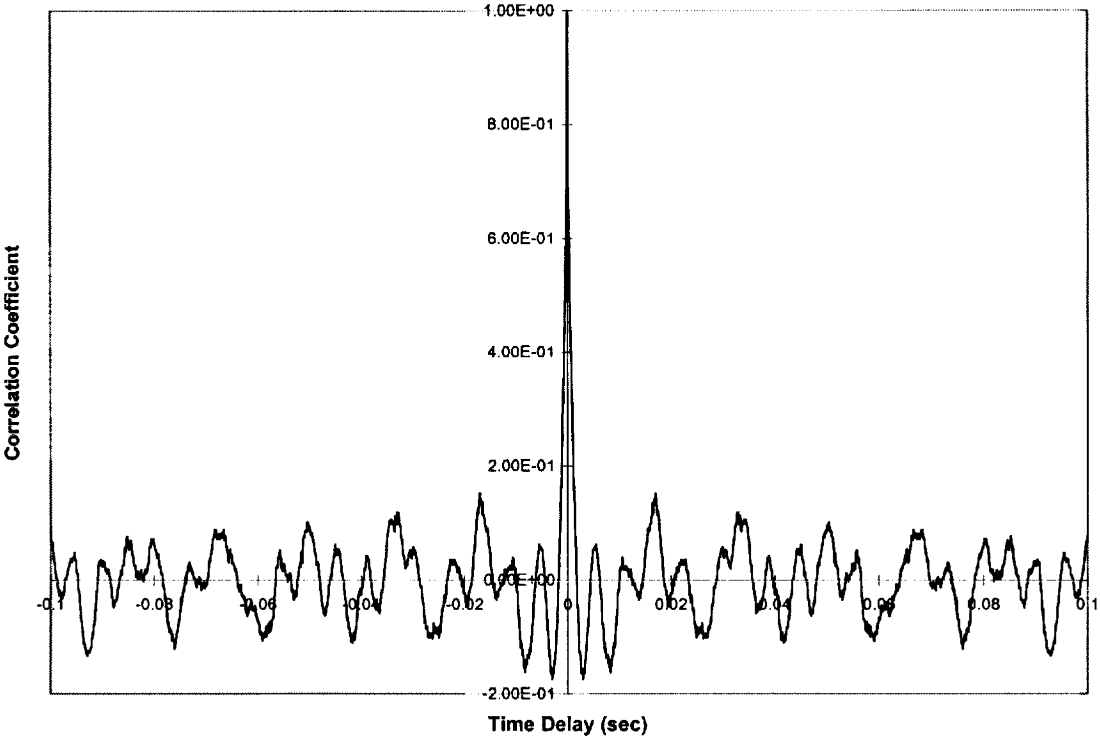

Figure 6.23. Streamwise PDV correlation coefficient, x/c = 0.30, z = 1.27 cm (0.5").

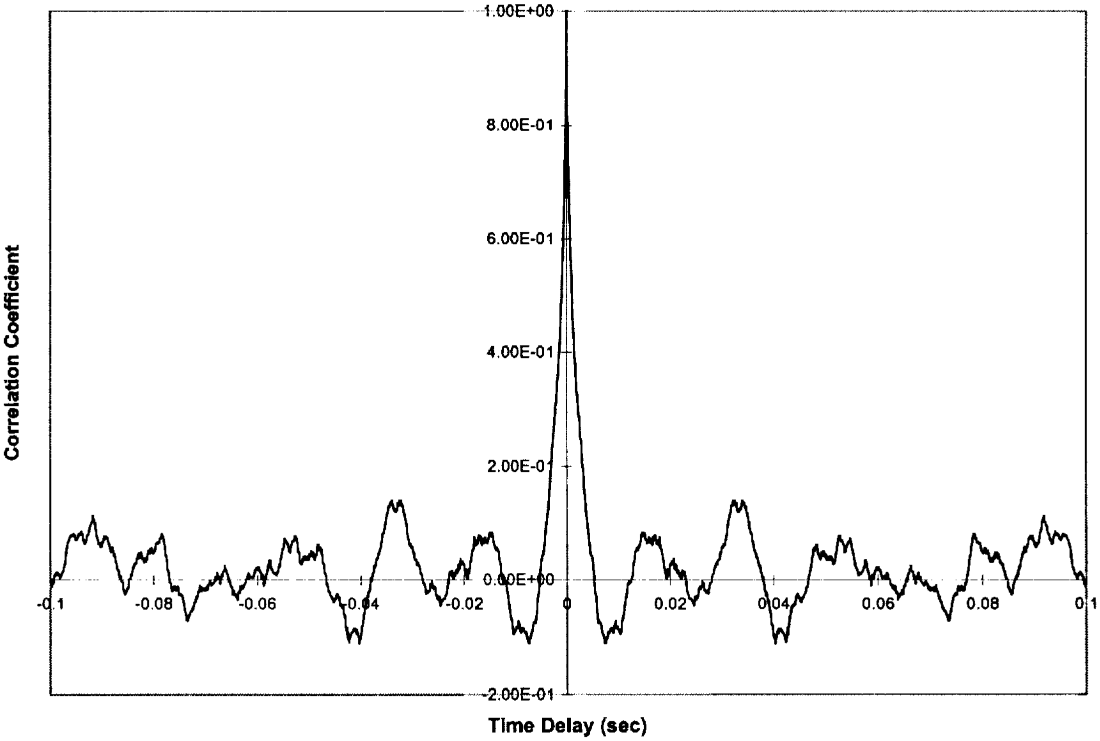

Figure 6.24. Streamwise PDV correlation coefficient, x/c = 0.89, z = 1.27 cm (0.5").

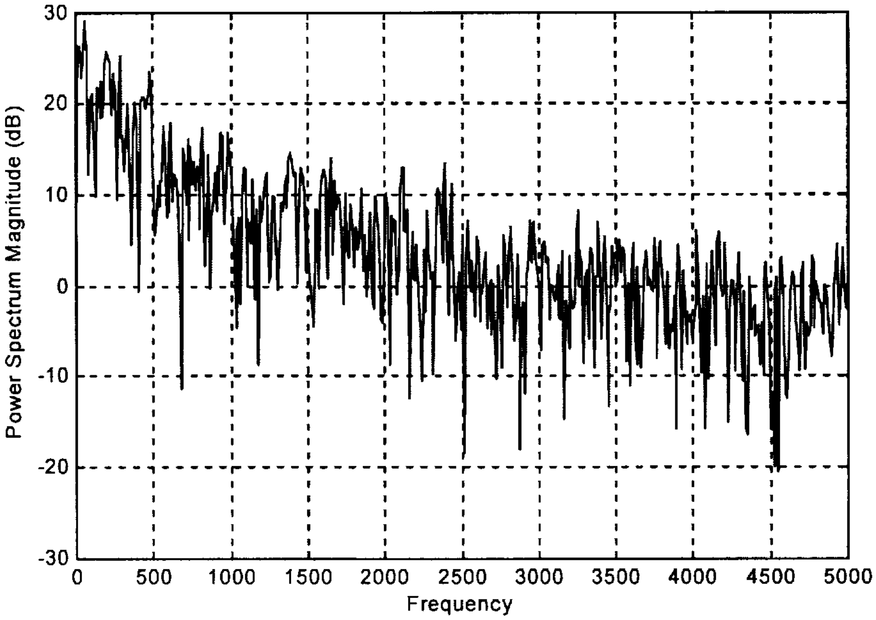

Figure 6.25. Streamwise hot wire power spectral density, x/c = 0.30, z = 1.27 cm (0.5").

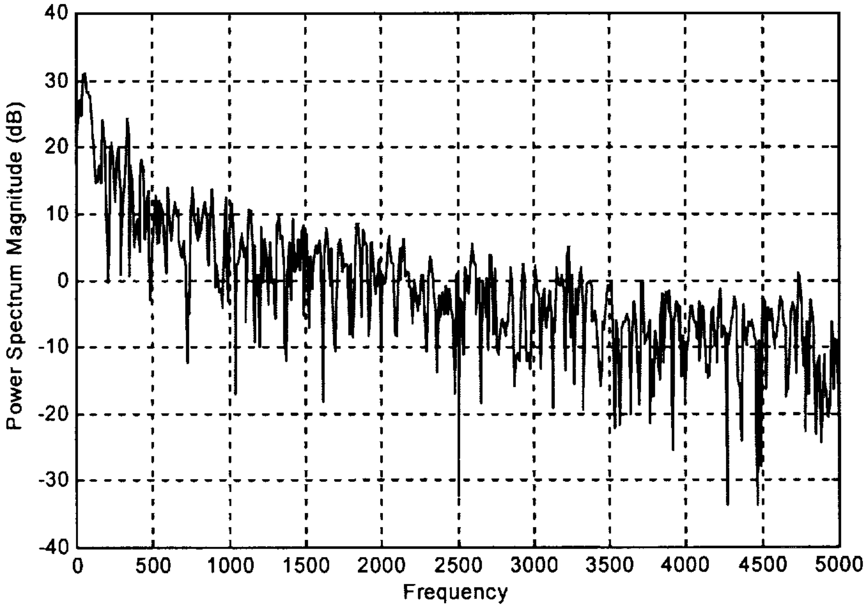

Figure 6.26. Streamwise hot wire power spectral density, x/c = 0.89, z = 1.27 cm (0.5").

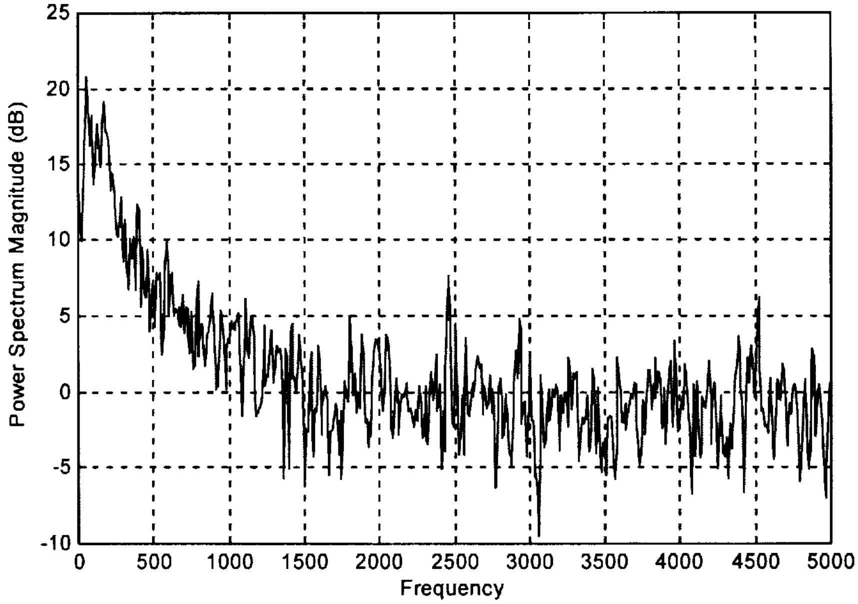

Figure 6.27. Streamwise PDV power spectral density, x/c = 0.30, z = 1.27 cm (0.5").

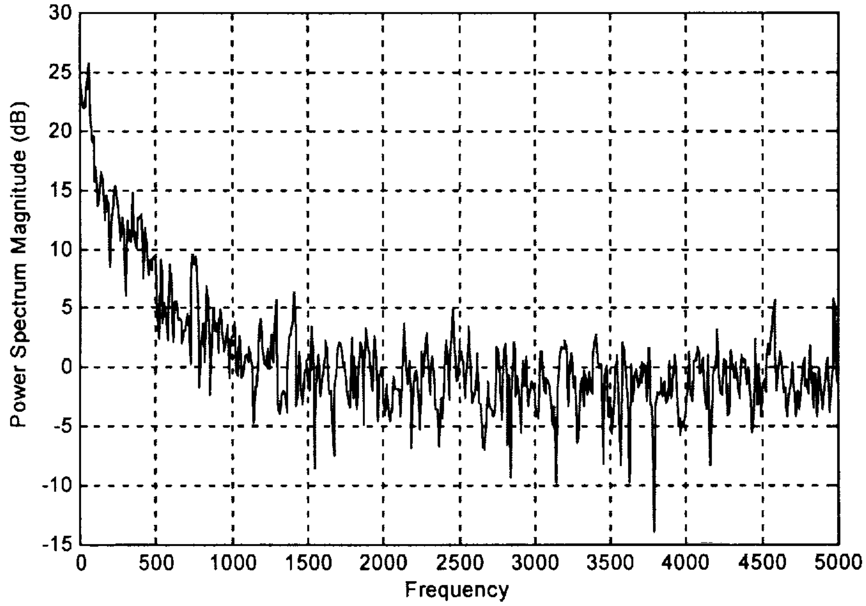

Figure 6.28. Streamwise PDV power spectral density, x/c = 0.89, z = 1.27 cm (0.5").

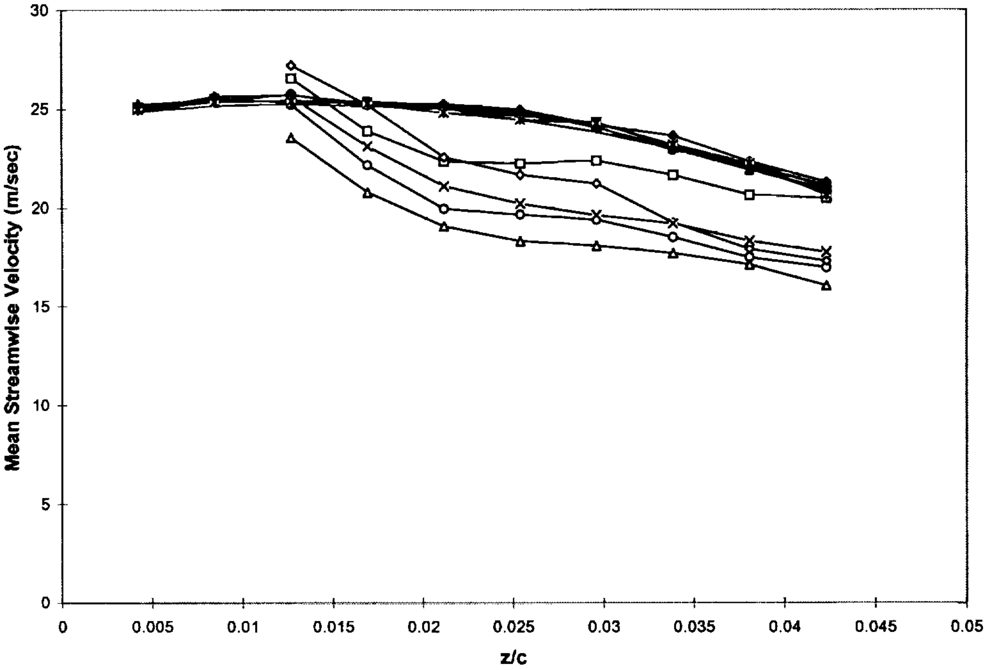

Figure 6.29. Comparison of hot wire and PDV mean streamwise velocity (open symbols - 5 repeat PDV runs, closed symbols - 6 repeat hot wire runs).

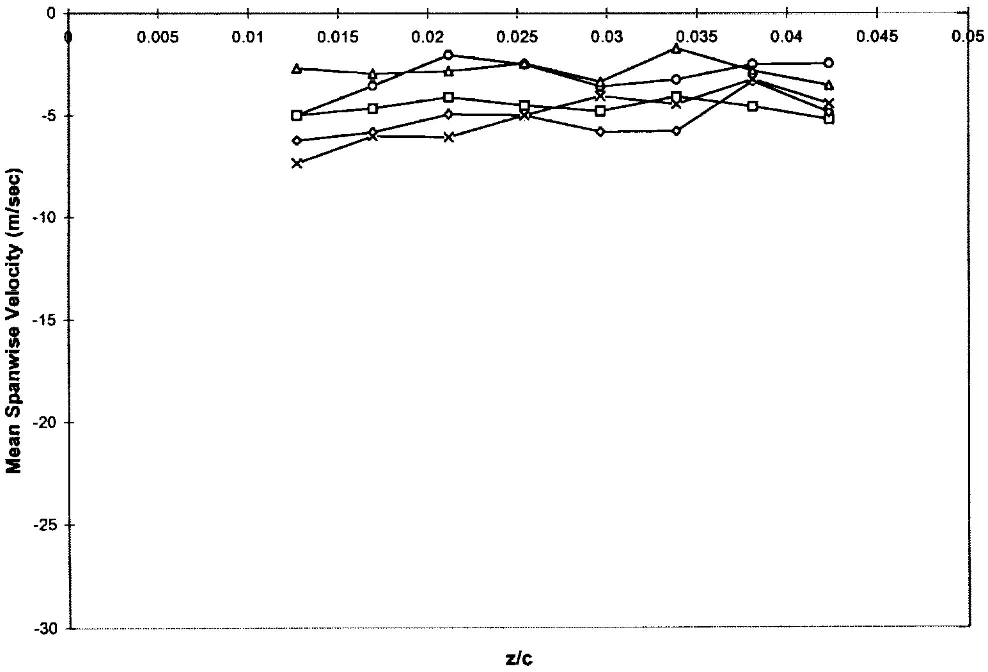

Figure 6.30. PDV mean spanwise velocity (5 repeat PDV runs).

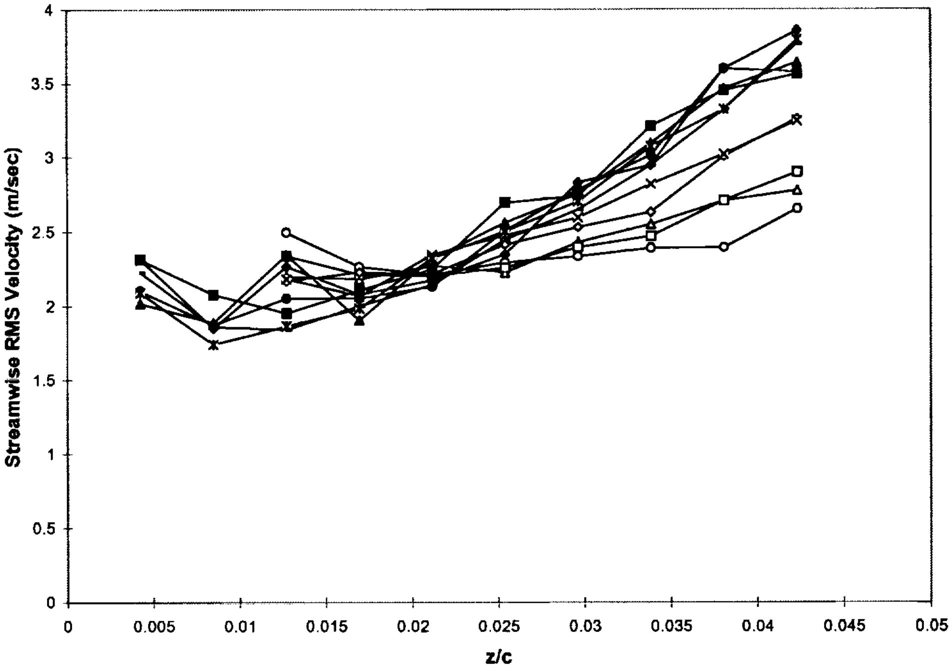

Figure 6.31. Comparison of hot wire and PDV streamwise RMS velocity (open symbols - 5 repeat PDV runs, closed symbols - 6 repeat hot wire runs).

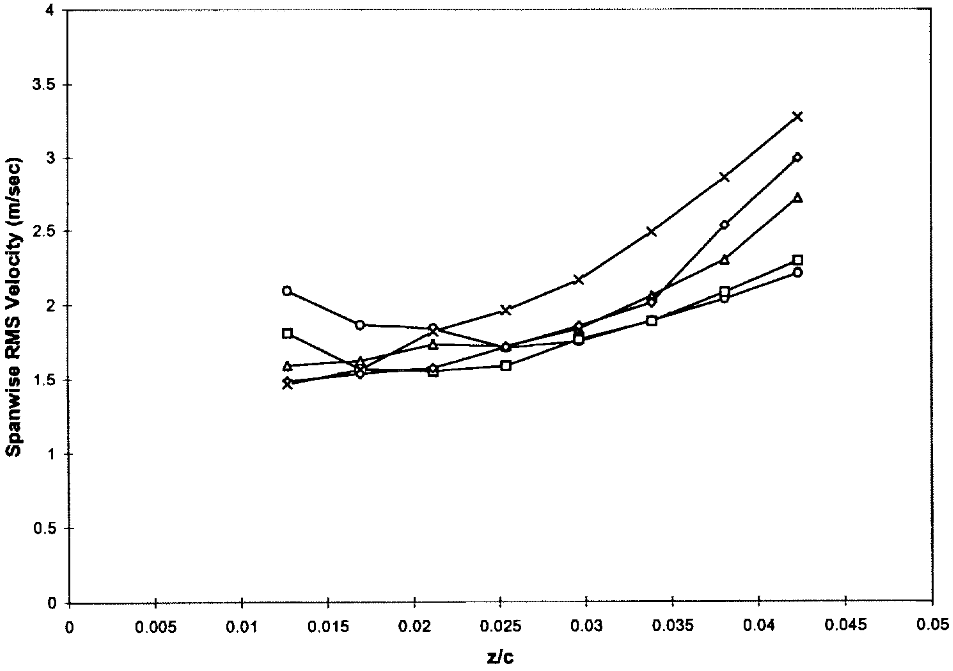

Figure 6.32. PDV spanwise RMS velocity (5 repeat PDV runs).

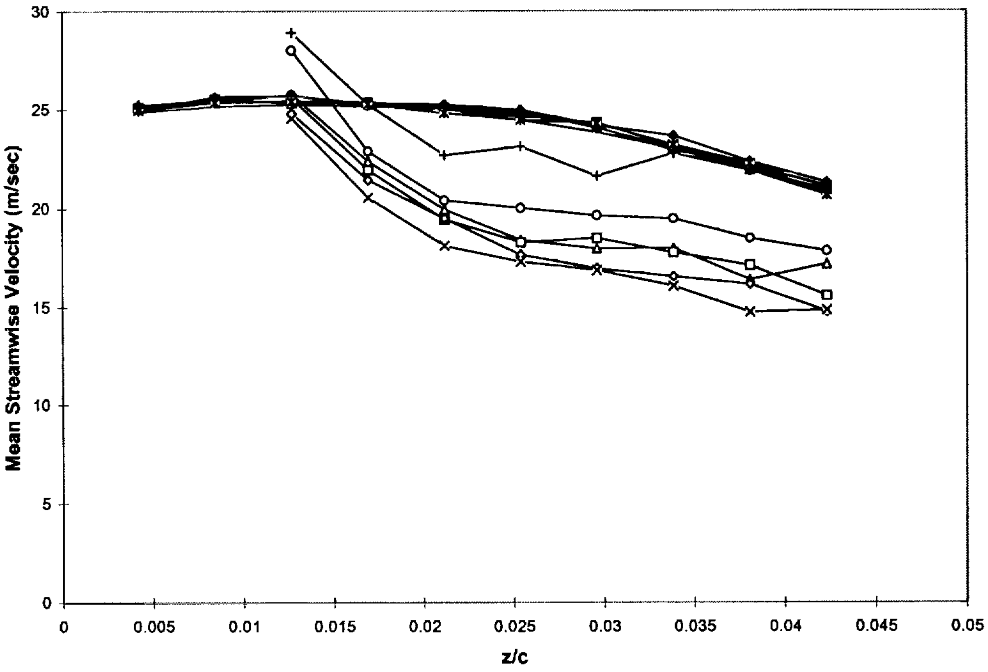

Figure 6.33. Comparison of hot wire and PDV mean streamwise velocity (open symbols - 6 repeat PDV runs, closed symbols - 6 repeat hot wire runs).

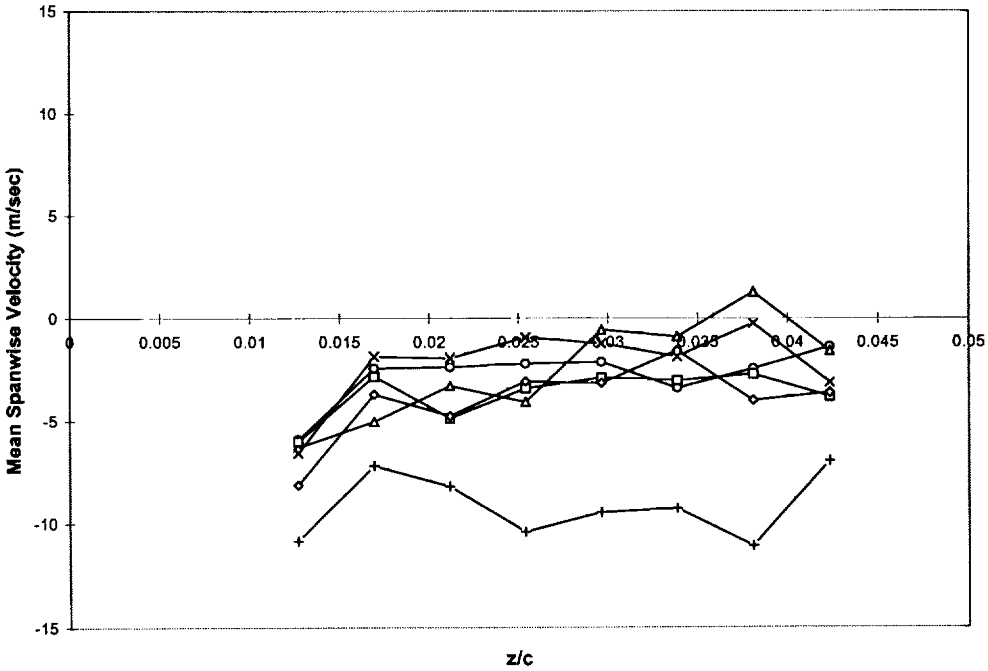

Figure 6.34. PDV mean spanwise velocity (6 repeat PDV runs).

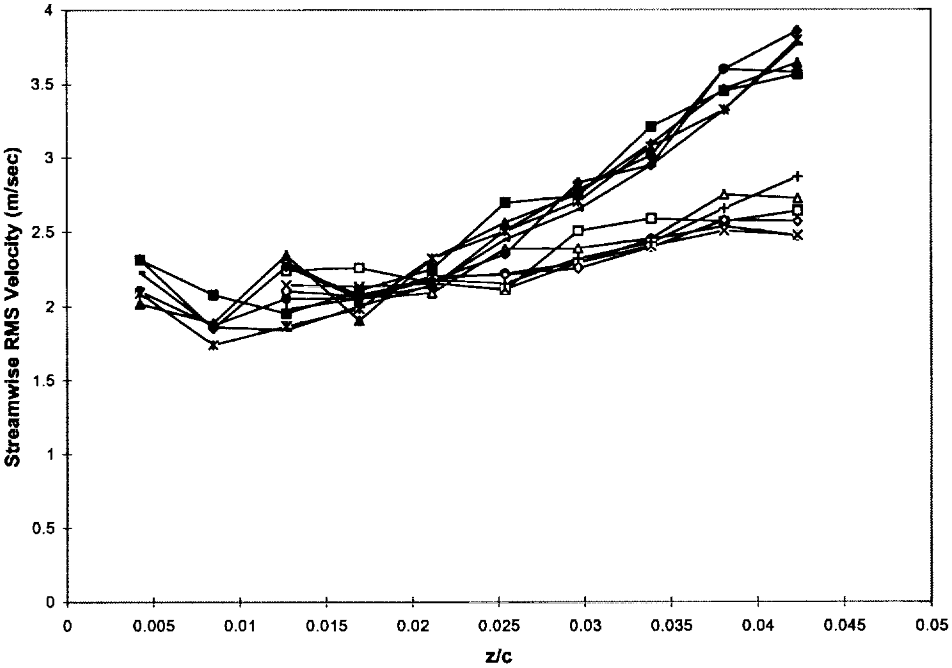

Figure 6.35. Comparison of hot wire and PDV streamwise RMS velocity (open symbols - 6 repeat PDV runs, closed symbols - 6 repeat hot wire runs).

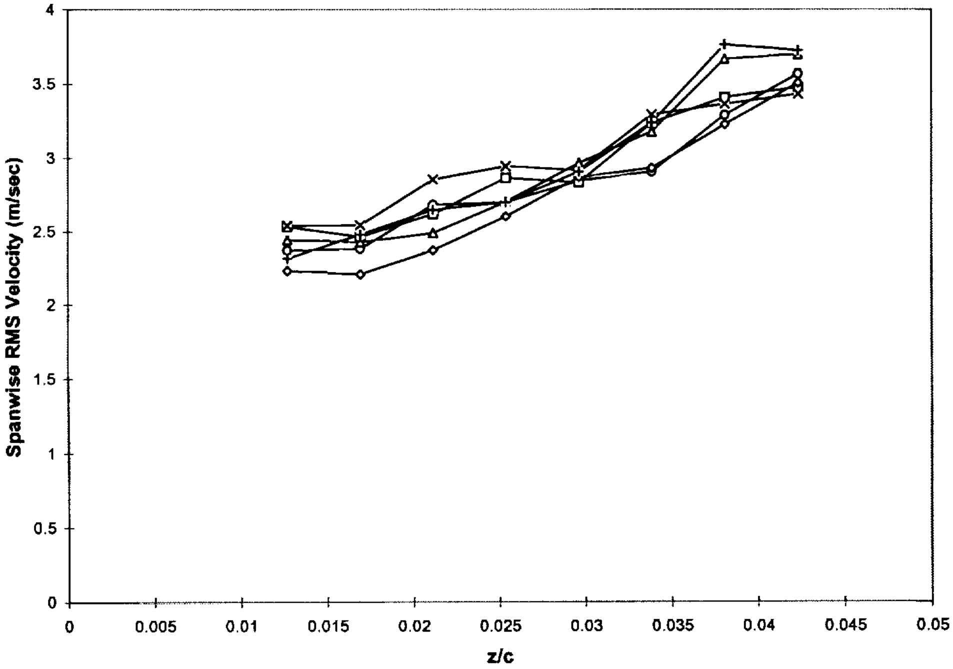

Figure 6.36. PDV spanwise RMS velocity (6 repeat PDV runs).

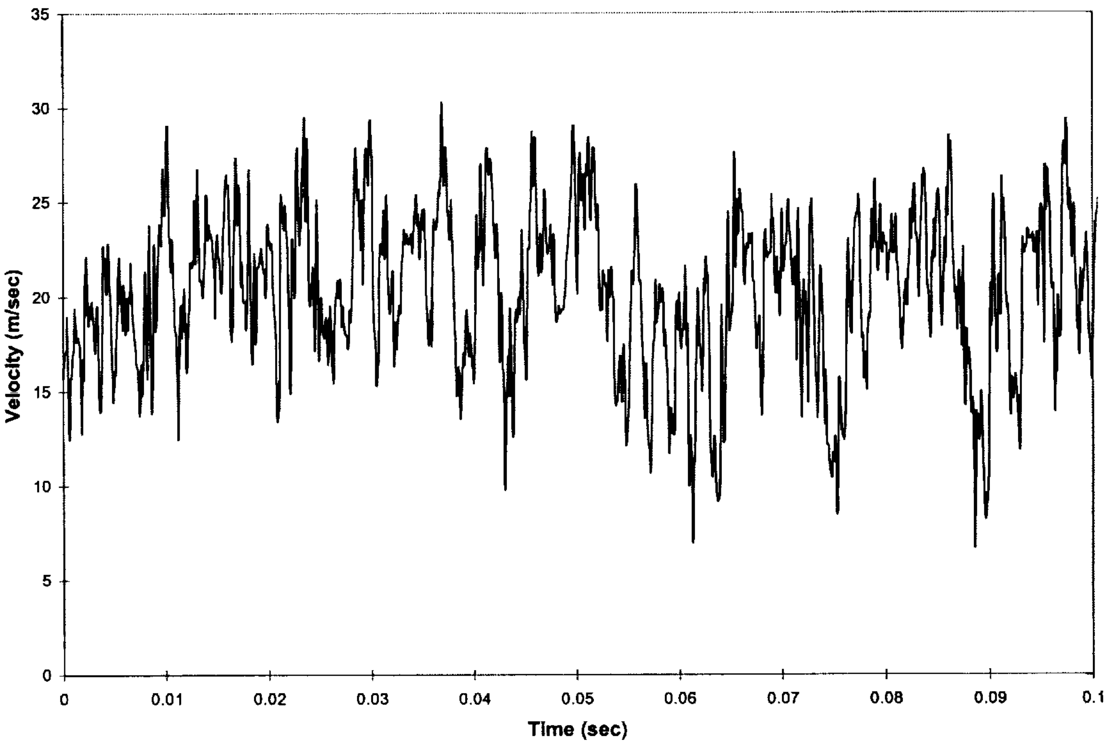

Figure 6.37. Streamwise hot wire time history, x/c = 0.30, z = 1.27 cm (0.5”).

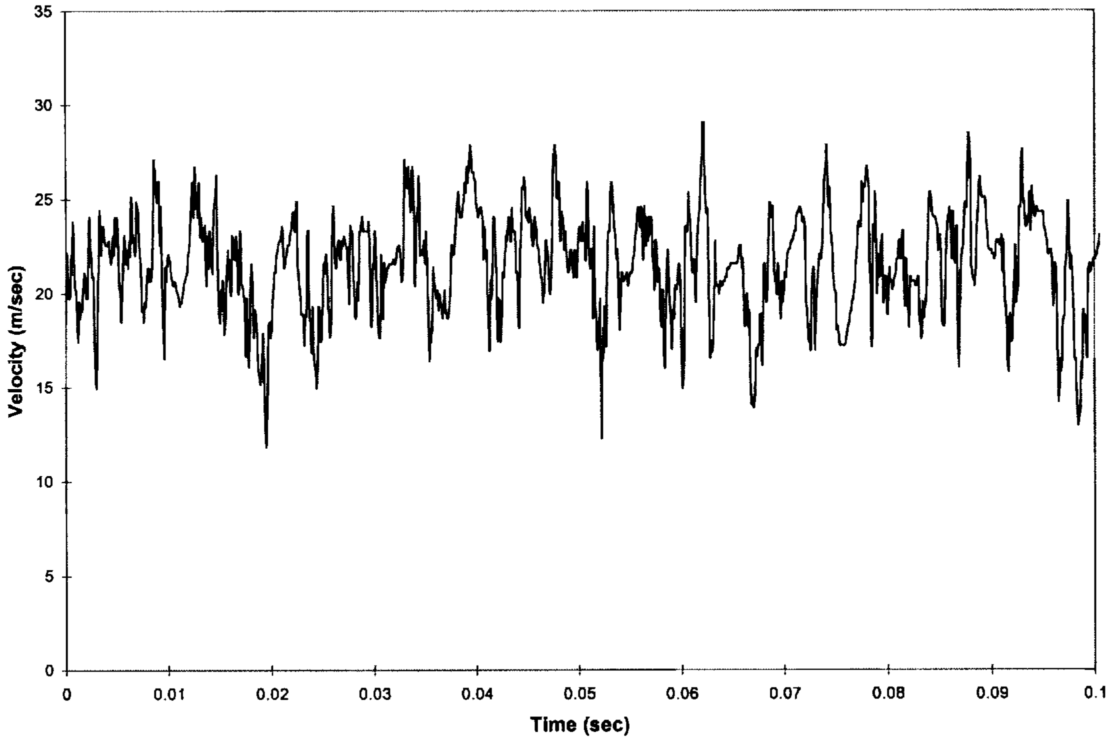

Figure 6.38. Streamwise hot wire time history, x/c = 0.30, z = 0.508 cm (0.2”).

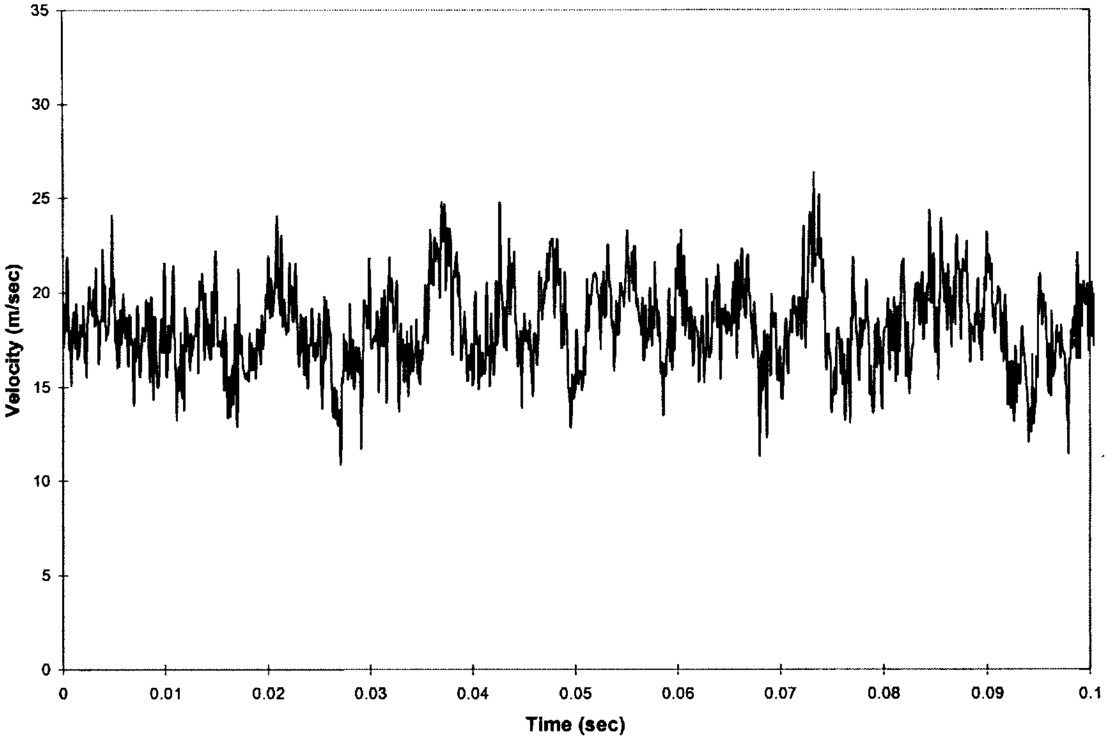

Figure 6.39. Streamwise PDV time history, x/c = 0.30, z = 1.27 cm (0.5”).

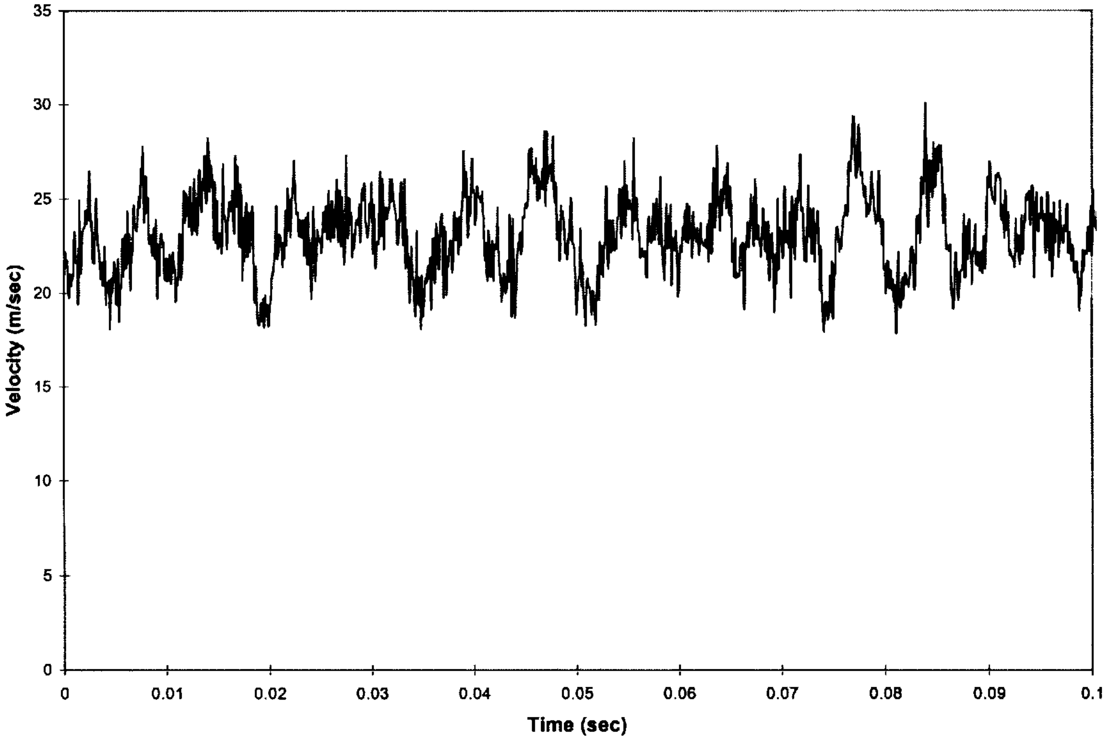

Figure 6.40. Streamwise PDV time history, x/c = 0.30, z = 0.508 cm (0.2”).

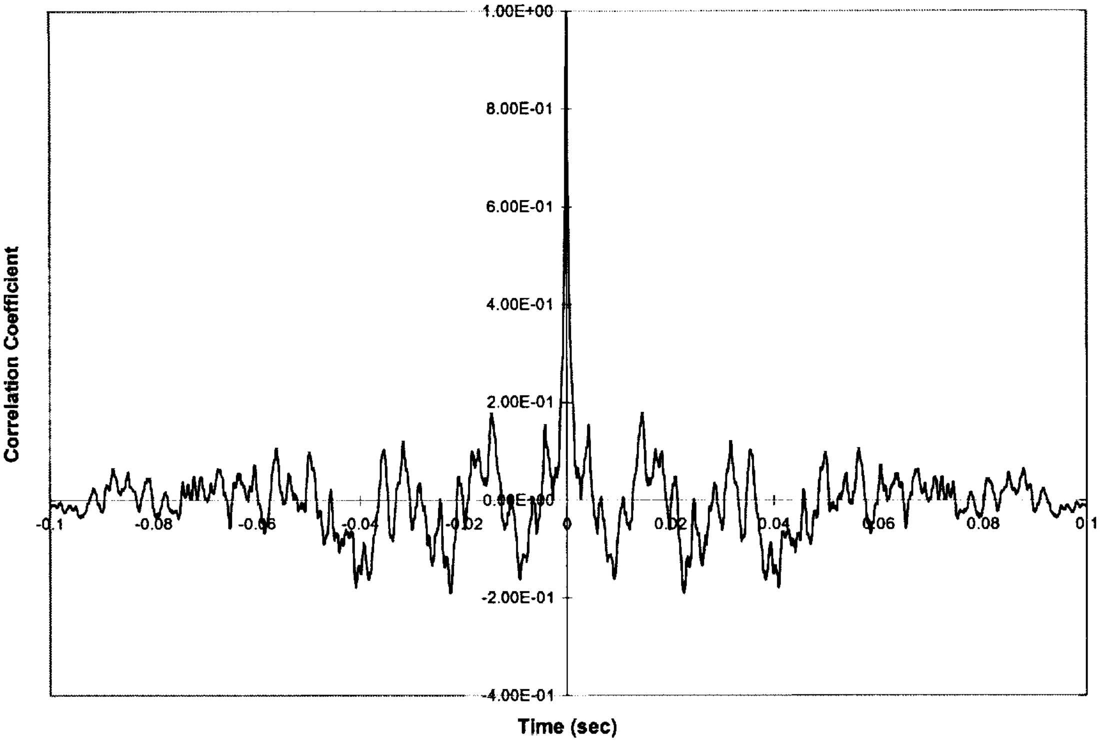

Figure 6.41. Streamwise hot wire correlation coefficient, x/c = 0.30, z = 1.27 cm (0.5").

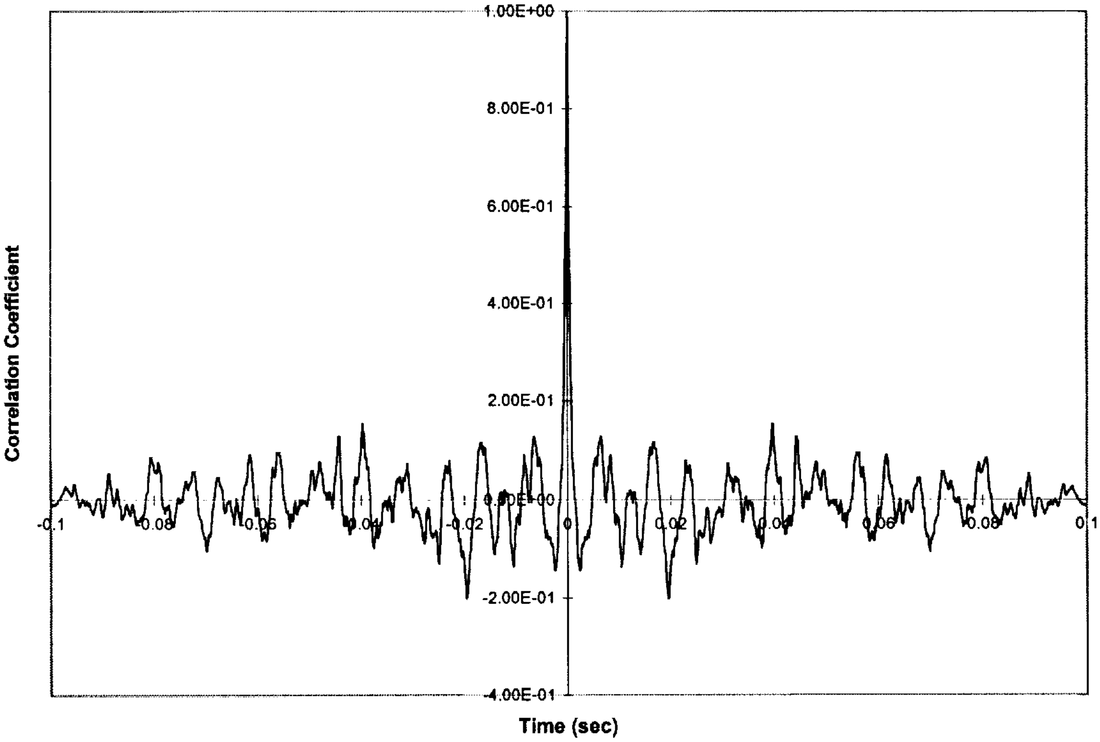

Figure 6.42. Streamwise hot wire correlation coefficient, x/c = 0.30, z = 0.508 cm (0.2").

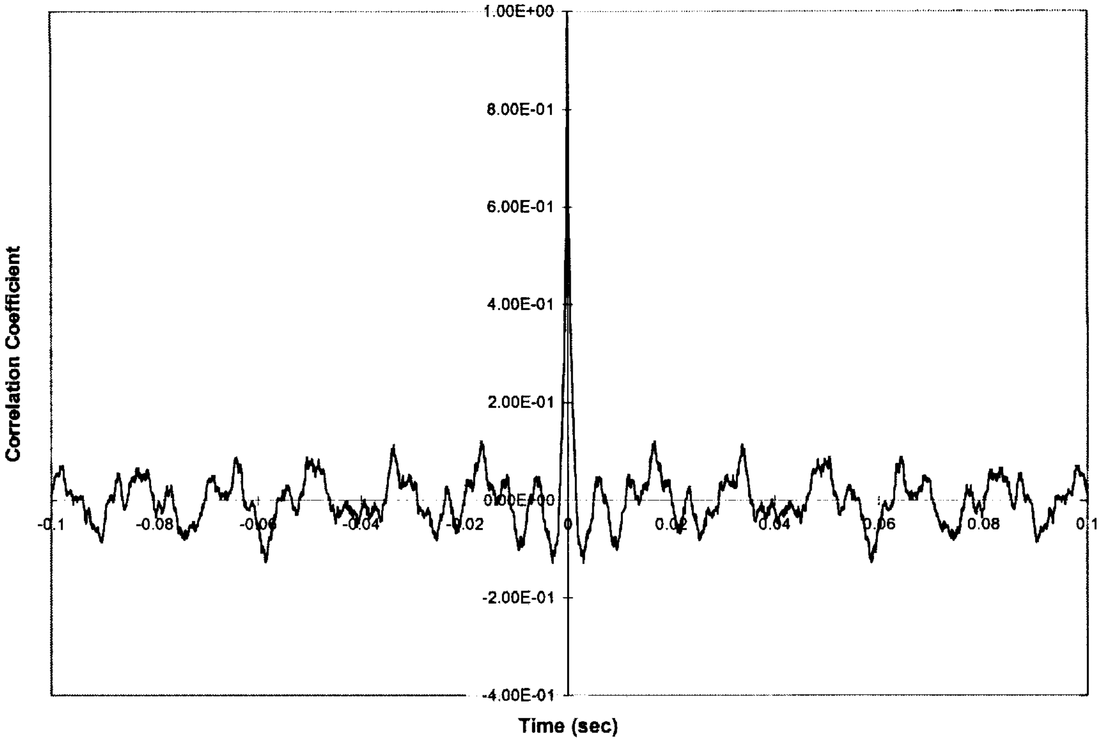

Figure 6.43. Streamwise PDV correlation coefficient, x/c = 0.30, z = 1.27 cm (0.5”).

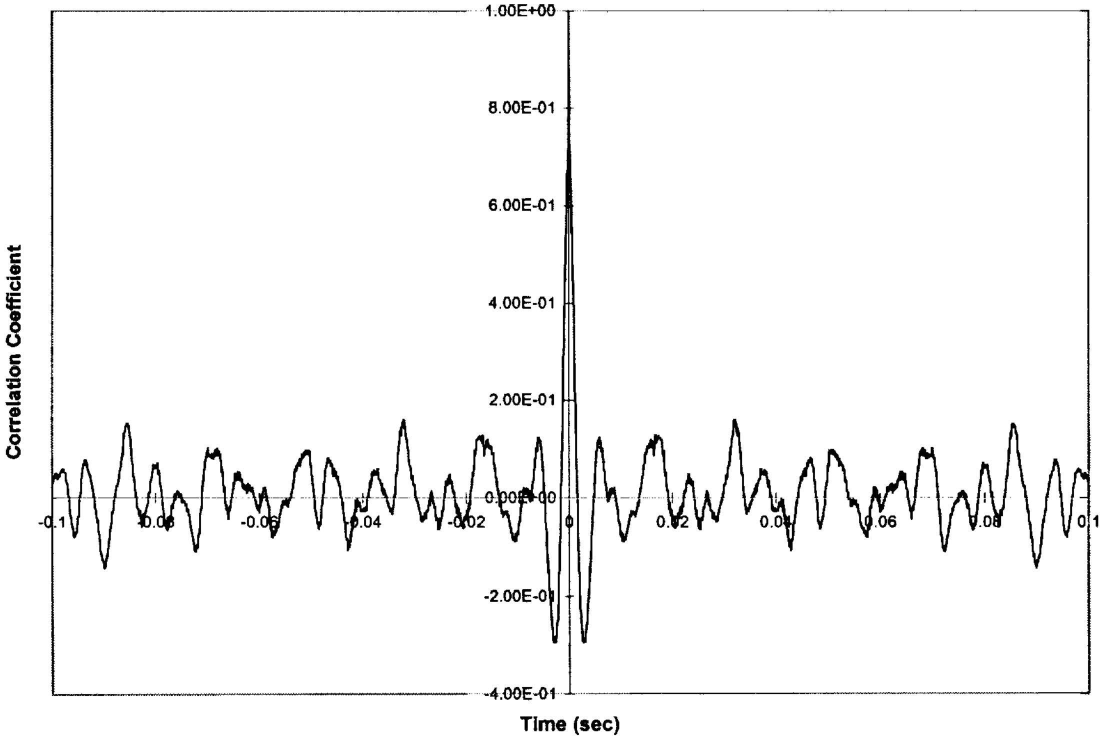

Figure 6.44. Streamwise PDV correlation coefficient, x/c = 0.30, z = 0.508 cm (0.2”).

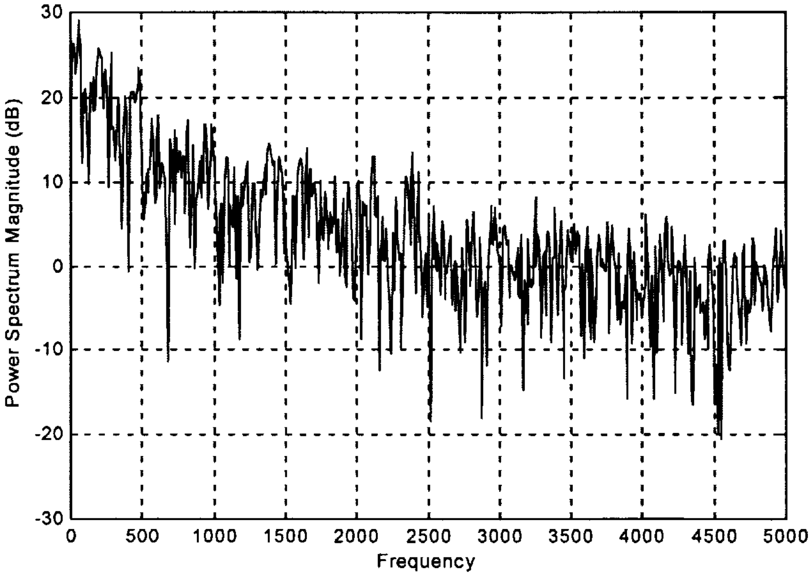

Figure 6.45. Streamwise hot wire power spectral density, x/c = 0.30, z = 1.27 cm (0.5").

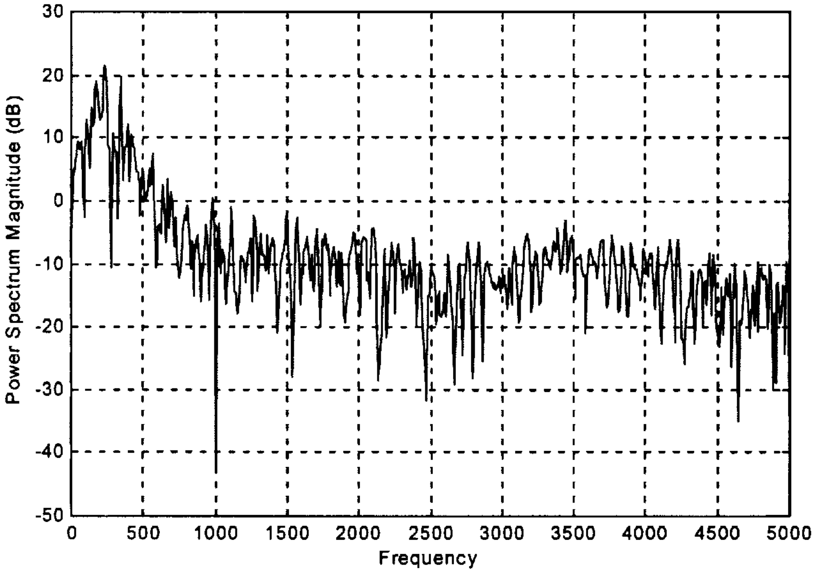

Figure 6.46. Streamwise hot wire power spectral density, x/c = 0.30, z = 0.508 cm (0.2").

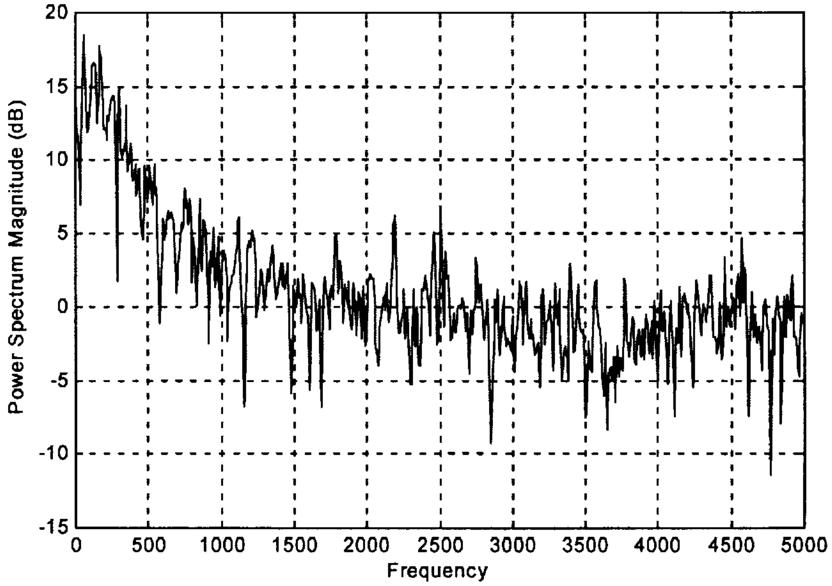

Figure 6.47. Streamwise PDV power spectral density, x/c = 0.30, z = 1.27 cm (0.5").

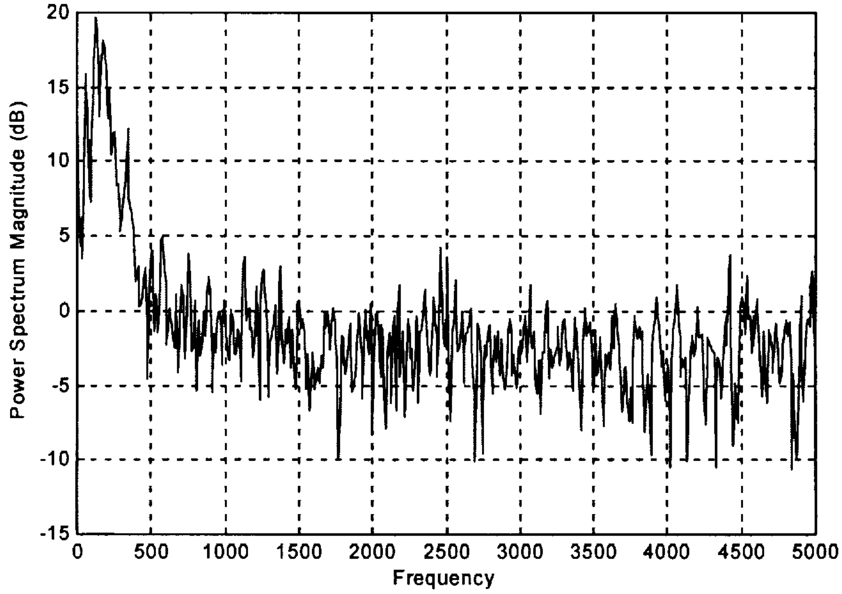

Figure 6.48. Streamwise PDV power spectral density, x/c = 0.30, z = 0.508 cm (0.2").

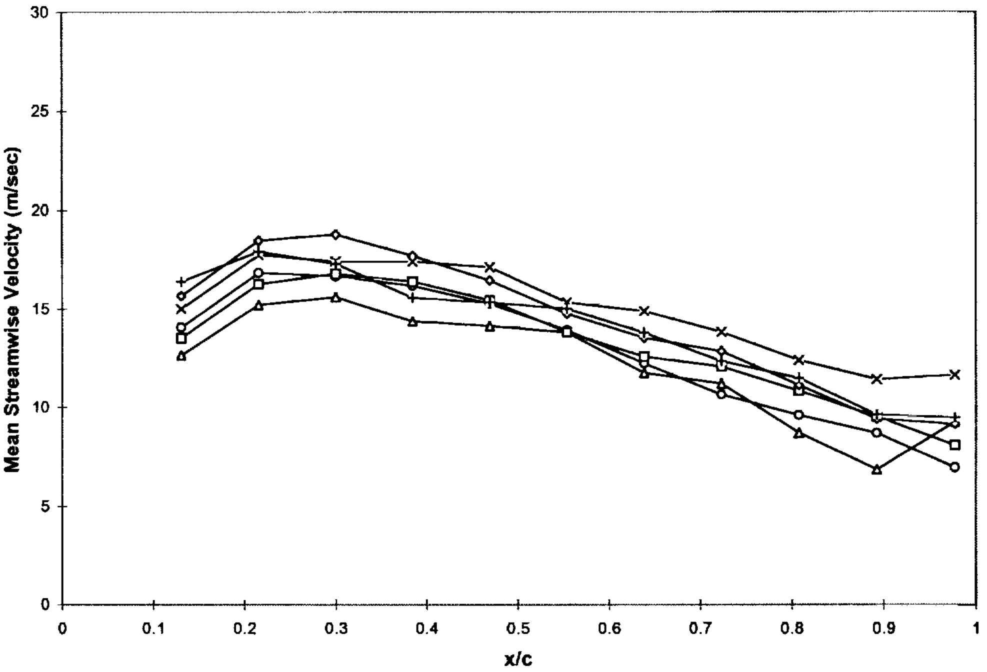

Figure 6.49. PDV mean streamwise velocity with polarizing film (6 repeat runs).

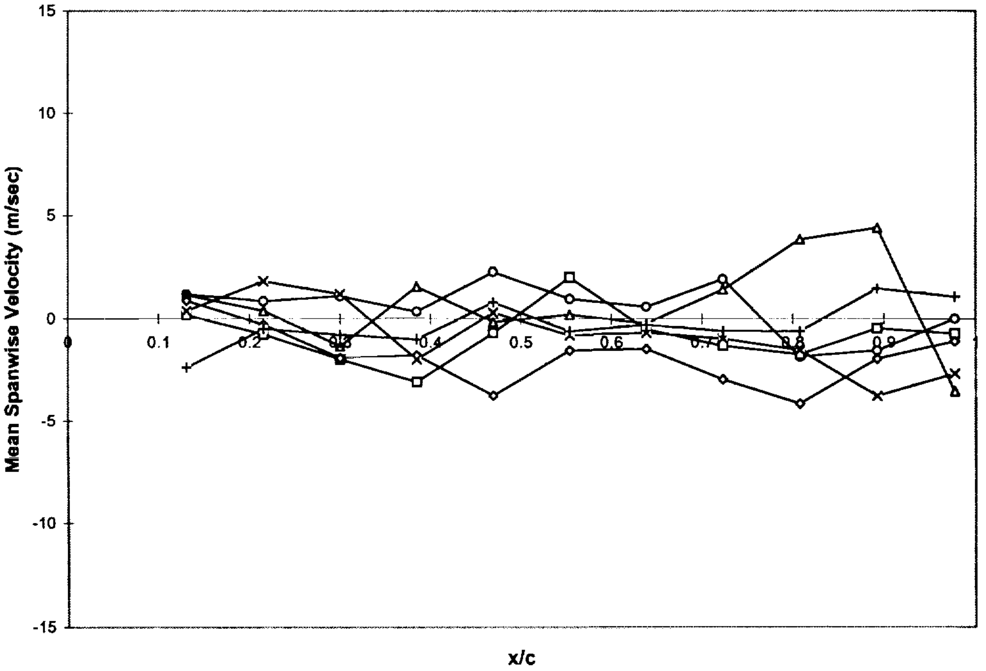

Figure 6.50. PDV mean spanwise velocity with polarizing film (6 repeat runs).

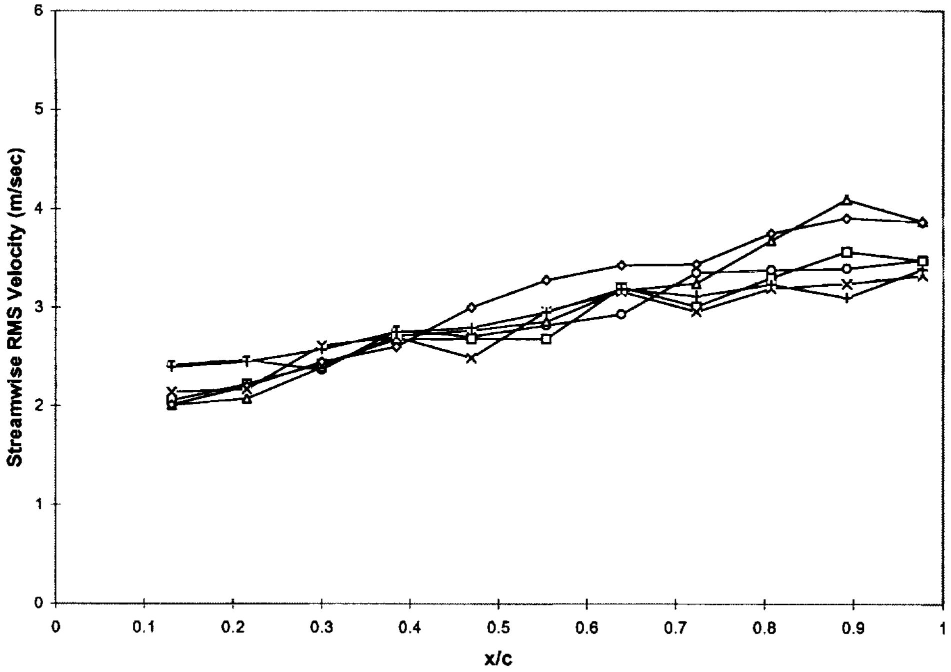

Figure 6.51. PDV streamwise RMS velocity with polarizing film (6 repeat runs).

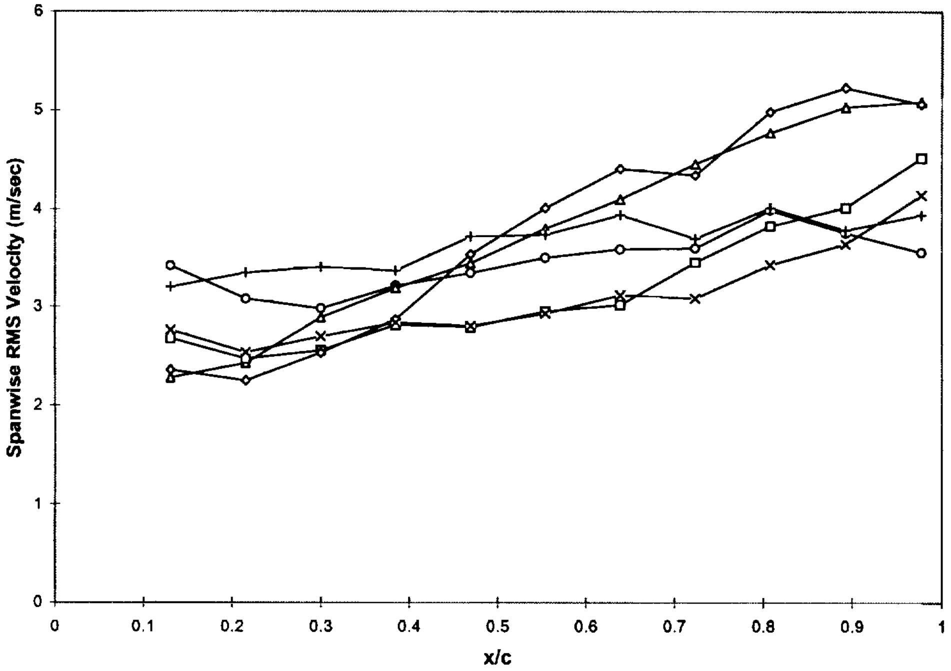

Figure 6.52. PDV spanwise RMS velocity with polarizing film (6 repeat runs).

DEVELOPMENT OF AND MEASUREMENTS USING A POINT DOPPLER VELOCIMETRY (PDV) SYSTEM

David L. Webb

THESIS

Submitted to the College of Engineering and Mineral Resources
West Virginia University
Morgantown, WV

In partial fulfillment of the requirements
for the degree of

Master of Science
in
Aerospace Engineering

Department of Mechanical and Aerospace Engineering

APPROVAL OF THE EXAMINING COMMITTEE

Mridul Gautam, Ph.D.

Charles F. Stanley, Ph.D.

Date

John M. Kuhlman, Ph.D., Chair